

L. William Pearce
Site Vice President

724-682-5234
Fax: 724-643-8069

November 24, 2003
L-03-188

U. S. Nuclear Regulatory Commission
Attention: Document Control Desk
Washington, DC 20555-0001

**Subject: Beaver Valley Power Station, Unit No. 1 and No. 2
BV-1 Docket No. 50-334, License No. DPR-66
BV-2 Docket No. 50-412, License No. NPF-73
Containment Conversion Pre-application Report**

FirstEnergy Nuclear Operating Company (FENOC) submitted letter L-03-127 which documented discussions held during an August 5, 2003 meeting between FENOC and the NRC staff to discuss the Beaver Valley Power Station Containment Conversion License Amendment Request. This letter stated that, in order to provide information on the results of the analyses performed using the modified MAAP code (MAAP-DBA) to the NRC in a timely manner, FENOC would provide a pre-application submittal in the Fall of 2003. As a follow-up to the August 5, 2003 meeting, FENOC met with the NRC staff on September 10, 2003. At this meeting FENOC discussed the three topics for which the NRC staff had requested additional information. These topics were revised mass and energy releases for the main steam line break case, treatment of loss of coolant accident blowdown generated aerosols, and MAAP-DBA code benchmarks to International Standard Problems. FENOC's plan to provide a pre-application submittal was also discussed at the September 10, 2003 meeting. In keeping with these previous meetings and discussions, enclosed is the Beaver Valley Power Station Containment Conversion Pre-application Submittal.

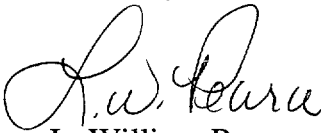
The enclosed report is being submitted for the purpose of obtaining NRC feedback on the methodology that will be used in the analyses that will support the revised Containment Conversion License Amendment Request that is being developed for submittal in early 2004. A meeting with the NRC staff is planned during the week of December 8, 2003 to discuss the methodology provided in the enclosed report. This meeting will be scheduled with the NRC Project Manager for Beaver Valley.

A001

Beaver Valley Power Station, Unit No. 1 and No. 2
Containment Conversion Pre-application Report
L-03-188
Page 2

No new commitments are contained in this submittal. If there are any questions concerning this matter, please contact Mr. Larry R. Freeland, Manager, Regulatory Affairs/Performance Improvement at 724-682-5284.

Sincerely,



L. William Pearce

Enclosure:

Beaver Valley Power Station Containment Conversion Pre-application Report

c: Mr. T. G. Colburn, NRR Senior Project Manager
Mr. P. C. Cataldo, NRC Sr. Resident Inspector
Mr. H. J. Miller, NRC Region I Administrator
Mr. D. A. Allard, Director BRP/DEP
Mr. L. E. Ryan (BRP/DEP)

Beaver Valley Power Station

Pre-Application Report

November 2003

TABLE OF CONTENTS

LIST OF TABLES iii

LIST OF FIGURESv

LIST OF ACRONYMS AND ABBREVIATIONS..... vii

EXECUTIVE SUMMARY ix

1 INTRODUCTION AND PURPOSE 1-1

 1.1 ANALYSES MODELS..... 1-2

 1.2 RESULTS FOR DESIGN LIMITING CASES 1-2

 1.3 SUMMARY AND CONCLUSION 1-2

2 OVERVIEW OF MAAP-DBA CONTAINMENT RESPONSE

 CALCULATIONAL APPROACH 2-1

 2.1 GENERAL CONTAINMENT MODELING FEATURES 2-2

 2.1.1 Pressure and Temperatures in a Region 2-2

 2.1.2 Flow Rates Between Containment Building Compartments 2-7

 2.1.3 Heat Transfer for Passive Heat Sinks..... 2-11

 2.1.4 Heat Removal by Active Systems 2-20

 2.2 SINGLE NODE CONTAINMENT MODEL 2-27

 2.3 MULTIPLE NODE CONTAINMENT MODEL 2-28

 2.4 BENCHMARKING OF MAAP-DBA MODEL 2-29

 2.4.1 GOTHIC Comparison 2-29

 2.4.2 Separate Effects Experiments 2-30

 2.4.3 Integral Effects Containment Experiments 2-31

 2.5 MASS AND ENERGY RELEASES FOR SMALL BREAK LOCA 2-35

 2.6 REFERENCES 2-36

3 RESULTS FOR BVPS-1 AND BVPS-2..... 3-1

LIST OF TABLES

Table ES	Pre-Application and Final LAR Summary	x
Table 2-1	Recent Licensing Precedence	2-40
Table 2-2	Input Conditions for MAAP-DBA and GOTHIC Comparison	2-40
Table 2-3	Summary of MAAP-DBA and GOTHIC Comparison	2-41
Table 2-4	Separate Effects Tests Used for MAAP-DBA Containment Response Benchmark	2-41
Table 2-5	Comparison of MAAP-DBA Average Condensation Heat Transfer Coefficients for the Wisconsin Square Channel Experiments	2-41
Table 2-6	Integral Effects Tests Used for MAAP-DBA Containment Response Benchmark	2-42
Table 2-7	CASP1 Fraction of the Blowdown Mass Collected as Water in the Node	2-43
Table 2-8	CASP2 Fraction of the Blowdown Mass Collected as Water in the Node	2-44
Table 2-9	Interpretation of Water Mass Distribution for CASP1	2-45
Table 2-10	Interpretation of Water Mass Distribution for CASP2	2-46
Table 3-1	Key Model Assumptions Used by MAAP-DBA for BVPS	3-2
Table 3-2	BVPS Containment Response Results	3-2

LIST OF FIGURES

Figure 2-1 Description in Terms for Estimating the Rates of Flashing and Rainout..... 2-47

Figure 2-2 Two Compartments Connected by a Junction 2-48

Figure 2-3 Structure of Heat Transfer Subroutines..... 2-49

Figure 2-4 Sensitivity of Containment Pressure to LOCA Airborne Water Fraction 2-50

Figure 2-5 MAAP-DBA Containment Nodalization for BVPS-1 and BVPS-2 2-51

Figure 2-6 Comparison of Pressure Results from MAAP-DBA and GOTHIC for Large LOCA (BVPS Case 8L)..... 2-52

Figure 2-7 Comparison of Gas Temperature Results from MAAP-DBA and GOTHIC for Large LOCA (BVPS Case 8L)..... 2-53

Figure 2-8 Comparison of Pressure Results from MAAP-DBA and GOTHIC for Large LOCA (BVPS Case3L) 2-54

Figure 2-9 Comparison of Temperature Results from MAAP-DBA and GOTHIC for Large LOCA (BVPS Case3L)..... 2-55

Figure 2-10 Comparison of Pressure Results from MAAP-DBA and GOTHIC for MSLB (BVPS Case15M)..... 2-56

Figure 2-11 Comparison of Temperature Results from MAAP-DBA and GOHTIC for MSLB (BVPS Case15M)..... 2-57

Figure 2-12 Comparison of Pressure Results from MAAP-DBA and GOTHIC for MSLB (BVPS Case 16M)..... 2-58

Figure 2-13 Comparison of Temperature Results from MAP-DBA and GOTHIC for MSLB (BVPS Case 16M)..... 2-59

Figure 2-14 PHEBUS FTP0 Pressure Profile..... 2-60

Figure 2-15 PHEBUS FPT0 Condensation Rate Profile 2-61

Figure 2-16 Comparison of the MAAP-DBA Condensation Heat Transfer Model with the Experimentally Determined Steam-Air Condensing Heat Transfer Coefficients 2-62

Figure 2-17 MAAP-DBA Single Node Model Pressure Profile for JAERI Test PHS-1 2-63

Figure 2-18 MAAP-DBA Multiple Node Model Pressure Profile for JAERI Test PHS-1 ... 2-64

Figure 2-19 MAAP-DBA Pressure Profiles for Kulic Spray Tests 2-65

Figure 2-20 HDR-V44 Pressure Profile 2-66

Figure 2-21 HDR-V44 Gas Temperature Profile..... 2-67

Figure 2-22 HDR-T31.5 Pressure Profile..... 2-68

LIST OF FIGURES (cont.)

Figure 2-23	HDR-T31.5 Gas Temperature Profile	2-69
Figure 2-24	Comparison of NUPEC M-7-1 Preheat Phase Gas Temperatures and Containment Pressure	2-70
Figure 2-25	Comparison of CVTR Test 3 Containment Pressure	2-71
Figure 2-26	Comparison of CVTR Test 4 Containment Pressure	2-72
Figure 2-27	Comparison of BFMC D-16 Pressure History in the Break Compartment	2-73
Figure 2-28	Comparison of BFMC D-16 Pressure History for Outer Room	2-74
Figure 2-29	Comparison of BFMC D-16 Temperature History for Break Room	2-75
Figure 2-30	Comparison of BFMC D-16 Temperature History for Outer Room.....	2-76
Figure 2-31a	Comparison of 2 Inch Cold Leg Releases for SBLOCA Analysis.....	2-77
Figure 2-31b	Comparison of 2 Inch Cold Leg Releases for SBLOCA Analysis.....	2-78
Figure 2-32a	Comparison of 3 Inch Cold Leg Releases for SBLOCA Analysis.....	2-79
Figure 2-32b	Comparison of 3 Inch Cold Leg Releases for SBLOCA Analysis.....	2-80
Figure 2-33a	Comparison of 4 Inch Cold Leg Releases for SBLOCA Analysis.....	2-81
Figure 2-33b	Comparison of 4 Inch Cold Leg Releases for SBLOCA Analysis.....	2-82
Figure 2-34a	Comparison of 6 Inch Cold Leg Releases for SBLOCA Analysis.....	2-83
Figure 2-34b	Comparison of 6 Inch Cold Leg Releases for SBLOCA Analysis.....	2-84
Figure 2-35a	Comparison of 2 Inch Cold Leg Releases.....	2-85
Figure 2-35b	Comparison of 2 Inch Cold Leg Releases.....	2-86
Figure 2-36a	Comparison of 2 Inch Hot Leg Releases	2-87
Figure 2-36b	Comparison of 2 Inch Hot Leg Releases	2-88
Figure 3-1	BVPS Large LOCA Pressure Profile (Tagami).....	3-3
Figure 3-2	BVPS MSLB Pressure Profile (Uchida).....	3-4
Figure 3-3	BVPS Large LOCA Gas Temperature Profile (Tagami).....	3-5
Figure 3-4	BVPS MSLB Gas Temperature Profile (Uchida)	3-6

LIST OF ACRONYMS AND ABBREVIATIONS

AFW	Auxiliary Feedwater
ANS	American Nuclear Society
ANSI	American National Standards Institute
AST	Alternative Source Term
BFMC	Battelle Frankfurt Model Containment
BVPS	Beaver Valley Power Station
CASP	Containment Analysis Standard Problem
CH/SI	Charging/Safety Injection
CSE	Containment System Experiment
CVTR	Carolinas and Virginia Test Reactor
DBA	Design Basis Accident
DEHL	Double Ended Hot Leg
EAB	Exclusion Area Boundary
ECCS	Emergency Core Cooling System
EQ	Equipment Qualification
FAI	Fauske & Associates Incorporated
FENOC	FirstEnergy Nuclear Operating Company
GCM	Generalized Containment Model
GDC	General Design Criteria
GOTHIC	Generation of Thermal Hydraulic Information for Containments
HDR	Heiss Dampf Reaktor
HMTA	Heat and Mass Transfer Analogy
HPI	High Pressure Injection
IET	Integral Effects Test
IGPM	Imperial Gallons Per Minute
ISPs	International Standard Problems
JAERI	Japan Atomic Energy Research Institute
LAR	License Amendment Request
LOCA	Loss of Coolant Accident
LPI	Low Pressure Injection
M&E	Mass and Energy
MAAP	Modular Accident Analyses Program
MAAP-DBA	Modular Accident Analyses Program DBA Version
MSIV	Main Steam Isolation Valve
MSLB	Main Steamline Break
MWt	Megawatts Thermal
NOTRUMP	Nodal Transient Small Break Universal Modeling Program
NPSH	Net Positive Suction Head
NPSHA	Net Positive Suction Head Available
NRC	Nuclear Regulatory Commission
NSSS	Nuclear Steam Supply System
NTU	Number of Transfer Units
NUPPSCO	Nuclear Power Plant Standards Consensus
Pa	Calculated Peak Accident Pressure

LIST OF ACRONYMS AND ABBREVIATIONS (cont.)

PSIA	Pounds Square Inch Absolute
PSIG	Pounds Square Inch Gauge
PWR	Pressurized Water Reactor
RCP	Reactor Coolant Pump
RCS	Reactor Coolant System
RG	Regulatory Guide
RS	Recirculation Spray
RTP	Reactor Thermal Power
SBLOCA	Small Break Loss of Coolant Accident
SER	Safety Evaluation Report
SG	Steam Generator
SI	Safety Injection
SIS	Safety Injection System
Tavg	Temperature Average
WCAP	Westinghouse Commercial Atomic Power

EXECUTIVE SUMMARY

FirstEnergy Nuclear Operating Company (FENOC) plans to convert both Beaver Valley Power Station Unit 1 (BVPS-1) and Beaver Valley Power Station Unit 2 (BVPS-2) from sub-atmospheric to atmospheric containment design.

The containment analysis will be done with the Modular Accident Analyses Program-Design Basis Analysis (MAAP-DBA) code version. This code version is consistent with the Standard Review Plan and uses Tagami and Uchida heat transfer. It takes no credit for forced convection or water entrainment. This is consistent with analysis previously reviewed by the NRC for other applications that have been approved.

This is a pre-application report submitted for the purpose of obtaining NRC feedback on the MAAP-DBA containment analysis methodology that will be used in the analyses to support a Licensing Amendment Request (LAR) in 2004.

This report describes the efforts planned and underway to support the containment atmospheric conversion, and specifically describes the analytical models being used, the benchmarking effort, and the results to date. The benchmarking results presented illustrate that there is good agreement in the peak containment pressures and temperatures calculated with the MAAP-DBA computer program and the NRC accepted Generation of Thermal Hydraulic Information for Containments (GOTHIC) version 6.0a computer program (Ref. 34) for the limiting containment pressure cases for BVPS-1 and -2. Furthermore, the analysis results for the limiting pressure cases presented show that both BVPS-1 and -2 will remain within the currently licensed containment design pressure of 45 psig when operated at an uprated power of 2900 MWt Reactor Thermal Power (RTP).

The work on the final submittal is in progress, and the anticipated submittal of the revised BVPS Containment Conversion LAR in early 2004.

The scope of this pre-application report and that of the final LAR submittal are summarized in the following Table ES.

Table ES Pre-Application and Final LAR Summary						
Parameter	Mass/Energy	Containment Model Used	Containment Methods	Precedents	MAAP-DBA Benchmarks	Results To Date and NRC Submittal Schedule
LOCA: Peak Pressure Gas Temperature Cont. Liner Temp	NRC Approved WCAP 10325-P-A	Single Node MAAP-DBA	Std Review Plan Tagami Heat Transfer No Entrainment 10% Airborne Water	NRC Approved: W-312 C-E #1 W-212 In NRC Review: C-E #2	GOTHIC 6.0a HDR – V44 HDR – T31.5 BFMC D-16	Model Description This Pre-Application Report Limiting Pressure Case: <45 psig Both Units This Pre-Application Report Remaining Cases: LAR 2004
MSLB Peak: Peak Pressure Gas Temperature Cont. Liner Temp	NRC Approved WCAP 8822-P-A	Single Node MAAP-DBA	Std Review Plan Uchida Heat Transfer No Entrainment 8% Re vaporization	NRC Approved: W-312 C-E #1 W-412 W-212 In NRC Review: C-E #2	GOTHIC 6.0a CVTR #3 CVTR #4 CVTR #5	Model Description This Pre-Application Report Limiting Pressure Case: <45 psig Both Units This Pre-Application Report Remaining Cases: LAR 2004
LOCA: NPSH	NRC Approved WCAP 10325-P-A	Multi Node MAAP-DBA	Std Review Plan Natural Convection No Entrainment 10% Airborne Water	NRC Approved M&E Current Licensing Methods	N/A	Model Description This Pre-Application Report Plant Analysis: LAR 2004
SBLOCA: Cont. Pressure NPSH Sump Water Inventory	MAAP Generated M/Es	Multi Node MAAP-DBA	Std Review Plan Natural Convection No Entrainment 10% Airborne Water	Cook Station	NOTRUMP NUPEC M-7-1	Benchmarking: This Pre-Application Report Plant Analysis: LAR 2004

1 INTRODUCTION AND PURPOSE

The Beaver Valley Power Station (BVPS) containments were originally licensed to operate at sub-atmospheric pressure, such that following a Loss of Coolant Accident (LOCA) the containment may endure a pressure transient up to its design pressure, 45 psig, but would then return to sub-atmospheric pressure within 60 minutes. This design permitted terminating the release from the containment in the radiological dose consequence analyses at 60 minutes, instead of at the usual accident termination time of 30 days specified for an atmospheric containment. Using this design allowed BVPS to demonstrate compliance with 10CFR100, using the original accident source term specified in Regulatory Guide (RG) 1.4, although the exclusion area boundary (EAB) is fairly close to the containment (approximately 2000 ft.).

In September 2003, the NRC approved BVPS-1 and -2 for a selective application of the Alternative Source Term (AST) for LOCA in Reference 28 in accordance with 10CFR50.67. Using AST, revised radiological dose consequence analyses demonstrated that federal dose limits are met both at the EAB and in the control room, even considering that the containment leakage may continue for up to 30 days. The BVPS-1 and -2 submittal and the NRC approval considered that conclusion to be valid for both a sub-atmospheric containment and an atmospheric containment. Consequently, the sub-atmospheric design is no longer necessary to protect the public and the plant operators from the radiological hazards of an accident occurring inside containment.

This is a pre-application report being submitted for the purpose of obtaining NRC feedback on the methodology that will be used in the analyses to support a Licensing Amendment Request (LAR) in 2004.

This report describes the efforts planned and underway to support the containment atmospheric conversion, and specifically describes the analytical models being used, the benchmarking effort, and the results to date. The benchmarking results presented illustrate that there is good agreement in the peak containment pressures and temperatures calculated with the MAAP-DBA computer program and the Generation of Thermal Hydraulic Information for Containments (GOTHIC) version 6.0a computer program for the limiting containment pressure cases for BVPS-1 and -2.

Based on analyses performed to date, this report shows that, using previously NRC approved modeling methodologies and reasonable adjustments to design input parameters, both BVPS-1 and -2 will remain within the currently licensed containment design pressure. Analyses results for the limiting design cases for BVPS-1 and -2 are reported. The results show both units remain within the currently licensed 45 psig design pressure.

Based upon the NRC's approval of AST, the containment analyses models and preliminary analyses results described in this report, and the final analyses to be submitted as a Licensing Amendment Request in 2004, FENOC plans to change both BVPS-1 and -2 to atmospheric containment design.

1.1 ANALYSES MODELS

Both BVPS-1 and -2 containment analyses are currently licensed using the computer code, LOCTIC (Ref. 32).

FENOC plans to revise the containment analysis code from LOCTIC to the MAAP-DBA code. Section 2 of this report describes the MAAP-DBA methodology and its comparisons with relevant large scale and small-scale experimental data. Comparisons to GOTHIC version 6.0a are also presented.

The MAAP-DBA code was developed to allow the calculation of containment response attributes for a spectrum of postulated LOCA and main steamline break sequences as part of design basis calculations for BVPS-1 and -2 containments. The containment assessments for design basis application will be implemented in a manner consistent with the NRC guidance provided in the Standard Review Plan. This will include the use of the Tagami and Uchida heat transfer correlations for the quantification of the passive heat sink responses. The spectrum of containment response attributes to be quantified include the peak containment pressure, the short and long-term containment temperature, the containment liner temperature, the long-term sump water temperature, the available NPSH for ECCS and containment spray pumps, and the maximum service water outlet temperature for the containment heat removal heat exchanger. To address this set of containment response attributes for the spectrum of loss of coolant accident break sizes, both single node and multiple node containment models are used. The single node models apply for those design basis sequences and attributes that employ the Tagami and Uchida heat transfer correlations. For the multiple node applications, a heat and mass transfer analogy based on natural convection is used. The MAAP-DBA model features and fundamental equations that apply to these applications are described in Section 2.

A single node model is used to calculate peak containment pressure and containment liner temperature as well as post accident containment global gas temperature profiles for equipment qualification. A multi-node model is used for NPSH and sump water temperature. This provides improved accountability of water hold up for NPSH and debris transport calculations. However, this report presents only containment pressure and gas temperature results from the single-node model.

1.2 RESULTS FOR DESIGN LIMITING CASES

Section 3 of this report provides analyses to date results for the limiting design cases for both BVPS-1 and -2. Those results show both units remain within the currently licensed 45 psig containment design pressure.

1.3 SUMMARY AND CONCLUSION

FENOC plans to revise the containment analysis code from LOCTIC to the MAAP-DBA code. The methodology described in this report and utilized in the MAAP-DBA code is consistent with the Standard Review Plan, the current licensing basis for BVPS-1 and -2, and with that approved by the NRC recently for other applications.

Comparisons presented in this report demonstrate that MAAP-DBA results are consistent with GOTHIC version 6.0a peak pressure and temperature results. GOTHIC version 6.0a has been accepted by the NRC for use in design basis applications at other plants.

The results of benchmarking calculations using MAAP-DBA demonstrate good agreement with separate effects experiments, which represent key phenomena for containment integrity analyses. The results of benchmarking calculations for an array of integral effects tests shows that MAAP-DBA maintains a level of conservatism of at least 10% with respect to the peak containment pressure attribute.

The results of comparisons with NOTRUMP show that MAAP-DBA conservatively calculates mass and energy releases for SBLOCA events, and is therefore acceptable for this purpose.

The results for BVPS-1 and -2 to date show that the containment peak pressure associated with limiting LOCA and MSLB cases do not exceed the current design pressure.

2 OVERVIEW OF MAAP-DBA CONTAINMENT RESPONSE CALCULATIONAL APPROACH

Single node assessments will be used to quantify the containment peak pressure, gas temperature, and maximum liner temperature; while multiple node assessments will be used to quantify available NPSH and long-term sump temperature responses. MAAP-DBA will be applied consistent with the Standard Review Plan as identified in Table ES in the Executive Summary. MAAP-DBA has the capability to model containment as a single node or as multiple nodes interconnected by flow junctions. This capability has been referred to as the generalized containment model (GCM) that replaced the fixed node and junction scheme included in previous versions of MAAP. Mass and energy balances are performed for each containment node. The rates-of-exchange of mass and energy between multiple nodes are quantified. The rates-of-exchange of mass and energy with active containment heat removal spray systems as well as passive heat sinks are also quantified.

The calculational procedure implemented in MAAP-DBA involves:

- an initialization step,
- the calculation of the auxiliary variables, such as the gas pressure and temperature, the water temperature, and various gas properties,
- the calculation of the rates-of-change of dynamic variables for each compartment by summing the rates-of-change of the physical phenomena and processes modeled,
- the saving of selected variables, and
- the output of selected variables to files for subsequent printing and plotting.

All compartments and heat sinks are initialized to the appropriate initial conditions, which are designated in the parameter file. Parameters that are initialized include the gas and water masses, the gas and water internal energy, compartment pressure and temperatures, and heat sink temperatures. The calculations of auxiliary variables update the gas pressure and temperature, the compartment water temperature, and various gas properties for nodes containing water, steam, and non-condensable by a call to MAAP-DBA subroutine PTCAL. In this manner, for each compartment the gas enthalpy, gas mole fraction, and water level are computed.

The calculation of the rates-of-change of the dynamic variables are compiled from various phenomenological models. These rates-of-change over the time step of interest are then integrated and then these changes in mass and energy are used to determine the new state and auxiliary variables. The calculation of the rates-of-change of mass and energy and heat sinks temperatures begins by setting the rates-of-change to zero. Then different processes are each computed, such as:

- engineered safeguards systems,
- passive metal and concrete heat sinks,

- flashing rates and pool evaporation,
- heat and mass transfer to spray droplets (computed using subroutine SPRAY),
- heat and mass transfer to suspended water droplets are calculated using subroutine RATES1, and
- flow rates between the primary system and the containment node, plus water and gas flow between multiple containment nodes.

The details of this functional scheme are described below. First, those procedures that are applicable to both single node and multiple node containment models are described in Section 2.1. Subsequently, the unique features and capabilities that apply for single node (see Section 2.2) and multiple node (see Section 2.3) calculations are discussed. Section 2.4 discusses applicable benchmarks for MAAP-DBA.

2.1 GENERAL CONTAINMENT MODELING FEATURES

2.1.1 Pressure and Temperatures in a Region

Subroutine PTCAL calculates the temperatures and pressure in a region containing water, steam, and non-condensable gases. The RATES1 subroutine calculates the mass transfer processes that result from flashing and boiling, condensation (rainout) of water droplets, and evaporation of suspended water droplets and steam condensation on them.

The important input quantities are the total gas, plus water volume, V ; total internal energies, U_w and U_g , of water and gas; and the masses, m_w , m_s , and m_i , of water, steam, and non-condensable gases, respectively. The important output quantities are the temperatures, T_w and T_g , of water and gas; the pressure, P . Other outputs include miscellaneous physical properties, such as the specific volume, v , the specific enthalpy, h , the specific internal energy, u , and the specific heat, c_v , etc., of water and steam.

An uncoupled model where the water and gas phases are allowed to have different temperatures is appropriate for large volumes containing a small amount of water, such as a containment region. The generalized containment model (GCM) uses an uncoupled model to quantify containment responses.

2.1.1.1 Gas Phase Temperature

The gas phase temperature, T_g , is computed for a given volume from the total internal energy and steam and non-condensable gas masses:

$$U_g = m_s u_s (T_g, v_s) + T_g \sum_i m_i c_{vi} \quad (2-1)$$

where U_g (total internal energy), m_s , and m_i are given as inputs; $u_s (T_g, v_s)$ is the saturated or superheated steam-specific internal energy per unit mass given by a call to the appropriate property subroutine; and c_{vi} is the constant volume specific heat capacity of non-condensable gas

component i . The gas potential and kinetic energies are assumed to be small and are neglected. The steam and non-condensables are assumed to be in thermal equilibrium. The specific volume of steam, v_s , appearing as an argument in equation (2-1) is determined by subtracting the volume occupied by water from the total nodal volume and dividing by the mass of steam (m_s)

$$v_s = \frac{V - m_w v_w - m_{sw} v_{sw}}{m_s} \quad (2-2)$$

where m_w is the water mass in the node's pool and m_{sw} is the suspended water mass in the node. The specific volumes of water in the pool and the suspended water are given by v_w and v_{sw} , respectively.

2.1.1.2 Total Pressure

The total gas pressure is computed from the Gibbs-Dalton law assuming the non-condensables are perfect gases:

$$P = P_{st} + P_{\text{non-condensables}} = P_{st} + \frac{NRT_g}{V_g} \quad (2-3)$$

where N is the total moles of non-condensable gases, R is the universal gas constant, and $V_g = V - m_w v_w$ is the gas volume of the region. The value of the partial pressure of steam, P_{st} , used in equation (2-3) is obtained by a final call to the property subroutine after convergence on gas temperature, T_g .

2.1.1.3 Specific Volume of Gas

The specific volume of the gas is determined by taking into account the mass of suspended water. That is,

$$V_g = \frac{V - m_w v_w}{m_s + \sum_i m_i + m_{sw}} \quad (2-4)$$

where m_i is the mass of the non-condensable gases (nitrogen, oxygen, hydrogen, carbon monoxide, and carbon dioxide).

2.1.1.4 Steam Generation and Rainout Rates

Steaming rates are calculated when the water pool is superheated due to heat addition or depressurization. These processes tend to increase the pool superheat (water temperature minus the saturation temperature). The steam generation rate, W_{st} , is determined from the mass of water flashed (m_{fl}) and the time step (Δt), as follows:

$$W_{st} = \frac{m_{fl}}{\Delta t} = \frac{m_w (h_w - h_{w,sat(P)})}{(h_{st,sat(P)} - h_{w,sat(P)}) \Delta t} \quad (2-5)$$

where P is the total pressure, (sat) refers to saturation, and h_w is the specific enthalpy of the water in the pool. It is assumed for water that the work term (P_{vw}) is negligible such that the specific internal energy and specific enthalpy are equal. The steaming rate as given by equation (2-5) is refined using implicit solution techniques. Figure 2-1 illustrates the system with energy addition to the water, inlet, and outlet water flow rates, steaming into a gas volume, and gas flow in and out of that volume.

The rainout rate is calculated when the steam is supersaturated. The rainout rate, $W_{rainout}$, is determined from the mass of steam, m_{st} , as follows:

$$W_{rainout} = \frac{m_{st} (u_{st} - u_{st,sat}(P_{sat}))}{(h_{w,sat}(P_{st}) - u_{st,sat}(P_{st})) \Delta t} \quad (2-6)$$

where P_{st} is the steam partial pressure and u_{st} is the steam specific internal energy.

2.1.1.5 Suspended Water

Water droplets can be produced in containment and become suspended in the gas space. The suspended water droplets can influence the heat and mass transfer processes that occur within the containment and on its passive heat sink surfaces. The possible sources of suspended water considered in MAAP-DBA include droplet formation from bulk condensation in a containment node, two-phase LOCA blowdowns, and spray system operation. MAAP-DBA does not credit any water that might be entrained off heat sink surfaces water pools when determining suspended water. The default mode for MAAP-DBA is to treat containment sprays per a separate subroutine (see discussion in Section 2.1.4.1). However, the spray flow may alternatively be treated as a source of suspended water.

The duration that water is suspended in a node's gas space influences the amount of heat and mass transfer with the surrounding gas. The dissipation of the suspended water droplet mass can occur due to evaporation and deposition. Deposition is modeled by settling. Assuming a well-mixed node, the suspended water droplet deposition rate (\dot{m}_{dep}) is given by

$$\dot{m}_{dep} = \lambda_{sw} m_{sw} \quad (2-7)$$

where λ_{sw} is the settling decay constant and m_{sw} is the mass of suspended water droplets.

The settling rate is also represented by

$$\dot{m}_{dep} = \frac{m_{sw} A_{sed} U_{term}}{V} \quad (2-8)$$

where A_{sed} is the node's sedimentation area, U_{term} is the water droplet terminal velocity, and V is the node's volume.

These two expressions for (\dot{m}_{dep}) result in an expression for the suspended water decay constant, λ_{sw}

$$\lambda_{sw} = \frac{A_{sed} U_{term}}{V_t} \quad (2-9)$$

The decay constant can be quantified for a given node once the droplet's terminal velocity is determined. The desired expression for the droplet terminal velocity is developed based on a force balance on a droplet and the law of resistance for a rigid spherical particle.

The force balance on a spherical particle falling with terminal speed U_{term} which equates the gravitational force to the force due to fluid resistance, gives

$$\frac{4}{3} \pi \left(\frac{d_p}{2} \right)^3 \rho_p g = \frac{C_D}{2} \pi \left(\frac{d_p}{2} \right)^2 \rho_\infty U_{term}^2 \quad (2-10)$$

where d_p is the particle diameter, ρ_p is the particle density, ρ_∞ is the surrounding fluid density, g is the gravitational constant, and C_D is the drag coefficient for a sphere. The law of resistance for a rigid spherical particle is (Ref. 19)

$$C_D = \frac{24}{Re_p} \left(1 + 0.15 Re_p^{0.667} \right) \quad (2-11)$$

where Re_p is the particle Reynolds number:

$$Re_p = \frac{\rho_\infty d_p U_{term}}{\mu_\infty} \quad (2-12)$$

In equation (2-12), μ_∞ is the fluid viscosity.

Equations (2-10) to (2-12) comprise a non-linear equation set from which U_{term} is calculated once the properties of the host fluid and the particle size d_p are specified. The solution for U_{term} is formulated to apply over the entire range of droplet diameters that applies from small droplet diameter (Stoke's law regime) situations to large droplet diameter situations.

The deposition of suspended water can alternatively be modeled in MAAP-DBA by treating it with the fission product aerosol deposition models.

2.1.1.6 Heat and Mass Transfers Between Suspended Water and Gases

The model calculates heat transfer between suspended water and the bulk gas. Also, the model calculates evaporation of suspended water or condensation of steam on the suspended water, depending on temperatures and partial pressure of steam.

The rate of heat transfer (Q_{gsw}) is given by

$$Q_{gsw} = h_g N A_d (T_g - T_{sw}) \quad (2-13)$$

where h_g is the heat transfer coefficient, N is the number of droplets, and A_d is the droplet surface area. Droplet population can be related to the suspended water mass (m_{sw}) by

$$N = \frac{6 m_{sw}}{\rho_w \pi d_d^3} \quad (2-14)$$

where ρ_w is the saturated water density and d_d is the droplet diameter. Since a droplet's surface area is given by

$$A_d = \pi d_d^2 \quad (2-15)$$

Equation (2-13) can be written as

$$Q_{gsw} = h_g \frac{6 m_{sw}}{\rho_w d_d} (T_g - T_{sw}) \quad (2-16)$$

The heat transfer coefficient h_g is calculated from a correlation (Ref. 16) given by

$$Nu = 2.0 + 0.65 Re_d^{1/2} Pr^{1/3} \quad (2-17)$$

where

Nu = Nusselt number,

Re_d = Reynolds number of droplet = $\frac{\rho_g d_d U_{term}}{\mu_g}$, (2-18)

U_{term} = Terminal velocity of droplet, and

Pr = Prantdl number.

The evaporation of suspended water or steam condensation on the surface of the suspended water is calculated by

$$W_{gsw} = h_m 6 \frac{M_{sw}}{\rho_w d_d} (P_{sat,d} - P_{st}) \quad (2-19)$$

where

h_m = $\frac{PM_w D_{dif} Sh}{P_{am} d_d R_u T_g}$, (2-20)

M_w = Molecular weight of water,

D_{dif} = Diffusivity of water vapor in the gas,

$$\begin{aligned}
 T_g &= \text{Gas temperature,} \\
 Sh &= \text{Sherwood number,} \\
 &= 2.0 + 0.65 \text{Re}_d^{1/2} \text{Sc}^{1/3} \qquad (2-21)
 \end{aligned}$$

$$P_{\text{sat,d}} = P_{\text{sat}}(T_{\text{sw}}), \qquad (2-22)$$

$$P_{\text{st}} = \text{Steam partial pressure,}$$

$$P_{\text{am}} = \frac{(P - P_{\text{st}}) - (P - P_{\text{sat,d}})}{\ln\left(\frac{P - P_{\text{st}}}{P - P_{\text{sat,d}}}\right)}, \qquad (2-23)$$

$$R_u = \text{Universal gas constant,}$$

$$\begin{aligned}
 Sc &= \text{Schmidt number, and} \\
 &= \frac{\mu_g}{\rho_g D_{\text{dif}}} \qquad (2-24)
 \end{aligned}$$

The heat and mass transfer rates in equations (2-13) and (2-19) are solved semi-implicitly using the approximate end of time step values of T_g , T_{sw} , $P_{\text{sat}}(T_{\text{sw}})$, and P_{st} .

2.1.2 Flow Rates Between Containment Building Compartments

2.1.2.1 Gas Flows

Subroutine AUXFLO computes gas flow rates between containment building compartments. Normally, pressure differences between compartments drive flows through junctions connecting the compartments. However, because flows in turn affect compartment pressures, an implicit numerical method is used where gas flow rates are computed based on end-of-time step pressures. Solving flow rates based on current pressures would be numerically stiff and require very small time steps.

Pressures are also dependent on gas temperatures, which in turn depend on gas to heat sink heat transfers inside the compartments. The scheme used in AUXFLO combines the implicit flow calculation with an implicit heat transfer calculation; that is, heat transfer is based on the end-of-time step gas temperature. The heat sink surface temperature is assumed to vary negligibly over the time step, and hence, its beginning-of-time step value is always used.

When the pressure difference across a junction is small, counter-current exchange flow through it may arise due to a density difference between the two compartments it joins. This counter-current flow is superimposed on the pressure-driven unidirectional flow. The maximum counter-current flow rate determined based on the Froude number versus L/D (length-to-diameter ratio) of the junction is found using beginning-of-time step properties. The actual counter-current flow

rate is a lower value depending on the unidirectional flow strength. Thus, counter-current flows are also included in the unified implicit scheme.

There are other special cases and considerations which add to the complexity of the scheme. They include treatment of shut-off junctions, choked flow, junctions which exhaust into a water pool, and parallel flow paths. The details of these treatments are provided in the MAAP4 User's Manual (Ref. 35).

Implicit flow and temperature equations are derived by considering two volumes and assuming constant density in each volume connected by a junction as shown in Figure 2-2. Under quasi-steady conditions, the flow through the junction is related to the pressures in the two compartments as

$$K |W^{n-1}| W = P_1 - P_2 - \rho_1 g(Z_1 - L) + \rho_2 g Z_2 \quad (2-25)$$

where K is a junction flow resistance and n is an exponent which is determined by the flow regime. By convention, the thermo-dynamically calculated pressures are those which would be measured at the bottom of the compartment. The pressure gradient in a volume is described by

$$\frac{dP}{dZ} = -\rho(P) g \quad (2-26)$$

For an ideal gas, the solution of equation (2-26) assuming homogenous, constant temperature for each volume becomes

$$P(Z) = P_0 e^{-\left(\frac{\rho}{P_0}\right) g Z} \quad (2-27)$$

Using the variable density, equation (2-25) becomes

$$K |W^{n-1}| W = P_1 e^{-\frac{\rho_1}{P_1} g(Z_1 - L)} - P_2 e^{-\frac{\rho_2}{P_2} g(Z_2)} \quad (2-28)$$

For a containment building with many junctions and compartments, the above equation can be generalized for each junction j as

$$K |W_j^{n_j-1}| W_j = P_{d_j} e^{-\left(\frac{\rho_{d_j}}{P_{d_j}}\right) g Z_{j,d}} - P_{r_j} e^{-\left(\frac{\rho_{r_j}}{P_{r_j}}\right) g Z_{j,r}} \quad (2-29)$$

where subscript "d_j" designates the donor compartment of junction j . Similarly, r_j designates the receiver compartment. $Z_{j,d}$ and $Z_{j,r}$ can be defined appropriately depending on whether the junction is horizontal or vertical.

The reference donor and receiver compartments are pre-assigned for each junction. When a negative flow is calculated for the junction, the reference donor compartment is actually downstream of the flow and the reference receiver compartment is actually upstream.

The implicit pressures in equation (2-29) can be expressed in terms of the “extrapolated” compartment pressure and the pressure change due to flows and gas temperature change. “Extrapolated” pressure is defined as the end-of-time step pressure if no inter-compartment flows exist and if the compartment gas temperature is constant. That is,

$$P_{d_j} = P_{d_j}^{ex} + \sum_{k \in d_j} I_{sense}(k, d_j) \frac{\partial P_{d_j}}{\partial W_k} W_k + \frac{P_{d_j}}{T_{d_j}} \delta T_{d_j} \quad (2-30)$$

where (k, d_j) means for every junction k connected to the compartment d_j (donor compartment for junction j). $I_{sense}(k, d_j)$ has a value of 1 if d_j is the reference receiver of flow W_k ; otherwise, it has a value of -1. For brevity, the I_{sense} will be written without compartment and flow designators hereafter. Because in containment rates calculations the AUXFLO subroutine is called after all other processes are evaluated, the necessary information to determine the “extrapolated” compartment pressure is available. The “extrapolated” pressure is calculated as

$$P^{ex} = P + \frac{\Delta t RT}{V} \sum_i \frac{\dot{m}_i}{Mw_i} + \frac{\Delta t P \dot{m}_w v_w}{V} \quad (2-31)$$

where

- P = beginning-of-time step pressure,
- R = ideal gas constant,
- T = compartment gas temperature
- \dot{m}_i = rate-of-change of gas species i ,
- Mw_i = molecular weight of gas species i (corrected for the non-ideality of steam),
- \dot{m}_w = rate-of-change of water mass, and
- V = gas volume.

Substituting equation (2-30) into equation (2-29) gives

$$\begin{aligned}
 & -K_j |W_j^{n_j-1}| W_j + \left(P_{d_j}^{\text{ex}} e^{-\frac{\rho_{d_j}}{P_{d_j}} g Z_{j,d}} + \sum_{k \in d_j} I_{\text{sense}} \frac{\partial P_{d_j}}{\partial W_k} + \frac{P_{d_j}}{T_{d_j}} \delta T_{d_j} \right) \\
 & - \left(P_{r_j}^{\text{ex}} e^{-\frac{\rho_{r_j}}{P_{r_j}} g Z_{j,r}} + \sum_{k \in r_j} I_{\text{sense}} \frac{\partial P_{r_j}}{\partial W_k} W_k + \frac{P_{r_j}}{T_{r_j}} \delta T_{r_j} \right) = 0
 \end{aligned} \tag{2-32}$$

Equation (2-32) represents J flow equations in terms of J unknown flows and N unknown temperature changes where J is the number of junctions and N is the number of compartments. The junction resistance K_j and the exponent n_j are calculated based on the beginning-of-time step condition. For unchoked junctions, the resistance is

$$K = \frac{v_g}{2 A^2 C_D^2} \tag{2-33}$$

where

- v_g = specific volume of gas,
- A = effective junction area (at present, the frictional loss due to finite length is ignored), and
- C_D = discharge coefficient (nominally 0.75), and

the exponent $n = 2$.

2.1.2.2 Water Flows

Subroutine AXWFLO computes the flow rate of water between containment compartments. Its philosophy and mathematical treatment are very similar to AUXFLO, which does the same job for the gas flows. The calculation is slightly complicated here, however, since junctions can be uncovered as the flow rates are converged; this cannot happen with the gas flow calculation. An additional complication is the possibility of water-solid regions.

As in subroutine AUXFLO, the unidirectional water flows are computed by iteratively solving a set of equations which define the flow on each junction. Flow W_j on a normal junction J is defined by an equation of the form:

$$O = B_j = KI_j \Delta P - W_j |W_j| \tag{2-34}$$

where

- KI = inverse flow resistance,

$$= 2 AO_j A_j \rho_D C_D^2, \text{ and}$$

$$\Delta P = \Delta P = g \{ \rho_1 (ZW_1 - Z_1) - \rho_2 (ZW_2 - Z_2) \} + \Delta P_j + (P_1 - P_2)$$

Here

AO_j = beginning of time step water-covered flow area on the donor side of the junction,

A_j = current (this iteration) water-covered flow area on donor side,

ρ_D = donor-side water density,

C_D = discharge coefficient (FCDJ(J), common block variable for J'th junction),

g = acceleration of gravity,

ρ_1, ρ_2 = density on either side of the junction,

Z_1, Z_2 = elevation of junctions 1 and 2 above the floor of their respective compartments,

ZW_1, ZW_2 = current (this iteration) water level in each compartment computed using function ZRBLVL,

$$\Delta P_j = \left[\frac{\rho_1 + \rho_2}{2} \right] L_j g,$$

L_j = $\begin{cases} \text{length of junction - for vertical junctions,} \\ 0 \text{ for horizontal junctions} \end{cases}$, and

P_1, P_2 = gas or "solid" pressure in each compartment.

2.1.3 Heat Transfer for Passive Heat Sinks

Subroutine HSNKRB manages the containment passive heat sink calculations, as illustrated in Figure 2-3. Heat sinks may be modeled as distributed (single- or double-sided) or as lumped. Subroutine HTWALLN calculates heat transfer to distributed heat sinks. This subroutine treats a wall or floor as a slab, assigns individual heat sink properties to the slab, nodalizes the slab, and specifies boundary heat fluxes imposed to the sides of the slab. Subroutine HTEQPT calculates the heat transfer rate and the temperature rate-of-change of the metal equipment heat sinks. The heat transfer coefficients, steam condensation rate, and energy exchange rate for the heat sinks are quantified. Serial thermal resistances due to painted surfaces, metal liners, gaps, and concrete are included.

The default mode of containment heat transfer for both distributed and lumped heat sinks is to use the mechanistic heat transfer coefficients for natural convection. The BVPS-1 and -2 atmospheric containment assessment uses this default mode for the multiple node containment model. The correlations for the natural convection heat transfer coefficient use an average Nusselt number (Nu) formulation based on the compositional Grashof number (Gr), as described below. The modified Reynolds analogy using the Stanton number (St) is used for the forced convection heat transfer coefficient benchmark with the Wisconsin flat plate data. Optional modes of containment heat transfer are also available for performing design basis analyses in compliance with the Standard Review Plan requirements. Specifically, the Tagami and Uchida heat transfer correlations can be selected, including the use of a multiplier for assessing equipment and containment liner responses.

2.1.3.1 Mechanistic Heat Transfer

The heat transfer coefficients for radiation and natural and forced circulation to a surface in containment are calculated by subroutine HTSHCR1. No credit is taken for forced convection if the calculated value exceeds calculated natural convection heat transfer coefficients. Natural convection heat transfer coefficients are determined through the use of a heat and mass transfer analogy (HMTA). The application of MAAP-DBA for the BVPS atmospheric containment assessment only uses the HMTA analogy for the multiple node model. The single node model uses the Tagami and Uchida correlations as discussed in Section 2.1.3.2.1 and 2.1.3.2.2.

The radiation calculation assumes that the radiation properties of the gas and surface are represented adequately by (user-specified) emissivities E_g and E_{wl} , respectively. The heat transfer coefficient is given by

$$h_{\text{rad}} = \frac{\sigma (T_g^4 - T_{\text{FO}}^4)}{\left(\frac{1}{E_g} + \frac{1}{E_{wl}} - 1 \right) (T_g - T_{\text{FO}})} \quad (2-35)$$

where T_g and T_{FO} are the temperatures of the gas and surface, respectively, and σ is the Stefan-Boltzmann constant.

If the difference between the temperatures of the gas and surface is less or equal to 1 degree Kelvin, l'Hopital's rule is applied to equation (2-35) and the resulting heat transfer coefficient is evaluated as:

$$h_{\text{rad}} = \frac{4 \sigma T_g^3}{\left(\frac{1}{E_g} + \frac{1}{E_{wl}} - 1 \right)} \quad (2-35a)$$

The natural convection heat transfer coefficient h_{CONV} is calculated by correlations of the form for the average Nusselt number

$$\text{Nu} = a (\text{Ra})^n \quad (2-36)$$

where,

$$\text{Nu} = h_{\text{CONV}} \frac{L}{k_g}, \quad (2-37)$$

$$\text{Ra} = \text{Gr Pr}, \quad (2-38)$$

$$\text{Gr} = \frac{\rho_g^2 g |\Delta\rho_g| L^3}{\rho_g \mu_g^2}, \text{ and} \quad (2-39)$$

$$\text{Pr} = \frac{\mu_g C_{pg}}{k_g} \quad (2-40)$$

Here ρ_g is the density of the bulk gas and $|\Delta\rho_g|$ is the density difference, C_{pg} is the specific heat of the gas at constant pressure, μ_g is the dynamic viscosity of the gas, k_g is the thermal conductivity of the gas, and L is a characteristic length of the surface. The gravitational constant, g , is adjusted for surfaces inclined between the horizontal and vertical orientations. Ra , Gr , and Pr are the standard Rayleigh, Grashof, and Prandtl numbers, respectively.

$|\Delta\rho_g|$ is the density difference between the bulk gas and the gas at condensate film interface on the heat sink wall. Assuming an ideal gas for the steam-gas mixture and constant pressure in the bulk and at the film interface, this term can be evaluated in the form of density ratio as;

$$P = \rho_g R_g T_g \quad (2-41)$$

$$\rho_g = \frac{P}{R_g T_g} \quad (2-42)$$

$$d\rho_g = - \frac{Pd T_g}{R_g T_g^2} - \frac{Pd R_g}{R_g^2 T_g} \quad (2-43)$$

$$d\rho_g = - \frac{P_g d T_g}{T_g} - \frac{P_g d R_g}{R_g} \quad (2-44)$$

$$\begin{aligned} \frac{|\Delta\rho_g|}{\rho_g} &= -\frac{\Delta T_g}{T_g} - \frac{\Delta R_g}{R_g} \\ &= \frac{T_g - T_i}{T_g} + \frac{R_g - R_{gi}}{R_g} \end{aligned} \quad (2-45)$$

where

- T_i = condensate film interface temperature,
 R_g = specific gas constant of the bulk gas, and
 R_{gi} = specific gas constant at film interface.

The gas constant term in the equation above actually represents the change in molecular weight of the steam-gas mixture and can be evaluated from

$$\frac{R_g - R_{gi}}{R_g} = \frac{(M_{W_{nc}} - M_{W_{stc}})(f_{st} - f_{st,i})}{M_{W_{nc}} f_{st} + M_{W_{stc}} f_{nc}} \quad (2-46)$$

where

- $M_{W_{nc}}$ = molar mass of non-condensable gases,
 $M_{W_{stc}}$ = molar mass of steam,
 f_{st} = mass fraction of steam at bulk, and
 $f_{st,i}$ = mass fraction of steam at film interface.

The constants a and n are given by:

<u>Situation</u>	<u>a</u>	<u>n</u>	<u>Reference</u>
Vertical Surface, $Ra < 10^9$.555	.25	(Ref. 12)
Vertical Surface, $Ra > 10^9$.021	.4	(Ref. 18)
<u>Horizontal Surface Facing Upward:</u>			
1. $Gr < 2 \times 10^7, T_g < T_{FO}$.54	.25	(Ref. 12)
2. $Gr \geq 2 \times 10^7, T_g < T_{FO}$.14	.333	(Ref. 12)
3. $Gr < 2 \times 10^7, T_g \geq T_{FO}$		$Nu = 2$	
4. $Gr \geq 2 \times 10^7, T_g \geq T_{FO}$		$Nu = 2$	

<u>Situation</u>	<u>a</u>	<u>n</u>	<u>Reference</u>
<u>Horizontal Surface Facing Downward:</u>			
1. $Gr < 2 \times 10^7, T_g \leq T_{FO}$		$Nu = 2$	
2. $Gr \geq 2 \times 10^7, T_g \leq T_{FO}$		$Nu = 2$	
3. $Gr < 2 \times 10^7, T_g > T_{FO}$.54	.25	(Ref. 12)
4. $Gr \geq 2 \times 10^7, T_g > T_{FO}$.14	.333	See Footnote 1.

For forced convection as used in the Wisconsin flat plate benchmark, the modified Reynolds analogy is used for both laminar and turbulent flow to calculate the heat transfer coefficient using the Stanton (St) number:

$$St = \frac{Nu}{Re Pr} \tag{2-47}$$

and

$$St = \frac{f}{2} Pr^{-2/3} \tag{2-48}$$

Combining equations (2-47) and (2-48) results in

$$Nu = \frac{f}{2} Re Pr^{1/3} \tag{2-49}$$

where Re is a Reynolds number and f is a friction factor. The Reynolds number and the friction factor depend on heat sink type, which can be a flat plate or round tube:

- Flat Plate:

$$\begin{aligned}
 f &= \frac{1.33}{Re_{,L}^{0.5}} & Re_{,L} &< 4 \times 10^5 \\
 &= \frac{0.072}{Re_{,L}^{0.2}} & Re_{,L} &> 6 \times 10^5
 \end{aligned}
 \tag{2-50}$$

¹ NOTE: According to Reference 12, no correlation has been established in these regimes. The correlations shown are based on extrapolations of the correlations given in Reference 12.

- Round Tube:

$$\begin{aligned}
 f &= \frac{16}{\text{Re}_{,D}} & \text{Re}_{,D} < 2000 \\
 &= \frac{0.046}{\text{Re}_{,D}^{0.2}} & \text{Re}_{,D} > 6000
 \end{aligned}
 \tag{2-51}$$

where

$$\text{Re}_{,L} = \frac{\rho_g U_g L}{\mu_g}
 \tag{2-52}$$

$$\text{Re}_{,D} = \frac{\rho_g U_g D_h}{\mu_g}
 \tag{2-53}$$

- D_h = hydraulic diameter,
 L = length of a plate, and
 U_g = continuity velocity of a node.

In the transition zone from laminar to turbulent flows, f is estimated using the interpolation formulas as:

$$\ln(f) = A_1 \ln(\text{Re}) + B_1
 \tag{2-54}$$

The convective Nusselt number and heat transfer coefficient are taken to be the larger of the natural and the nodal continuity velocity values. Nodal continuity velocities are only calculated for multiple node containment nodalization models. Continuity velocity is not quantified for single node containment models.

The code also calculates the quotient of Sherwood number and length. This quotient is related to the inverse of the boundary layer thickness and is used for calculations of fission product vapor transport. A heat and mass transfer analogy is used (Ref. 6):

$$\frac{\text{Sh}}{L} = \frac{\text{Nu}}{L} \left(\frac{\text{Sc}}{\text{Pr}} \right)^n
 \tag{2-55}$$

where

$$Sc = \frac{\mu_g v_g}{D}, \text{ assumed equal to } Pr = \frac{\mu_g c_{pg}}{k_g} \quad (2-56)$$

D = diffusion coefficient,

n = exponent of Prandtl number dependence of Nu, and

v_g = specific volume of gas.

Finally, the following derivatives of the heat transfer coefficients are calculated by differentiating the appropriate correlations:

1. $\frac{dh_{rad}}{dT_g}$ from equation (2-35)
2. $\frac{dh_{CONV}}{dT_g}$ from equations (2-36), (2-37), and (2-49).

These derivatives are used by some of the calling programs to iteratively solve for the mass flow or the gas or surface temperatures.

2.1.3.2 Tagami and Uchida Heat Transfer Correlations

Subroutine HTTAGAMI calculates the heat transfer coefficient based on the Tagami correlation. The Tagami heat transfer coefficient is activated when the user sets flag ITAGAMI to 1. The single node LOCA calculations use the Tagami correlation.

Subroutine HUCHIDA calculates the heat transfer coefficient based on Uchida correlation. The Uchida heat transfer coefficient is activated when flag IUCHIDA is set to 1 by users. The single node MSLB calculations use the Uchida correlation.

2.1.3.2.1 Tagami

The Tagami heat transfer coefficient correlation (Ref. 20) is used in the containment LOCA analysis if a user-input flag ITAGAMI is equal to 1. The Tagami maximum heat transfer coefficient is given as

$$h_{max} = 75 \left(\frac{E_p}{V t_p} \right)^{0.6} \quad (2-57)$$

where

- h_{\max} = Tagami heat transfer coefficient (Btu/hr-ft²-°F),
 E_p = Integrated energy released to the containment at the time of the first peak pressure (Btu),
 V = Containment free volume (ft³), and
 t_p = Time of the first peak pressure (sec).

MAAP-DBA does all computations in SI units. In SI units, the above equation becomes

$$h_{\max} = 0.77 \left(\frac{E_{p,SI}}{V_{SI} t_p} \right)^{0.6} \quad (2-58)$$

where

- h_{\max} is in W/m²-°C,
 $E_{p,SI}$ is in joules,
 V_{SI} is in m³, and
 t_p is in sec.

Before the first peak pressure is reached, the heat transfer coefficient is calculated as:

$$h = h_{\max} (t / t_p) \quad (2-59)$$

where t is the time in seconds after the accident.

After the first peak pressure is reached, the following equation is used to calculate the heat transfer coefficient:

$$h = h_{\text{stag}} + (h_{\max} - h_{\text{stag}}) e^{-0.05(t-t_p)} \quad (2-60)$$

where

- h_{stag} = The stagnation heat transfer coefficient = 2 + 50 X (Btu/hr-ft²-°F), and
 X = Steam / Air mass ratio.

Once the heat transfer coefficient h is calculated, the heat transfer rate Q into a heat sink (steel or concrete) with area A is calculated by

$$Q = h A (T_{\text{sat}} - T_{\text{wall},0}) \quad (2-61)$$

where T_{sat} is the saturation temperature corresponding to the partial pressure of steam and $T_{wall,0}$ is the surface temperature of the heat sink. The full value of the Tagami heat transfer coefficient is used for both concrete and steel heat sinks. When a heat sink is painted, the total heat transfer coefficient is adjusted to include the resistance of the paint. A user-input parameter FTAGAMI is provided as a multiplier to the Tagami heat transfer coefficient for peak liner temperature quantification and sensitivity studies. The BVPS-1 and -2 peak liner temperature assessment uses a value of four (4) for this multiplier.

The condensation rate is calculated as

$$W_{cd} = Q / (h_{st} - h_{cd}) \quad (2-62)$$

and the energy removed from gas space becomes

$$Q_g = h A (T_{sat} - T_{wall,0}) + W_{cd} h_{cd} \quad (2-63)$$

where h_{st} is the heat of specific enthalpy of saturated steam at the partial pressure of steam and h_{cd} is an average enthalpy of the condensate.

2.1.3.2.2 Uchida

The Uchida heat transfer correlation (Ref. 21) is used in the containment MSLB analysis if a user-input flag IUCHIDA is equal to 1. The Uchida heat transfer coefficient is given as

$$h = H P_s / (3.25 P_t) \quad \text{if } 0.01 \leq (P_s / P_t) \leq 0.19 \quad (2-64)$$

or

$$h = H e^{-3.5 \left(1 - \frac{P_s}{P_t}\right)} \quad \text{if } (P_s / P_t) > 0.19 \quad (2-65)$$

where

- h = Uchida heat transfer coefficient (Btu/hr-ft²-°F),
- H = Heat transfer coefficient for pure steam (300 Btu/hr-ft²-°F),
- P_s = Partial pressure of steam, and
- P_t = Total pressure of containment atmosphere.

Once the heat transfer coefficient h is calculated, the heat transfer rate Q into a heat sink (steel or concrete) with area A is calculated by

$$Q = h A (T_{sat} - T_{wall,0}) \quad (2-66)$$

where T_{sat} is the saturation temperature corresponding to the partial pressure of steam and $T_{wall,0}$ is the surface temperature of the heat sink. When a heat sink is painted, the total heat transfer coefficient is adjusted to include the resistance of the paint. A user-input parameter FUCHIDA is

provided as a multiplier to the Uchida heat transfer coefficient for peak liner temperature quantification and sensitivity studies.

The condensation rate is calculated as

$$W_{cd} = Q / (h_{st} - h_{cd}) \quad (2-67)$$

and the energy removed from gas space becomes

$$Q_g = h A (T_{sat} - T_{wall,0}) + W_{cd} h_{cd} \quad (2-68)$$

where h_{st} is the specific enthalpy of saturated steam at the partial pressure of steam and h_{cd} is an average enthalpy of the condensate.

2.1.3.2.3 Revaporization

When the gas is super-heated, the convective heat transfer from the gas region to the condensate film could raise the temperature of the condensate to saturation temperature and evaporate some of the liquid film back to the gas space. This fraction of evaporation is modeled through a user-input parameter FEVAP. The BVPS atmospheric containment assessment uses a value of 0.08 for EVAP. Based on the FEVAP, the evaporation fraction FREVAP(i) for the i-th containment node is calculated based on the nodal gas temperature $T_g(i)$ and the saturation temperature based on the steam partial pressure $T_{sat}(P_{st}(i))$:

$$FREVAP(i) = FEVAP \text{ if } T_g(i) > T_{sat}(P_{st}(i)) + 3^\circ\text{C} \quad (2-69)$$

$$FREVAP(i) = FEVAP (T_g(i) - T_{sat}(P_{st}(i)) - 1) / 2$$

$$\text{if } T_{sat}(P_{st}(i)) + 3^\circ\text{C} > T_g(i) > T_{sat}(P_{st}(i)) + 1^\circ\text{C} \quad (2-70)$$

$$FREVAP(i) = 0 \text{ if } T_g(i) < T_{sat}(P_{st}(i)) + 1^\circ\text{C} \quad (2-71)$$

When the evaporation fraction FREVAP(i) is greater than 0, the condensation rate is adjusted as

$$W_{cd} = (1 - FREVAP(i)) Q / (h_{st} - h_{cd}) \quad (2-72)$$

where h_{cd} is the average enthalpy of the condensate.

2.1.4 Heat Removal by Active Systems

2.1.4.1 Containment Spray

Heat and mass transfer to spray droplets is quantified in subroutine SPRAY. The important input quantities for the spray model are the flow rate W_o , the water temperature T_o , the initial droplet diameter d_o , and the nozzle height z_o above the liquid pool surface. The important gas phase input quantities are the pressure P , the gas temperature T_g , and the partial pressure of water vapor

P_{ps} . Subroutine SPRAY computes the mass and energy flow rates in the droplets striking the water surface and the mass and energy flow rates transferred to the gas phase by evaporation, condensation, and convective heat transfer. It also calculates the rate at which the containment volume is swept by the spray for use in calculating aerosol removal rates.

SPRAY assumes the droplets enter at an effective height z_o , at terminal velocity and drift downward until either they strike the water pool surface ($z = 0$) or they evaporate ($m = 0$). Typically, the droplets enter at a cold temperature below the dew point, $T_{sat}(P_{ps})$, of water vapor in the gas. Moisture in the gas condenses on the droplets, which are heated by convective heat transfer as well as by latent heat. The droplets rise in temperature past the dew point and begin to evaporate. They asymptotically reach a wet bulb temperature where the convective heat transfer to the droplet is just balanced by evaporative cooling. The evaporating droplet continues to drift downward until it is entirely evaporated ($m = 0$) or it has reached the water pool surface in the containment node.

2.1.4.1.1 Condensation and Evaporation

A droplet of mass m increases (or decreases) in mass by condensation (or evaporation) according to diffusion theory (Ref. 11)

$$\frac{d_o m}{dt} = K_g A [P_{ps} - P_{sat}(T_d)] \quad (2-73)$$

with initial condition m_o given by the initial droplet diameter (d_o). In equation (2-73), the droplet surface area A is given by,

$$A = 4\pi r^2 \quad (2-74)$$

where, in turn, the droplet radius r is given in terms of the droplet mass by,

$$r = \left(\frac{3m}{4\pi\rho} \right)^{1/3} \quad (2-75)$$

The mass transfer coefficient K_g is given by,

$$K_g = \frac{M_w D_{dif} P}{T_g R P_{am}} \cdot \frac{Sh}{d} \quad (2-76)$$

In equation (2-76), M_w is the molecular weight of water vapor, D_{dif} is the diffusivity of water vapor in the gas, T_g is the absolute gas temperature, R is the gas constant, and P_{am} is the log mean non-condensable gas pressure at the condensing surface and in the free gas phase. In terms of P_{ps} and $P_{sat}(T_d)$, P_{am} is defined as

$$P_{\text{am}} = \frac{\left| (P - P_{\text{ps}}) - (P - P_{\text{sat}}(T_d)) \right|}{\ln \left| \frac{P - P_{\text{ps}}}{P - P_{\text{sat}}(T_d)} \right|} \quad (2-77)$$

The Sherwood number (Sh) in equation (2-76) can be interpreted as giving the thickness δ of the diffusion layer of non-condensable gases surrounding the droplet, $\delta = d / \text{Sh}$. Subroutine SPRAY determines the Sherwood number from a correlation (Ref. 16),

$$\text{Sh} = 2.0 + 0.6 \text{Re}^{1/2} \text{Sc}^{1/3} \quad (2-78)$$

where the Schmidt number is

$$\text{Sc} = \frac{\mu_g}{\rho_g D_{\text{dif}}} \quad (2-79)$$

The Reynolds number appearing in equation (2-78) is for a spherical droplet in a gas,

$$\text{Re} = \frac{\rho_g U_{\text{term}} d}{\mu_g} \quad (2-80)$$

where the droplet velocity is given by the terminal velocity,

$$U_{\text{term}} = \left[\frac{4 g d (\rho - \rho_g)}{3 \rho_g C_D} \right]^{1/2} \quad (2-81)$$

Equation (2-81) is obtained by balancing the buoyancy force with the drag force. A one millimeter diameter droplet of water in air has a drift velocity of 5 m/sec and a Reynolds number of 340 if we assumed a drag coefficient of $C_D = 0.44$ suitable for large Reynolds numbers.

2.1.4.1.2 Heat Transfer

Heat is transferred to the droplet by convection and by the latent heat during condensation,

$$m c_p \frac{dT_d}{dt} = h A (T_g - T_d) + K_g A h_{fg} [P_s - P_{\text{sat}}(T_d)] \quad (2-82)$$

with initial condition T_0 , the spray temperature. In equation (2-82), the heat transfer coefficient h is given in terms of the Nusselt number by definition

$$h = \frac{k_g \text{Nu}}{d} \quad (2-83)$$

and the Nusselt number is given by the correlation (Ref. 16),

$$\text{Nu} = 2.0 + 0.6 \text{Re}^{1/2} \text{Pr}^{1/3} \quad (2-84)$$

where the gas phase Prandtl number is,

$$\text{Pr} = \frac{\mu_g c_{pg}}{k_g} \quad (2-85)$$

Equation (2-82) assumes the entire droplet is at one temperature, T. This is a good approximation for small diameter droplets because the characteristic time for conduction

$$\tau = \frac{0.3\rho_w c_{pw}}{k_w} \left(\frac{d}{2}\right)^2 \quad (2-86)$$

is much smaller than the drift time z_o/U . For one-millimeter diameter droplets of water, τ is about 0.5 sec. The drift time for these droplets to fall 20 meters is about 4 seconds.

The Nusselt number correlation, equation (2-84), in terms of the Prandtl number is the same as the Sherwood number correlation equation (2-78), in terms of the Schmidt number. This is a statement of the analogy between heat and mass transfer. A typical value of Nu and Sh for one millimeter diameter droplets is 13, corresponding to a heat transfer coefficient of about $380 \text{ W/m}^2 \text{ K}$.

2.1.4.1.3 Droplet Drift

The water droplets drift downward according to the differential equation

$$\frac{dz}{dt} = -U_{\text{term}} \quad (2-87)$$

with the initial condition z_o , the effective height of the spray nozzles above the water surface. The downward velocity is taken to be the terminal drift velocity.

2.1.4.2 Engineered Safeguard Features

Subroutine GENESF is a generalized Pressurized Water Reactor (PWR) engineered safeguards model. It allows flexibility in specifying pump operation and alignment. The model features user-control of seven completely independent pump systems: charging pumps, high pressure injection (HPI), low pressure injection (LPI) (two trains), and three containment spray systems. Each pump system can have its own water source and discharge location(s), thus allowing users to model the exact pump lineups at their plants. Additionally, heat exchangers can be placed downstream of any pump and several options exist to model net positive suction head (NPSH) enhancement flows for any pump. Finally, several sets of pump characteristics can be defined for each pump system to simulate pump performance under normal or degraded conditions as

well as variations in pump performance due to pump lineup changes. The details of these models are provided in the MAAP4 User's Manual (Ref. 35).

2.1.4.3 Heat Exchanger Performance

Subroutine HTEXCH is a model for a shell and tube heat exchanger used for the emergency core cooling systems (ECCS) and other systems in MAAP-DBA. MAAP-DBA has other models to assess containment fan cooler performance. However, since the BVPS containment systems do not include safety-related fan coolers, these models are not discussed in this document. Specifically, this model calculates the exit temperatures from the shell and tube sides based on the inlet temperatures, flow rates, and the heat exchanger geometry. Two kinds of shell and tube heat exchangers are considered by the model:

1. Counter-flow straight tube, with a single pass in the shell and the tube, and
2. U-tube with a single shell pass and two (2) tube passes.

The exit temperatures from the shell and the tube are calculated from the heat exchanger effectiveness which is a function of the number of transfer units (NTU) and the operating conditions of the heat exchanger. This subroutine may be used by either specifying the number of transfer units as input or providing the necessary details of the heat exchanger geometry such that the number of transfer units can be calculated by the model.

The heat exchanger is modeled by assuming that the service or component cooling water flows in the shell side at a constant inlet temperature T_{si} and flow rate W_s . Hotter circulated emergency cooling water flows inside the tube with a given inlet temperature T_{ti} and flow rate W_t . These tube-side operating conditions are time-dependent, and therefore, a quasi-steady model is used to determine the exit temperatures assuming a short response time for the heat exchanger relative to the global time step.

The effectiveness of the heat exchanger, ϵ , is defined as (Ref. 8):

$$\epsilon = \frac{\text{actual heat transfer rate}}{\text{maximum possible heat transfer rate}}$$

The maximum possible heat transfer rate is that obtained by the fluid stream that has the minimum specific heat \times flow rate product (minimum fluid) undergoing the maximum temperature difference. This maximum temperature difference is the difference between the hot and the cold stream temperatures. Therefore, if the minimum fluid is in the tube side, the effectiveness is:

$$\epsilon = \frac{C_t (T_{ti} - T_{to})}{C_t (T_{ti} - T_{si})} = \frac{C_s (T_{so} - T_{si})}{C_t (T_{ti} - T_{si})} \quad (2-88)$$

where $C_t = W_t c_t$ is the heat capacity rate of the tube-side (minimum) fluid and $C_s = W_s c_s$ is the heat capacity rate of the shell-side fluid. Equation (2-88) can be rearranged to yield the tube-side and shell-side exit temperatures

$$T_{to} = T_{ti} - \varepsilon (T_{ti} - T_{si}) \quad (2-89)$$

and

$$T_{so} = T_{si} + \varepsilon \frac{C_t}{C_s} (T_{ti} - T_{si}) \quad (2-90)$$

Similarly, if the minimum fluid flows in the shell then

$$T_{to} = T_{ti} - \varepsilon \frac{C_s}{C_t} (T_{ti} - T_{si}) \quad (2-91)$$

and

$$T_{so} = T_{si} + \varepsilon (T_{ti} - T_{si}) \quad (2-92)$$

The effectiveness of the heat exchanger is a function of the ratio of the heat capacity rates and the number of transfer units NTU. This number is defined as

$$NTU = \frac{U A}{C_{min}} \quad (2-93)$$

where U is the overall heat transfer coefficient, A is the heat transfer area, and C_{min} is the heat capacity rate of the minimum fluid.

As given in (Ref. 8), the effectiveness of a counter-flow straight tube heat exchanger is

$$\varepsilon = \frac{1 - \exp[-NTU(1-C)]}{1 - C \exp[-NTU(1-C)]} \quad C \neq 1 \quad (2-94)$$

and

$$\varepsilon = \frac{NTU}{1 + NTU} \quad C = 1 \quad (2-95)$$

where

$$C = \frac{C_{min}}{C_{max}} \quad (2-96)$$

The effectiveness of a U-tube heat exchanger is (Ref. 8)

$$\varepsilon = 2 \left\{ 1 + C + (1 + C^2)^{1/2} \frac{1 + \exp \left[-NTU (1 + C^2)^{1/2} \right]}{1 - \exp \left[-NTU (1 + C^2)^{1/2} \right]} \right\}^{-1} \quad (2-97)$$

Equations (2-89) through (2-97) are used to evaluate the exit temperatures in terms of the inlet temperatures, flow rates, and the number of transfer units. It is currently assumed that this number, if supplied, remains constant for all flow rates and inlet temperatures.

If the number of heat transfer units is not specified by the user, it is calculated as follows.

2.1.4.3.1 The Number of Transfer Units

The number of the transfer units, as defined in equation (2-93), is calculated from the overall heat transfer coefficient which is evaluated as the reciprocal of the sum of the individual heat resistances between the bulks of the two fluids

$$U = \frac{1}{\frac{1}{h_t} + \frac{x_t}{k_t} + \frac{d_i}{h_s d_o} + R_f} \quad (2-98)$$

where h_t is the heat transfer coefficient inside the tube, x_t and k_t are the tube wall thickness and thermal conductivity, d_i and d_o are the tube inner and outer diameters, and R_f is the total fouling resistance as specified by the user.

The convective heat transfer coefficient inside the tube is calculated by the Dittus-Boelter correlation (Ref. 8) as

$$h_t = 0.023 \frac{k}{d_i} \left(\frac{4 W_t}{\pi n_t d_i \mu} \right)^{0.8} \left(\frac{c \mu}{k} \right)^{0.4} \quad (2-99)$$

where k , μ , and c are the thermal conductivity, viscosity, and specific heat, and n_t is the number of tubes. To avoid an iterative solution all the physical properties are taken at the inlet temperature.

The convective heat transfer coefficient in the shell side is calculated from the Colburn - j factor correlation (Ref. 13) assuming no leakage area between the tubes and the baffle

$$h_s = j_k j_b c \frac{W_s}{A_s} \left(\frac{k}{c \mu} \right)^{2/3} \quad (2-100)$$

where j_k is the ideal tube bank factor, j_b is the baffle configuration correction factor, and A_s is the shell-side cross sectional flow area between baffle at the centerline. The length of the shell pass

between baffles is $L / (n_b + 1)$, where L is the length of the heat exchanger and n_b is the number of baffles. Thus, the shell flow area is (Ref. 15)

$$A_s = \frac{L}{n_b + 1} \left[2x_g + \frac{d_b - d_o}{s} (s - d_o) \right] \quad (2-101)$$

where x_g is the shell-to-bundle gap, d_b is the effective bundle diameter, d_o is the tube outer diameter, and s is the tube pitch. The effective bundle diameter is calculated by assuming a triangular pitch in the bundle

$$d_b = \sqrt{\frac{4}{\pi} n_t J \frac{s^2 \cos 30^\circ}{2}} \quad (2-102)$$

where J is the number of tube passes (1 for straight tube and 2 for a U-tube).

The ideal tube bank j_k factor in equation (2-100) depends on the shell-side Reynolds number which is defined as (Ref. 15)

$$Re_s = \frac{d_o W_s}{\mu A_s} \quad (2-103)$$

By a fit to the curves presented in (Ref. 15) (Figure 10-19), this factor is calculated as:

$$j_k = \begin{cases} Re_s^{-0.65} & Re_s < 10^2 \\ 0.27 Re_s^{-0.37} & 10^2 < Re_s < 10^5 \end{cases} \quad (2-104)$$

The baffle correction factor, j_b in equation (2-100), is also calculated by a fit to (Ref. 15) curves (Figures 10-16 and 10-20) as

$$j_b = 1.5 - 1.95 \frac{b}{d_s} \quad (2-105)$$

where b is the baffle cut and d_s is the shell inner diameter.

The overall heat transfer coefficient calculated by equation (2-98) is based on the area of the inner tubes. Thus, the number of transfer units is

$$NTU = \frac{U}{C_{min}} J n_t \pi d_i L \quad (2-106)$$

2.2 SINGLE NODE CONTAINMENT MODEL

The design basis containment response calculations were implemented consistent with the intent of the Standard Review Plan. The containment peak pressure and temperature responses for

large LOCA and main steamline breaks use the Tagami and Uchida heat transfer correlations to conservatively quantify the participation of the passive heat sinks. The implementation of these heat transfer correlations leads to the use of a single node containment model. Thus, the total containment volume and passive containment heat sinks are incorporated in a single node containment model that is applied for quantifying the peak pressure, peak gas temperature, and maximum containment liner temperature for the spectrum of main steamline break and large LOCA breaks. The containment liner temperature response is biased by using a multiplier of four (consistent with NUREG-0588) on the Tagami and Uchida heat transfer coefficients per the BVPS-1 and -2 current licensing basis. The characterization of the mass and energy release histories for these design basis accidents were supplied externally through the application of the Westinghouse-approved methodologies.

The containment spray system impact varies by the accident sequence type. For the short-term large LOCA peak pressure and temperature responses, the time interval to the peak values is short and no containment spray system operation occurs prior to the peak condition. For the main steamline breaks, the peak conditions occur in the order of several hundred seconds following the postulated break. Thus, the quench spray system will be activated and delivering spray to the containment atmosphere for a part of the main steamline break sequence. A spray water droplet size of 1000 microns is modeled for heat and mass transfer. No credit is taken for the recirculation sprays in determining the long-term temperature response for main steamline break calculations. For the main steamline breaks, the Uchida heat transfer correlation is used to quantify the response of the passive containment heat sinks. The model used for the single node representation uses an 8% value (consistent with NUREG-0588 and NRC approved GOTHIC version 6.0a) for the percent of condensate that is revaporized into the gas space while it is experiencing superheated conditions.

The model will credit the impact of airborne water droplets originating in the blowdown jet following LOCA accidents. During and following the blowdown transients, airborne water acts as a heat sink for steam to minimize or eliminate superheat as well as to condense some of the steam mass. With the large surface-to-volume ratio, and high water density and specific heat compared to steam, a relatively small droplet water mass is sufficient to eliminate steam superheat from the containment atmosphere. During the blowdown the fraction of available liquid airborne is specified to be 10% of the non-flashed liquid blowdown. This is discussed further in benchmark Section 2.4.3 and the MAAP-DBA code using Tagami heat transfer correlation demonstrates a low sensitivity using this value. See Figure 2-4. A droplet size for the airborne liquid mass of 100 microns is assigned. Following the end of the blowdown, the fraction of available liquid airborne is specified to be 0%. Following blowdown, the remaining airborne water droplets decay due to deposition and possibly spray operation. Table 2-1 summarizes other containment analysis submittals that have used a similar single node modeling approach and credited an airborne water fraction for large design basis LOCA sequences. This helps establish a licensing precedence for the single node model and its application.

2.3 MULTIPLE NODE CONTAINMENT MODEL

The assessment of some of the long-term containment response attributes is conducted with a multiple node containment model. Specifically, the large break LOCA NPSH, the small break LOCA NPSH, and the small break LOCA sump water temperature attributes implement a

multiple node model (see Figure 2-5). The sump water level history is a key input in quantifying these specific attributes. Thus, the relative rate of delivery and removal of water inventory from the containment sump and lower compartment influence the NPSH and sump temperature histories. The hold-up of water from the break or spray injection sources in other regions of the containment directly influences the sump water level and temperature histories. Additionally, the distribution of containment sprays as they are collected on the operating deck floor can also influence these attributes. Thus, a multiple node containment configuration that identifies the elevations and sizes of junctions connecting the various containment regions is implemented for these evaluations. Additionally, the results for the water distribution can provide insights regarding other containment issues, such as the transport paths for debris generated during these energetic blowdowns.

The methods used to quantify the available NPSH for BVPS-1 and -2 are consistent with the current licensing basis. The BVPS-1 available NPSH method continues to include the overpressure credit, while the BVPS-2 available NPSH assessment does not credit overpressure.

The multiple node model will use natural convection heat transfer models for calculating the energy transfer to the containment heat sinks distributed through these multiple nodes. The natural convection heat transfer models will be biased to minimize the calculated available NPSH. Like the single node model, the airborne fraction of LOCA blowdown will be set to 10% with the droplet size set to 100 microns. Likewise, the spray system behavior will be modeled in the same fashion as for the single node model.

The mass and energy releases from the primary system to containment for the spectrum of small and intermediate size LOCAs will be generated using the MAAP-DBA code. The MAAP-DBA mass and energy release histories are benchmarked with Westinghouse Small Break LOCA ECCS Evaluation Mode (NOTRUMP) results in Section 2.5. The mass and energy releases for the large break LOCA NPSH calculations will be biased to yield the maximum sump water temperature by mixing the streams from the two sides of the guillotine break. The mass and energy release histories for each side of the break are quantified by applying the NRC approved Westinghouse methodologies (Ref. 23).

2.4 BENCHMARKING OF MAAP-DBA MODEL

2.4.1 GOTHIC Comparison

Results from MAAP-DBA and GOTHIC version 6.0a have been compared for the peak containment pressure and temperatures associated with the limiting cases for both BVPS-1 and -2 containments. For the large LOCA comparisons, Case 8L was used for BVPS-1 and Case 3L was used for BVPS-2. For the main steamline break comparisons of peak pressure and peak gas temperature, Case 15M was used for BVPS-1 and Case 16M was used for BVPS-2. The large LOCA Cases 8L and 3L are for double-ended hot leg breaks from 100% reactor power. The Case 15M is a 1.4 ft² double-ended rupture from 30% power assuming the failure of the main steamline check valve. The Case 16M is a 1.069 ft² double-end rupture from 0% power with a main steam isolation valve failure and a failure of one train of quench spray. Table 2-2 summarizes the key input conditions used for this comparison.

The results of the comparison are provided in Table 2-3. Figures 2-6 through 2-13 provide a graphical comparison of the LOCA and MSLB pressure and temperature transients from each computer code. The use of a single node containment model and the Tagami and Uchida heat transfer correlations yield good agreement for the peak containment response attributes.

2.4.2 Separate Effects Experiments

Several separate effects experiments (listed in Table 2-4) were used for benchmarking models used in the MAAP-DBA containment code. In particular, the condensation heat transfer models and the containment spray heat removal models were benchmarked against available separate effects tests. The condensation experiments used included the University of Wisconsin flat plate experiments (Ref. 9), the PHEBUS FPT0 experiments (Ref. 31), and the Dehbi experiments (Ref. 4 and 5). The containment spray heat removal benchmarks included the JAERI spray heat transfer tests (Ref. 10) and the Kulic spray heat transfer experiments (Ref. 13).

The Wisconsin flat plate steam condensation experiments in the presence of noncondensable gases (air) reported by Huhtiniemi, et al., (Ref. 9) are compared with the MAAP-DBA natural and forced convection heat transfer correlations by calculating the average heat transfer coefficients. MAAP-DBA calculated heat transfer coefficients for six different test conditions were compared with the data. The six tests included air-to-steam mass ratio of 0.29 to 3.5, bulk-to-surface temperature differentials of 20 to 60 degrees C, and flow velocities of 1 to 3 m/s.

In MAAP-DBA's validation, it was assumed that turbulence exists in the experiment due to mixing at the test section inlet such that the flat plate turbulent flow friction factor was used to calculate the forced convection heat transfer coefficient.

The comparisons of the MAAP-DBA calculated heat transfer coefficients against the Wisconsin flat plate data are shown in Table 2-5. As shown in the Table 2-5, the MAAP-DBA calculated heat transfer coefficients agree well with the data. At low air-to-steam mass ratios, the MAAP-DBA natural convection model is conservative.

The benchmark of the PHEBUS FPT0 (Ref. 31) test was performed to assess MAAP-DBA's condensation model. A comparison of the calculated containment vessel pressure against the measured pressure from PHEBUS FPT0 test is shown in Figure 2-14. Variations in the pressure history result from changes in the steam injection rate and the variation of the condenser surface temperature. MAAP-DBA over-predicted the peak pressure about 1.2 psi. In general, the calculated pressure transient follows the data very well for the most of the transient. Figure 2-15 shows the comparison between the measured and calculated condensation rates. The shape of the condensation rate transient follows the shape of the total pressure (i.e., the shape of the partial pressure of steam) and the calculated condensation rate agrees with the data. These results show that the natural convection heat and mass transfer model in MAAP-DBA is adequate to calculate the containment response under natural convection conditions.

The steam condensation experiments in the presence of noncondensable gases reported by Dehbi, et al. (Ref. 4 and 5) are compared with the MAAP-DBA natural convection heat transfer correlation by calculating the average heat transfer coefficients. Three system pressures for the

steam-air mixtures were studied with the steam mass fraction varied from very small concentration to values approaching 90% steam.

The correlation and the Dehbi data are compared in Figure 2-16. This figure illustrates the MAAP-DBA model prediction and the measured values (adjusted for curvature effects to represent a flat plate) for the different air mass fractions and pressures investigated in the experiments. As shown in this figure, the MAAP-DBA natural convection model reasonably predicts the measured heat transfer over the range of air mass fractions and containment pressures tested. An experimental uncertainty in the reported values of the "measured" heat transfer coefficients is $\pm 15\%$. The MAAP-DBA predicted heat transfer coefficient all are within this range of experimental uncertainty.

In the JAERI spray experiments (Ref. 10), a large, tall vessel was pressurized with steam and subsequently cooled by an internal spray. The MAAP-DBA spray model was investigated for both single node and multiple vertical node models. In particular, Test PHS-1 was investigated since this provides an evaluation of both the pressurization and depressurization phases. The comparisons for the single node system are given in Figure 2-17 and for the multiple node system in Figure 2-18. As illustrated by these comparisons, the multiple node system provides a better representation of the overall transient. The single and multiple node model results both demonstrate the proper performance of the MAAP-DBA spray model for calculating heat removal and depressurization.

A set of spray droplet heat removal experiments were performed by Kulic (Ref. 13) and used to benchmark the MAAP-DBA spray heat transfer model. Integral experiments were performed with water sprayed into a steam-air mixture contained in a large, closed vessel and the subsequent depressurization was recorded.

The MAAP-DBA calculated vessel depressurization was benchmarked against three Kulic tests, as shown in Figure 2-19. Test 1 illustrates the influence of heat losses from the test vessel when no spray flow was provided and confirms the initial and boundary conditions used for these benchmarks. Test 1A illustrates the influence of a single spray nozzle with a flow rate of 45 imperial gallons per minute (IGPM) at a temperature of 24°C (75°F). Test 1B illustrates the influence of five spray nozzles at a temperature of 24°C. The proper behavior of the MAAP-DBA spray model heat removal calculations is demonstrated by these single and multiple spray nozzle benchmarks.

2.4.3 Integral Effects Containment Experiments

The MAAP-DBA code has been benchmarked against integral effects containment experiments including several that have been used as International Standard Problems (ISPs). The containment design basis attributes of pressure and temperature will be quantified in these benchmarks and compared with the observations from the several integral experiments. Table 2-6 lists the integral effect experiments (IETs) used to benchmark the MAAP-DBA containment response.

These tests were used to demonstrate the prediction of the thermal-hydraulic response of large-scale multiple compartment containments. The comparisons show both the MAAP-DBA single

and multiple node models used for the BVPS-1 and -2 containment analyses are conservative in predicting containment pressures and temperatures. The results from these benchmarks are provided below.

The decommissioned Heiss Dampf Reaktor (HDR) nuclear reactor containment was used to run large-scale design basis (LOCA and MSLB) experiments. Tests HDR-V44 and HDR-T3.15 are International Standard Problems that have been used to benchmark the performance of MAAP-DBA for predicting peak containment pressure and temperature responses. A two node model has been used, such that one node is for inside the HDR containment and the second node is for the annular gap that surrounds it. Consistent with the modeling used for the BVPS-1 and -2 analyses, in these benchmarks the Tagami heat transfer correlation is used and it is assumed that 10% of the non-flashed blowdown water becomes airborne as suspended water.

Comparison of the calculated pressure against the data for HDR-V44 is shown in Figure 2-20. MAAP-DBA over-predicts the peak pressure demonstrating that the MAAP-DBA Tagami heat transfer correlation and 10% airborne water is conservative. In terms of the gas temperature, the one node model provides an average gas temperature of the whole containment which is highly compartmentalized. The gas temperature at the vicinity of the break source is higher than the average gas temperature and the gas temperature at the lower elevation is lower than the average temperature. Figure 2-21 shows comparison of the calculated gas temperature against the measured gas temperature in the upper compartment which accounts about 43% of the total internal containment volume. The Tagami correlation with 1-node model over-predicts the gas temperature in the dome region.

Comparison of the calculated pressure against the data for HDR-T31.5 is shown in Figure 2-22. MAAP-DBA also over-predicts the peak pressure for this test. Figure 2-23 compares the calculated gas temperature against the measured gas temperature in the upper compartment. The MAAP-DBA Tagami correlation and 10% airborne water with 1-node model also over-predicts the gas temperature in the dome region for these tests.

The NUPEC M-7-1 test is an International Standard Problem that has been used to benchmark the performance of MAAP-DBA for predicting design basis containment responses with natural convection and the heat and mass transfer analog (HMTA) correlation. This test had two phases. The first phase was a "pre-heat" that simply discharged steam into the 1/4-scale containment for three hours. This phase simulates a small LOCA sequence and is applicable to design basis events. The second phase initiated helium and steam injection plus containment spray operation to simulate a severe accident that experienced core damage and hydrogen generation. This phase of the M-7-1 test is not applicable to design basis events. The results for the pre-heat phase are reported here and used to benchmark MAAP-DBA's containment responses.

The predicted containment pressure and temperature responses for this multiple node MAAP-DBA model are compared to the test data in Figure 2-24. A multiple node model is used for small break LOCA in the BVPS analysis. The code underestimates the heat transfer from the gases to the passive heat sinks. The containment pressure and gas temperatures calculated by MAAP-DBA are shown to over-predict containment pressure when compared to the test data.

The decommissioned Carolina Virginia Tubular Reactor (CVTR) containment was used to run large-scale tests that simulated MSLBs with and without containment spray actuation (Ref. 38). The CVTR tests #3, #4, and #5 have been used to benchmark MAAP-DBA for predicting design basis containment responses with the Uchida heat transfer coefficient correlation. Test #3 did not include containment spray actuation, while the other two tests included sprays at two different flow rates. Measurements from the CVTR tests provide a set of large-scale containment response information to evaluate the dominant heat transfer processes associated with condensation, global natural circulation flows, counter-current natural circulation flows, and the influence of containment sprays.

Figure 2-25 illustrates the measured and calculated containment pressure and gas temperature histories for Test 3 using a single node MAAP-DBA model and demonstrates that a one node model overstates the containment pressurization, by more than 20%. Test 3 was selected because there are no sprays used, which is a more challenging test. (Once the containment sprays are turned on, the atmosphere is more homogenized and a single node gives an improved representation.) Furthermore, the calculation also overstates the containment temperature increase early in time and later in time, underestimates the temperature above the operating deck (TC-28) and overestimates the temperature below the operating deck (TC-5).

Figure 2-26 illustrates the measured and calculated containment pressure and gas temperature histories for Test 4 using a single node MAAP-DBA model. Once again, the single node model overstates the containment pressurization by more than 20%. Test 4 used containment sprays, and once they turned on, the containment pressurization and heat up were mitigated. A lower peak pressure was obtained than for Test 3, but significant margin is demonstrated. Likewise, the Test 4 calculation demonstrates a similar containment gas temperature response that overstates the temperature increase early in time and later in time, underestimates the temperature above the operating deck and overestimates it below the operating deck. Test 5 also included containment spray operation and its MAAP-DBA calculation demonstrated similar behavior as observed for Test 4.

The Battelle Frankfurt Model Containment (BFMC) Test D-16 is an International Standard Problem that has been used to benchmark the performance of MAAP-DBA for predicting design basis containment response with the Tagami heat transfer coefficient correlation and to provide a technical basis for the value used for the airborne water fraction of the non-flashed portion of LOCA blowdowns.

For containment integrity evaluations, the most important evaluations are the pressure histories in the compartment receiving the break discharge (break compartment) and the pressure imposed on the outer containment wall. Figure 2-27 compares the measured D-16 pressure in the break compartment with those calculated using MAAP-DBA. The corresponding calculated values for the pressure imposed on the model containment outer wall is given in Figure 2-28. The MAAP-DBA containment model calculated containment pressure conservatively bounds the measured values.

The calculated and measured temperatures in the break compartment are illustrated in Figure 2-29. Since a single node model is used for this benchmark, it yields the average containment temperature, and thus, under-predicts the temperature observed in the break node.

Figure 2-30 compares the predicted and measured temperatures in a node that is remote from the break node. Here the predicted peak gas temperature bounds the measured value.

All saturated water blowdown experiments, such as the HDR tests and those performed at the Battelle-Frankfurt model containment show the aerosolization and airborne transport of water. Airborne water is manifested in at least two ways, the first is that the measured gas temperatures remain close to the saturation value corresponding to the measured containment pressure and the second is that airborne water is directly observed in the HDR tests. In the Battelle-Frankfurt Tests D15 and D16, substantial amounts of water are transported to compartments away from the break room. At the end of test the measured water masses in these rooms are well in excess of those that could be accumulated in these locations due solely to condensation.

Of particular interest are the two Battelle Frankfurt tests (D-15 and D-16) that are identified as Containment Analysis Standard Problems CASP1 and CASP2. The former was configured to blowdown from the top of the high pressure vessel whereas the latter experienced a two-phase discharge from the bottom of the vessel with about four times the water inventory that was used in D-15. While Test D-16 is more representative of large break LOCA conditions, both tests experienced two-phase blowdown rates. Furthermore, the configuration of the containment rooms differed between the tests with Test D-15 having the rooms aligned in a chain and the second experiment having two parallel flow paths from the break room to the outer containment compartment. At the completion of the tests, the water inventory collected in the various rooms was measured.

Tables 2-7 and 2-8 list the measured water inventories in each of the rooms, i.e. approximately 956 kg were measured in CASP1 (D15) with 3873 kg being found in CASP2 (D16). Both tables also list the concrete surface areas associated within each containment room and these are used to estimate the condensation that could have occurred in each of the rooms. Tables 2-9 and 2-10 show the estimation of the water phase remaining after flashing and evaporation were complete. These analyses show that 562.1 kg remained as water for CASP1 and 2404 kg in CASP2. Assuming that the steam mass condensed can be partitioned between the rooms in proportion to the fraction of the concrete heat sink surface area in each room, the mass condensed can be estimated and is listed in each table. Subtracting this estimated mass from the measured water mass approximates the water mass transported to these rooms as water. These tables illustrate that substantial water masses are transported to rooms removed from the break room. Summing the water masses transported as liquid outside of the break room and dividing by the total water mass remaining after flashing and evaporation, gives a value of 0.49 for CASP1 and 0.65 for CASP2. (Of these two, the second is by far the more meaningful since the test was conducted under large LOCA like conditions.) Consequently, these experiments undergoing a high pressure two-phase critical discharge clearly have a large fraction of water transported away from the break room. It is also noted that these experiments were performed with an impingement (baffle) plate immediately downstream of the break. These results demonstrate that the assumed airborne water fraction of 10% used in the BVPS-1 and -2 atmospheric containment assessment is a conservatively low value.

As expected, the single node containment models that applied the Tagami and Uchida heat transfer correlations over-predicted the peak containment pressures observed in this set of Integral Effects Experiments. The single node containment models also over-predicted the peak

containment gas temperature, with the possible exception of the local break node temperature for LOCA simulations. For the measurements near the break room, the calculated values either exceed or are in close agreement with the reported values. Since a single node model yields the average containment gas temperature, it may under-predict the gas temperature after the peak occurs or in regions removed from the break location where non-condensables can accumulate for MSLB simulations.

2.5 MASS AND ENERGY RELEASES FOR SMALL BREAK LOCA

For the large break LOCA and main steamline breaks, the MAAP-DBA computer program used externally specified mass and energy release histories generated by NRC approved Westinghouse methodologies (Ref. 23, 24, and 25) to quantify the containment response for several design basis response attributes, i.e., peak pressure, gas temperature, and containment liner temperature.

For the small break loss of coolant accidents, the MAAP-DBA computer code was used to generate the mass and energy release histories to quantify containment pressure as well as additional containment response attributes (ECCS sump water level and temperature and available NPSH for the recirculation spray and low head injection pumps). As discussed below, there is a precedent for using MAAP-DBA to quantify SBLOCA mass and energy releases. The release histories for a spectrum of break sizes in both the hot leg and cold leg regions of the primary systems are calculated. Benchmarks are performed against an alternate computer code that is also used to quantify primary system mass and energy releases for small breaks.

MAAP-DBA predicted mass and energy release histories have been benchmarked against two sets of release histories as generated by the NOTRUMP computer code (Ref. 26) to confirm the acceptability of the MAAP-DBA predictions. In the first benchmark, an existing BVPS NOTRUMP application has been used. The NOTRUMP computer code was used to assess the BVPS reactor core (fuel temperature) response for a spectrum of small to medium break sizes. The mass and energy release histories that were quantified for 2, 3, 4, and 6 inch cold leg breaks by NOTRUMP have been used to benchmark the predicted mass and energy releases from the MAAP-DBA code. The 10CFR50 Appendix K requirements were incorporated in this NOTRUMP analysis. Thus, the decay heat curve based on the ANSI 1971 Decay Heat Standard with a 1.2 multiplier was used. Solely for the purpose of this comparison, the MAAP-DBA benchmark for these four cases also used this decay heat curve.

A second set of NOTRUMP mass and energy release histories were quantified specifically for benchmarking with MAAP-DBA. In this set of release histories both 2 inch diameter cold and hot leg breaks were calculated with NOTRUMP based on the ANSI 1979 Decay Heat Standard with a two standard deviation uncertainty. This is the decay heat curve that will be used in the BVPS-1 and -2 containment response quantification.

The integrated mass and energy release histories for each of these six cases are compared in Figures 2-31a through 2-36b. Good agreement is obtained for this spectrum of break sizes and locations. The trending of the releases is similar for MAAP-DBA and NOTRUMP. There are small instantaneous deviations for a given break size. The divergence in the initial release histories results from the more detailed models in NOTRUMP. However, the release histories tend to converge following the initial release interval and in some cases MAAP-DBA bounds

NOTRUMP. When the MAAP-DBA integral mass release lags the NOTRUMP release, the rate of increase in sump water level may be slightly slower; this is conservative regarding available NPSH calculations. When the MAAP-DBA integral energy release exceeds the NOTRUMP release, the sump water temperature will be higher; this is conservative regarding available NPSH and thermal stress on affected piping. A large spectrum of break sizes (1 inch through 12 inch diameter) are analyzed to conservatively envelope the observed divergences such that the impact of the limited uncertainty in the MAAP-DBA mass and energy releases histories is bounded.

The reactor coolant system (RCS) model used by MAAP-DBA is the same as the MAAP 4.0 RCS model that has been used to calculate mass and energy (M&E) releases to the containment during small break LOCAs and submitted on other licensing dockets. The derivation of the M&E releases for BVPS is consistent with that used in MAAP 4.0 in the 1999 analysis conducted by FAI for D. C. Cook. The mass released from the MAAP RCS model used in the D. C. Cook calculations were validated by comparison to the NOTRUMP code, considering a 2-in. diameter break. The comparison showed that the integrated break flow release to the containment calculated by the MAAP RCS module was about 10% less than the comparable calculation by NOTRUMP. The NRC validated and accepted the D. C. Cook calculations (Ref. 27) by comparisons to an audit calculation.

MAAP-DBA was also benchmarked with NOTRUMP in support of the AP600 project, considering a spectrum of small RCS hot leg break sizes ranging from 0.5-in. to 8.75-in. The results are documented in Reference 22. The benchmarking performed in this report shows good agreement between MAAP-DBA and NOTRUMP mass inventory calculations, except for one sequence that is specific to the AP600 design. The NRC accepted the use of MAAP4 in the AP600 PRA.

2.6 REFERENCES

1. Bergles, A. E. et al., *Two-Phase Flow and Heat Transfer in the Power and Process Industries*, New York: Hemisphere Publishing Corporation, pp. 334-343.
2. Colburn, A. P., and Hougen, O. A., 1934, "Design of Cooler Condensers for Mixtures of Vapours with Non-Condensing Gases." *Ind. Eng. Chem.*, Vol. 26, pp. 1178-1182.
3. Collier, J. G., 1981, *Convective Boiling and Condensation*, 2nd Edition, New York: McGraw-Hill.
4. Dehbi, A. A. et al., 1991a, "The Effects of Noncondensable Gases on Steam Condensation Under Turbulent Natural Convection Conditions," MIT Report MIT-ANP-TR-004.
5. Dehbi, A. A. et al., 1991b, "Condensation Experiments in Steam-Water and Steam-Air-Helium Mixtures Under Turbulent Natural Convection," *AICHE Symposium Series, Heat Transfer*, Volume 87, pp. 19-28.
6. Eckert, E. R. G., and Drake, 1972, "Analysis of Heat and Mass Transfer," McGraw-Hill, pg. 731.

7. Holman, J. P., 1968, Heat Transfer, 2nd Edition, New York: McGraw-Hill.
8. Holman, J. P., 1976, Heat Transfer, Chapter 10, 4th Edition, New York: McGraw-Hill.
9. Huhtiniemi, I. K. et al., 1993, "Condensation in the Presence of Noncondensable Gases," Nuclear Engineering and Design, 141.
10. Kitani, S., 1978, "Containment Spray Experiments for Pressure Suppression," Paper Presented at the 1st International Conference on Liquid Atomization and Spray Systems, Tokyo, Japan, August 27-31, pp. 355-359.
11. Kreith, F., 1958, Principles of Heat Transfer, International Textbook Company.
12. Kreith, F., 1973, "Principles of Heat Transfer," International Textbook Company, pp. 395-398, 419, and 442.
13. Kulic, E., 1976, "An Experimental and Theoretical Study of Simultaneous Heat and Mass Transfer Applied to Steam Dousing," Doctoral Thesis Presented to the Chemical Engineering Department, University of Waterloo, Ontario, Canada.
14. McCabe, W. L., and Smith, J. C., 1976, Unit Operations in Chemical Engineering, 3rd Edition, New York: McGraw-Hill, p. 300.
15. Perry, J. H., Perry, R. H., Chilton, C. H., and Kirkpatrick, S. K., 1984, "Chemical Engineering Handbook," Chapter 10, 6th Edition, New York: McGraw-Hill.
16. Ranz, W., and Marshall, W., 1952, Chem. Engr. Prog., Vol. 48.
17. Rohsenow, W. M., 1956, "Heat Transfer and Temperature Distribution in Laminar Film Condensation," Trans. ASME, Vol. 78, pp. 1645-1648.
18. Rohsenow, W. M., and Hartnett, J. K., 1973, "Handbook of Heat Transfer," McGraw-Hill, pp. 6-14.
19. Rose, P. N., 1961, "Drag Forces in a Hydraulic Model of a Fluidized Bed – Part II," Trans. Inst. Chem. Engrs., Vol. 39, pp. 175-180.
20. Slaughterbeck, D. C., 1970, "Review of Heat Transfer Coefficients for Condensing Steam in a Containment Building Following a Loss-of-Coolant Accident," Idaho Nuclear Corporation, National Reactor Testing Station, Idaho Falls, ID.
21. Uchida, H., Oyama, A., Togo, Y., 1964, "Evaluation of Post Incident Cooling Systems of Light-Water Power Reactors," in Proceedings of the Third International Conference on the Peaceful Uses of Atomic Energy held in Geneva on August 31 – September 9, Vol. 13, New York: United Nations, 1965, (A/CONF.28/P/436) (May 1964) pp 93-104.
22. Westinghouse, 1997, "MAAP4/NOTRUMP Benchmarking to Support the Use of MAAP4 for AP600 Success Criteria Analyses," WCAP-14869, April 1997.

23. WCAP-10325-P-A, (Proprietary), WCAP-10326-A (Nonproprietary), Westinghouse LOCA Mass & Energy Release Model for Containment Design – March 1979 Version, May 1983.
24. Westinghouse, WCAP-8822 (Proprietary) and WCAP-8860 (Nonproprietary), Mass and Energy Releases Following a Steamline Rupture; Sept 1976; incl. Supplements 1 and 2.
25. Westinghouse WCAP-8821-P-A (Proprietary) and WCAP-8859-A (Nonproprietary), TRANFLO Steam Generator Code description, September 1976; approved.
26. Rupprecht, S. D. et al., “Westinghouse Small Break LOCA ECCS Evaluation Model Generic Study with the NOTRUMP Code,” WCAP-11145-P-A (proprietary), October 1986.
27. Safety Evaluation by the Office of Nuclear Reactor Regulation Related to Amendment No. 234 to Facility Operating License No. DPR-58, and Amendment No. 217 to Facility Operating License No. DPR-74; Indiana Michigan Power Company Donald C. Cook Nuclear Plant, Units 1 & 2 Docket Nos. 5~315 & 5~316; Dec. 1999.
28. NRC letter to FENOC, Timothy G. Colburn to L. William Pearce TAC Nos. MB 5303 and MB 5304 Facility Operating License Amendments 257 (U1) and 139 (U2), September 10, 2003.
29. FENOC letter to NRC, L. William Pearce Letter L-03-079 Licensing Amendment Requests 300 and 172, June 6, 2003.
30. FENOC letter to NRC, Mark B. Bezilla letter L-03-038 Licensing Amendment Requests 300 and 172, March 31, 2003.
31. Von der Hardt, P., Jones A. V., Lecomie, C., and Tattegrain, A., 1994, “Nuclear Safety Research: The Phebus FP Severe Accident Experimental Program,” Nuclear Safety, Vol. 35, No. 2, July-December.
32. LOCTIC – A Computer Code to Determine the Pressure and Temperature Response of a Dry Containment to a Loss-of-Coolant Accident. Stone and Webster Engineering Corporation, Proprietary Report, September 1971).
33. MAAP-DBA – A computer Code use in Design Basis Analysis of Large Dry Containments as Submitted for BVPS Specific Application via FENOC Letter to NRC L-03-188.
34. NAI 8907-09 Rev. 4, “GOTHIC Containment Analysis Package Qualification Report,” Version 6.0, T. George et. al., December 1997.
35. EPRI, 1994, MAAP4: Modular Accident Analysis Program, User’s Manual, EPRI Report prepared by Fauske & Associates, Inc. (FAI), May.

36. NuReg-0800; Standard Review Plan for the Review of Safety Analysis Reports for Nuclear Power Plants – LWR Edition; Rev. 2, 07/1981.
37. Nureg-0588, Interim Staff Position on Environmental Qualification of Safety-Related Electrical Equipment, Revision 1; 07/01/1981.
38. Schmitt, R. C. et al., 1970, Simulated Design Basis Accident Test of the Carolinas Virginia Tube Reactor Containment – Final Report, Idaho Nuclear Corporation Report IN-FY03; USAEC Reactor Technology, TID-4500.

Application	Type	HTC	Airborne Water Fraction	Nodes	NRC Approval Status	Notes
W-312	Large Dry	Tagami/Uchida	100%	Single	Approved	GOTHIC Benchmarked to COPATTA
C-E	Large Dry	Tagami/Uchida	100%	Single	Approved	Benchmarked to CONTEMPT
W-412	Ice Condenser	Uchida	100%	Multi	Approved	Benchmarked to LOTIC
C-E	Large Dry	Tagami/Uchida	100%	Single	In Review	Benchmarked to CONTRANS
W-212	Large Dry	Tagami/Uchida	100%	Single	Approved	GOTHIC Benchmarked to COCO
AP600	Passive	Natural Conv.	5-100%	Multi	Approved	WGOTHIC

	GOTHIC Version 6.0a	MAAP-DBA
Nodes	Single	Single
Entrainment (Pools and Films)	Yes	No
Forced Convection	No	No
LOCA Airborne Water Droplet Fraction	10%	10%
Spray Droplet Diameter	1000 microns	1000 microns
LOCA Airborne Water Droplet Diameter	100 microns	100 microns
Re-vaporization	8%	8%
Initial Containment Pressure	14.2 psia	14.2 psia
LOCA: Heat Transfer (Short Term)	Tagami	Tagami
MSLB: Heat Transfer	Uchida with 8% revaporization	Uchida with 8% revaporization

Unit	Sequence	Results Comparison							
		LOCA				MSLB			
		Pressure (psia)		Gas Temperature (°F)		Pressure (psia)		Gas Temperature (°F)	
		MAAP-DBA	GOTHIC	MAAP-DBA	GOTHIC	MAAP-DBA	GOTHIC	MAAP-DBA	GOTHIC
1	Case 8L	57.57	57.41	267.4	266.3	—	—	—	—
2	Case 3L	58.99	58.29	269.7	268.2	—	—	—	—
1	Case 15M	—	—	—	—	56.8	57.8	342.6	341.3
2	Case 16M	—	—	—	—	51.5	52.9	327.1	329.8

Benchmark	Test	Application
1.	U. of Wisconsin Flat Plate	Condensation heat transfer (HMTA with forced convection used for multiple node models)
2.	PHEBUS FPT0	Condensation with non-condensables present
3.	Dehbi	Condensation with non-condensables present
4.	JAERI PHS-1	Spray heat removal
5.	Spray Droplet Heat Transfer (Kulic)	Spray droplet heat removal

Case #	T _{mix} , °C	T _w , °C	m _{air} / m _{steam}	V, m/s	h _{exp} *	h _{exp (max, min)} *	MAAP-DBA **
1	70	30	3.58	1	111.1	(122.2, 99.99)	113.9
2	70	30	3.58	3	213.9	(235.3, 192.5)	235.4
3	80	30	1.808	1	163.9	(180.3, 147.5)	165.2
4	80	30	1.808	3	305.6	(336.2, 275.0)	310
5	90	30	0.706	1	255.5	(281.1, 229.95)	256.3
6	95	45	0.31	1	546.	(600.6, 491.4)	402.9

* Heat transfer coefficient in w/m²/K.

** MAAP-DBA uses the maximum of the natural and forced convection values. At 1 m/s, the code is using the natural convection value.

Benchmark	Test	Application
1.	HDR-V44	Large loss of coolant accident (LOCA)
2.	HDR-T31.5	Large LOCA
3.	NUPEC M-7-1	Small LOCA
4.	CVTR #3	Main steamline break without containment spray
5.	CVTR #4, #5	Main steamline break with spray actuation
6.	BFMC D-16	Large LOCA

* Benchmark numbers 1, 2, 3, and 6 are International Standard Problems.

Table 2-7 CASP1 Fraction of the Blowdown Mass Collected as Water in the Node

Node Number*	Volume (m ³)	t = 600 s			t = 3840 s			Concrete Surface Area (m ²)	Fraction of Concrete Area
		Measured Water Level (cm)	Water Mass Measured (kg)	Fraction of the Total Water Mass	Measured Water Level (cm)	Water Mass Measured (kg)	Fraction of the Total Water Mass		
R6	41.26	8.0	315	0.432	9.1	400	0.418	90.1	0.088
R8	40.53	5.2	175	0.240	6.1	245	0.256	91.7	0.090
R7	46.4	0	21	0.029	0	21	0.022	76.6	0.075
R4	12.2	6.3	75	0.102	7.1	85	0.089	38.6	0.033
R5	41.05	0	18	0.025	0.2	20	0.021	76.1	0.075
R9 (R9 Annulus)	450 (300)	1.0	125 100	0.171 0.137	1.8	185 150	0.194 0.157	416.6	0.409
(R9 Center)	(150)	2.0	25	0.034	2.5	35	0.037	229.2	0.225
TOTAL	625		729	0.999		956	1.000	1018.9	1.000

*Listed in the order of the flow path from the break discharge room to the outer room.

Node Number*	Volume (m ³)	t = 840 s			t = 6480 s			Concrete Surface Area (m ²)	Fraction of Concrete Area
		Measured Water Level (cm)	Water Mass Measured (kg)	Fraction of the Total Water Mass	Measured Water Level (cm)	Water Mass Measured (kg)	Fraction of the Total Water Mass		
R4 (discharges into R5 and R7)	13.66	76.2	903	0.261	76.7	909	0.235	38.6	0.038
R5 (discharges into R9)	41.05	9.7	630	0.182	11.1	721	0.186	76.1	0.075
R7 (discharges into R8)	40.40	3.2	102	0.029	6.5	207	0.053	76.6	0.075
R8 (discharges into R9)	40.53	9.0	477	0.138	9.5	504	0.130	91.7	0.090
R9 (discharges into R6) (R9 Annulus) (R9 Center)	465.0	6.3 5.3	967	0.280	7.2	1107	0.286	416.6	0.409
	300		258	0.075	5.7	277	0.072	229.2	0.225
R6	41.26	4.7	122	0.035	5.7	148	0.038	90.1	0.086
TOTAL	641.9		3459	1.000		3873	1.000	1018.9	1.000

*Listed in the two parallel flow paths from the break discharge room (R4) to the outer room (R9) and eventually to R6.

Table 2-9 Interpretation of Water Mass Distribution for CASP1

Initial water temperature = 286°C

Initial water enthalpy: $h_o = 1.267 \times 10^6 \text{ J/kg}$

Two-phase mixture quality after blowdown: $x = \frac{h_o - h_f}{h_{fg}}$

Assume saturation at 50°C: $x = 0.444$

Steam in the atmosphere at 50°C ~ 55 kg

Total mass considered at 3840 secs = 1011 kg

Mass formed as steam due to blowdown = $0.444 \times 1011 \text{ kg} = 448.9 \text{ kg}$

Mass remaining as water after blowdown = $1011 - 448.9 = 562.1 \text{ kg}$

Average airborne density of water is uniformly distributed throughout

$$\bar{\rho}_o = \frac{562.1 \text{ kg}}{625 \text{ m}^3} = 0.90 \text{ kg/m}^3$$

Estimated mass of water collected as condensed steam

$$m_{w,con} = \text{Fraction of Concrete Surface Area} \times 448.9 \text{ kg}$$

Compartment (Room)	Water Mass Collected (kg)	Estimated Mass Condensed (kg)	Estimated Mass Transport as Water (kg)	$\bar{\rho} = \frac{m_v}{\text{Room Vol}}$ Airborne Density of Water	Fraction of Total Airborne $\bar{\rho}/\rho_o$
R6 (break room)	400	39.5	360.5		
R8	245	40.4	204.6	5.0	> 1.00
R7	21	33.7	0	0	
R7 and R8*	266	74.1	204.6	2.4	> 1.00
R4	85	14.8	70.2	5.8	> 1.00
R5	20	33.7	0	0	
R9 Annulus	150	183.6	0	0	
R9 Center	35	101.0	0	0	
Total Water Mass Outside of R6	956		274.8		

*Provided for reference.

Fraction of the depressurized water jet measured outside of the break discharge room

$$= \frac{274.8}{562.1} = 0.49$$

Table 2-10 Interpretation of Water Mass Distribution for CASP2

Initial water temperature = 260°C

Initial water enthalpy: $h_o = 1.134 \times 10^6 \text{ J/kg}$

Two-phase mixture quality after blowdown: $x = \frac{h_o - h_f}{h_{fg}}$

Assumed saturated conditions at 50°C: $x = 0.388$

Steam in atmosphere at 50°C ~ 55 kg

Total mass considered at 6480 secs = 3873 + 55 = 3928 kg

Mass formed as steam due to blowdown = $0.388 \times 3928 = 1524 \text{ kg}$

Mass remaining as water after blowdown = $3928 - 1524 = 2404 \text{ kg}$

Average airborne density if water is uniformly distributed throughout the model containment

$$\bar{\rho}_o = 2404/641.9 = 3.75 \text{ kg/m}^3$$

Estimated mass of water collected as condensed steam for a given compartment (room)

$$m_{w,con} = \text{Fraction of Concrete Surface Area} \times 1524 \text{ kg}$$

Compartment (Room)	Water Mass Collected (kg)	Estimated Mass Condensed (kg)	Estimated Mass Transport as Water (kg)	$\bar{\rho} = \frac{m_v}{\text{Room Vol}}$ Airborne Density of Water	Fraction of Total Airborne $\frac{\bar{\rho}}{\rho_o}$
R4 (break room)	909	57.9	851.1		
R5	721	114.3	606.7	14.8	1.00
R7	207	114.3	92.7	2.30	0.61
R8	504	137.2	366.8	9.05	1.00
R9 Annulus	1107	623.3	483.7	1.61	0.43
R9 Center	277	342.9	0	0	0
R6	148	134.1	13.9	0.03	0.008
Total Water Mass Outside of R4			1563.8		

Fraction of the depressurized water jet measured outside of the break discharge room

$$= \frac{1563.8}{2404} = 0.65$$

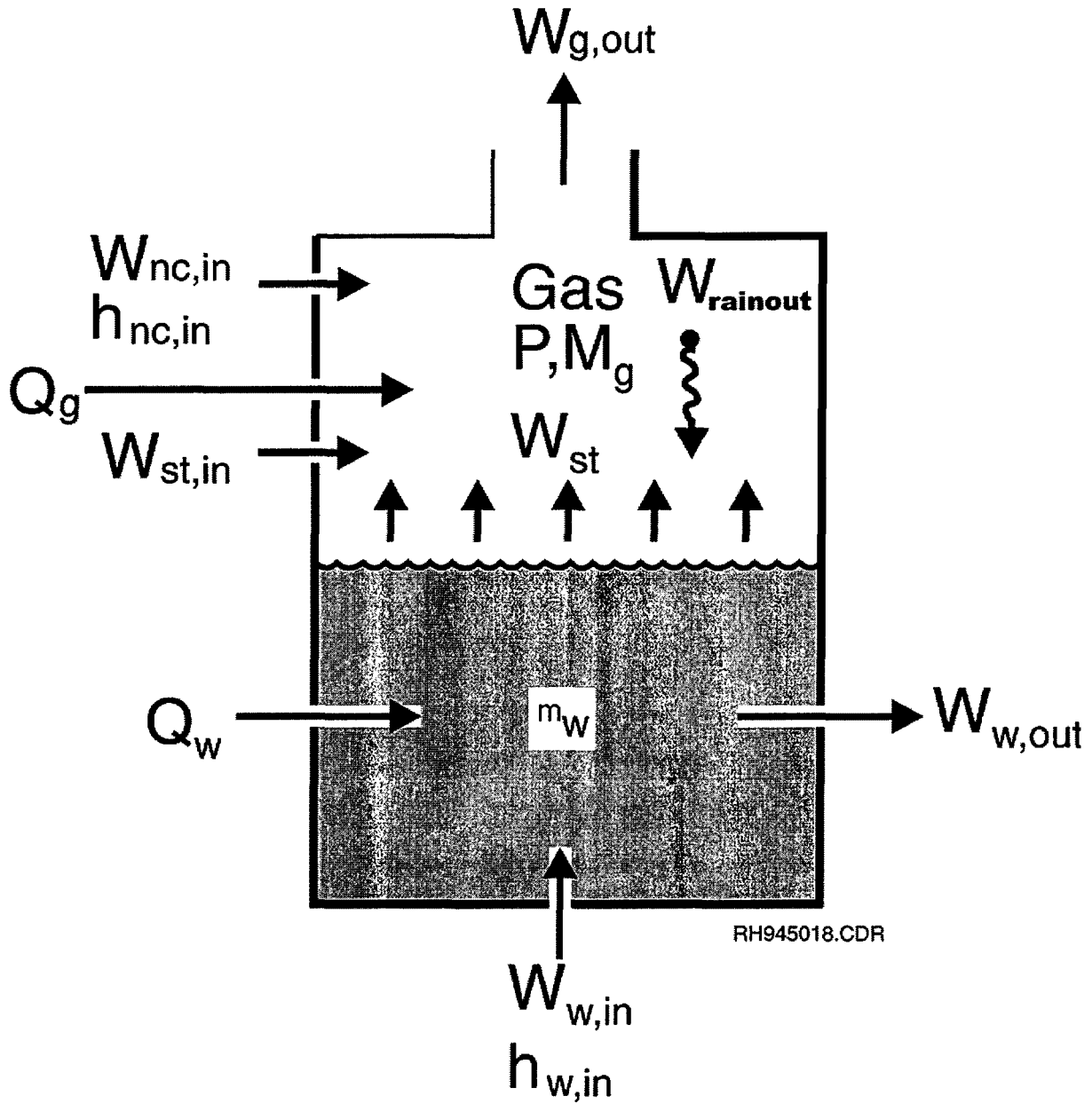


Figure 2-1 Description in Terms for Estimating the Rates of Flashing and Rainout

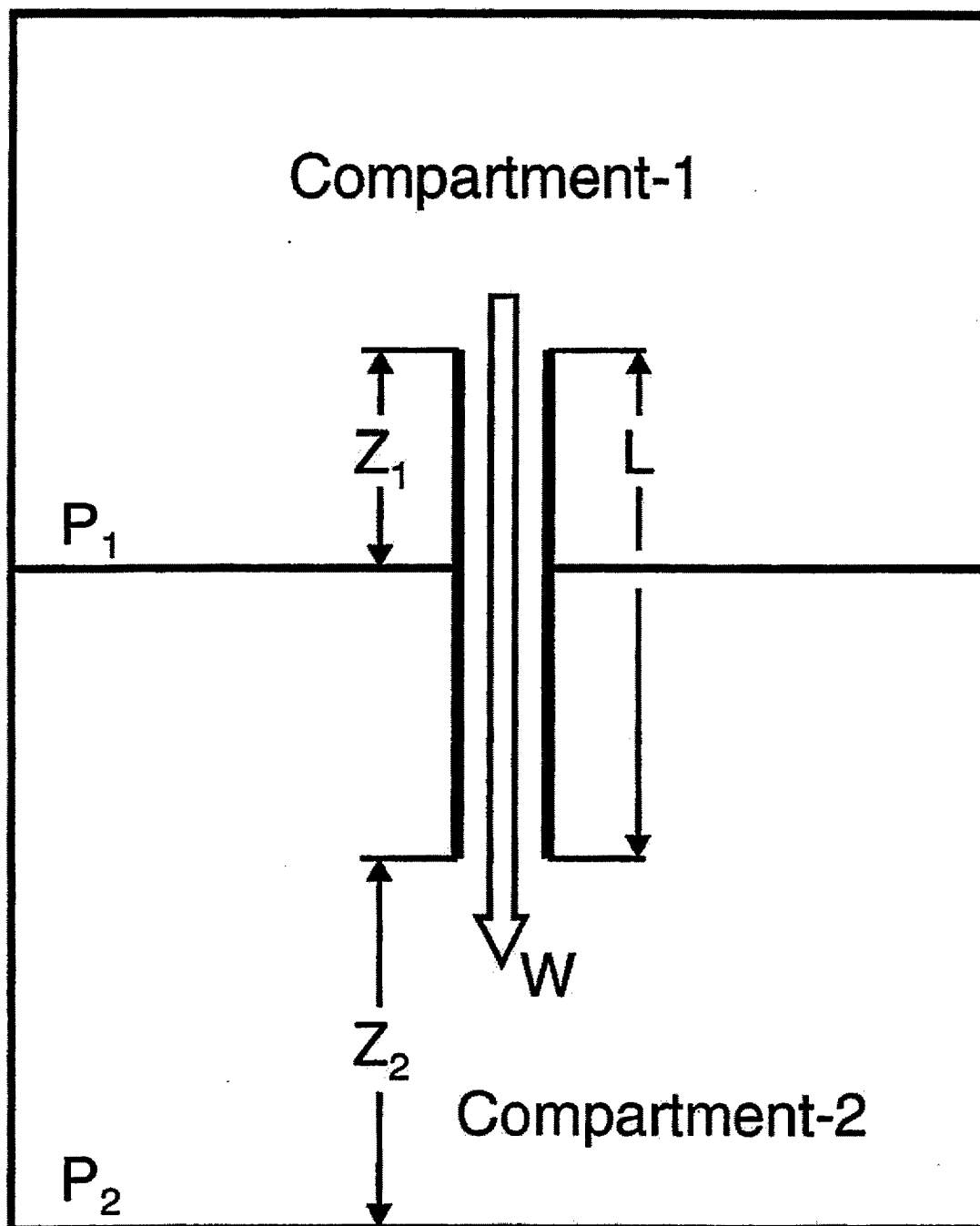


Figure 2-2 Two Compartments Connected by a Junction

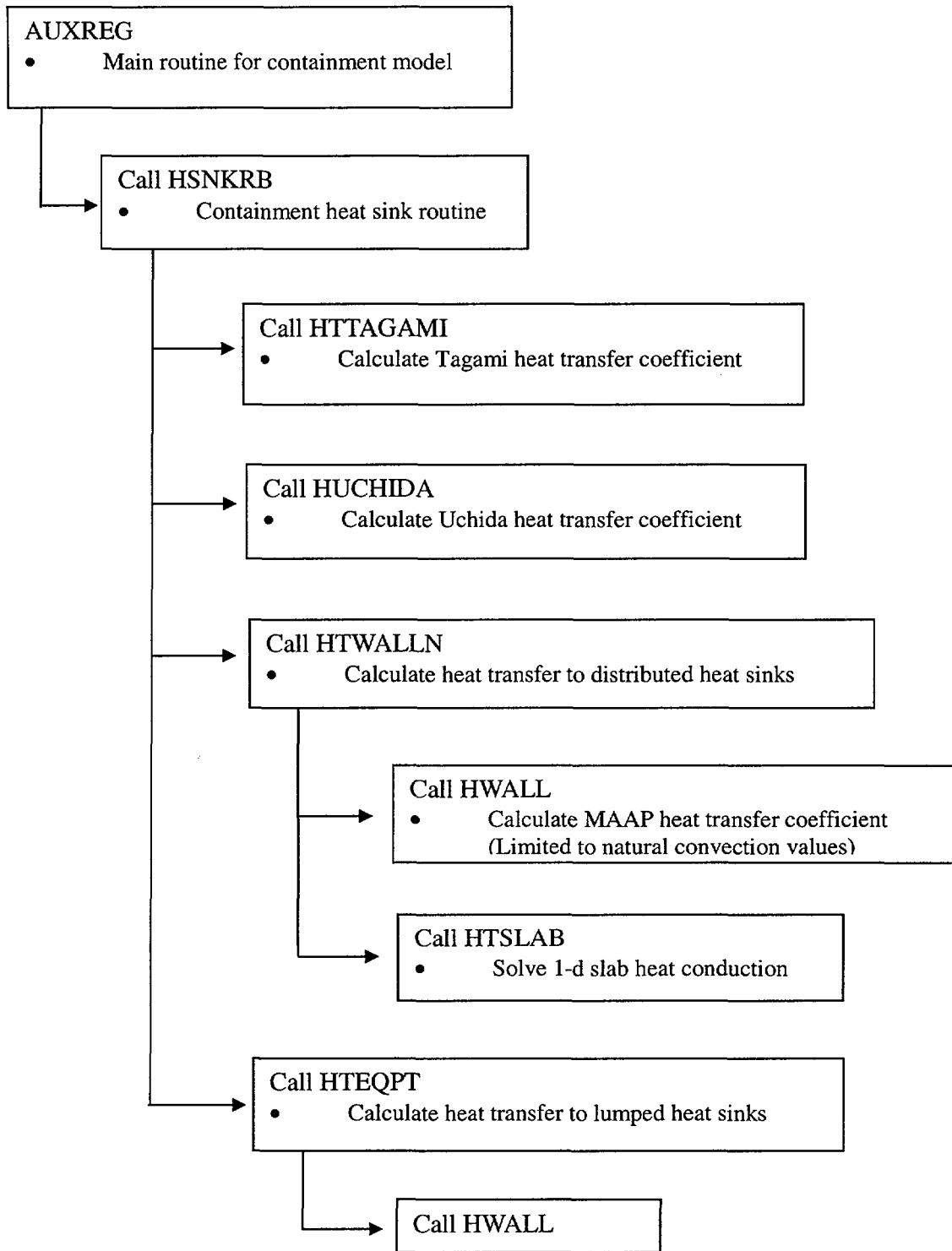


Figure 2-3 Structure of Heat Transfer Subroutines

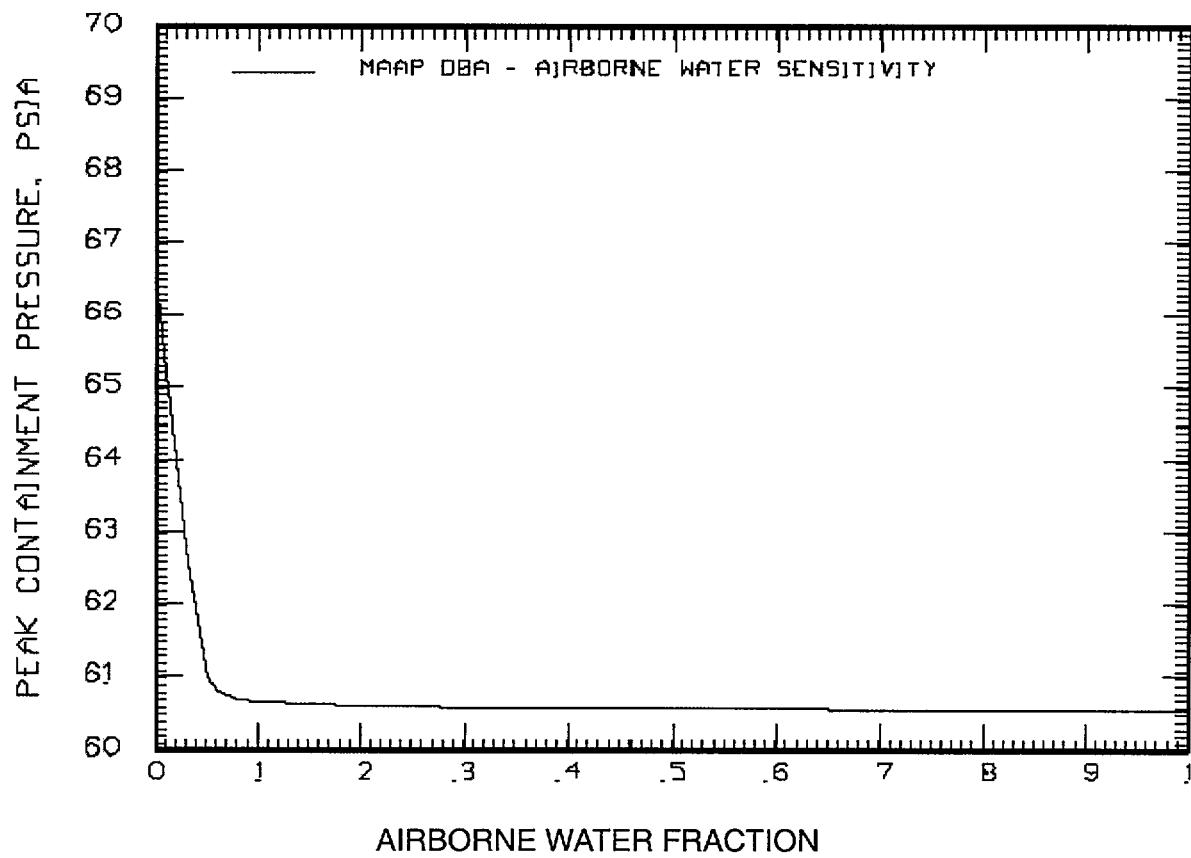
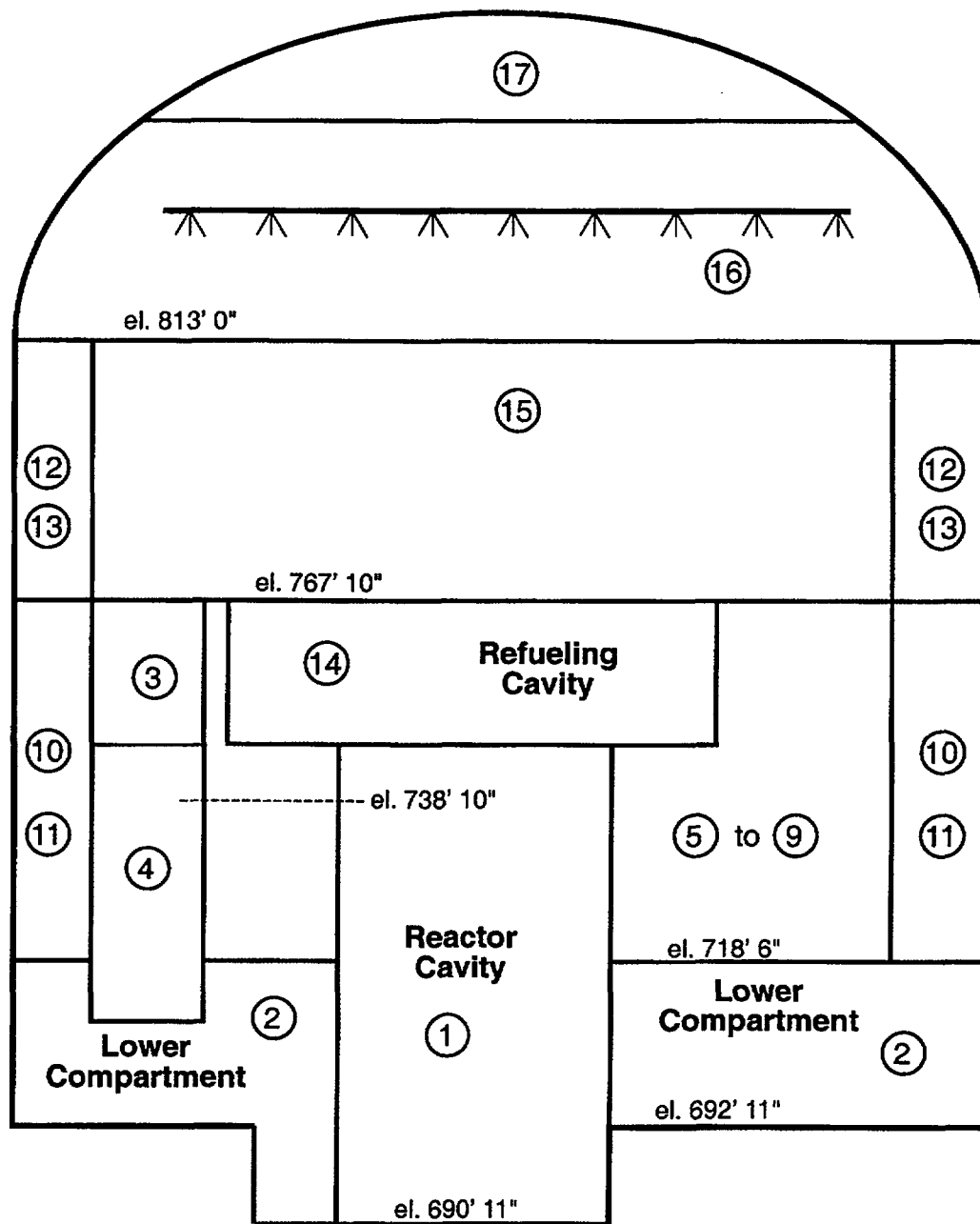


Figure 2-4 Sensitivity of Containment Pressure to LOCA Airborne Water Fraction



Note: The refueling cavity node (14) is divided into two nodes (14 and 18) for the BVPS-1 model.

Figure 2-5 MAAP-DBA Containment Nodalization for BVPS-1 and BVPS-2

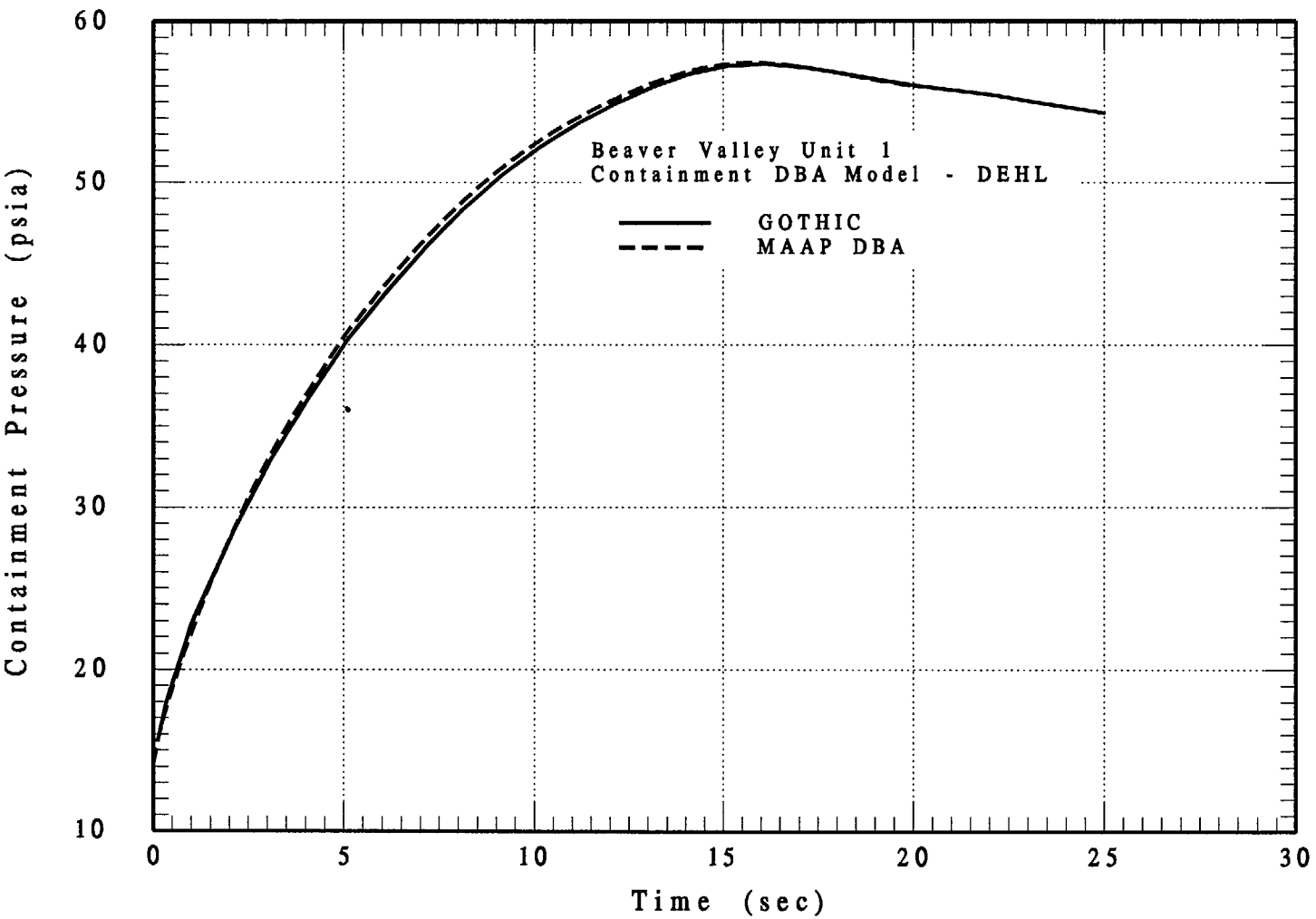


Figure 2-6 Comparison of Pressure Results from MAAP-DBA and GOTHIC for Large LOCA (BVPS Case 8L)

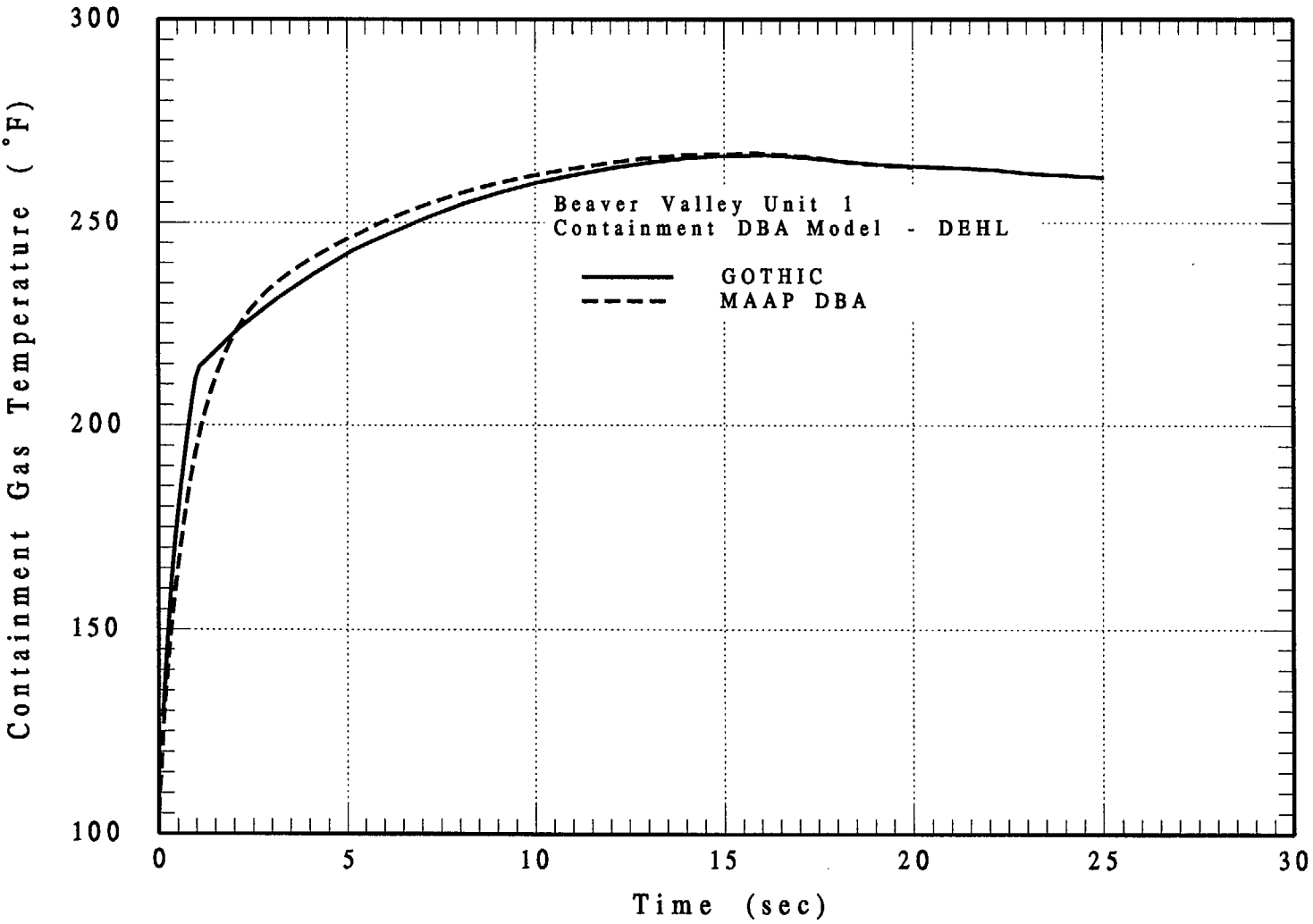


Figure 2-7 Comparison of Gas Temperature Results from MAAP-DBA and GOthic for Large LOCA (BVPS Case 8L)

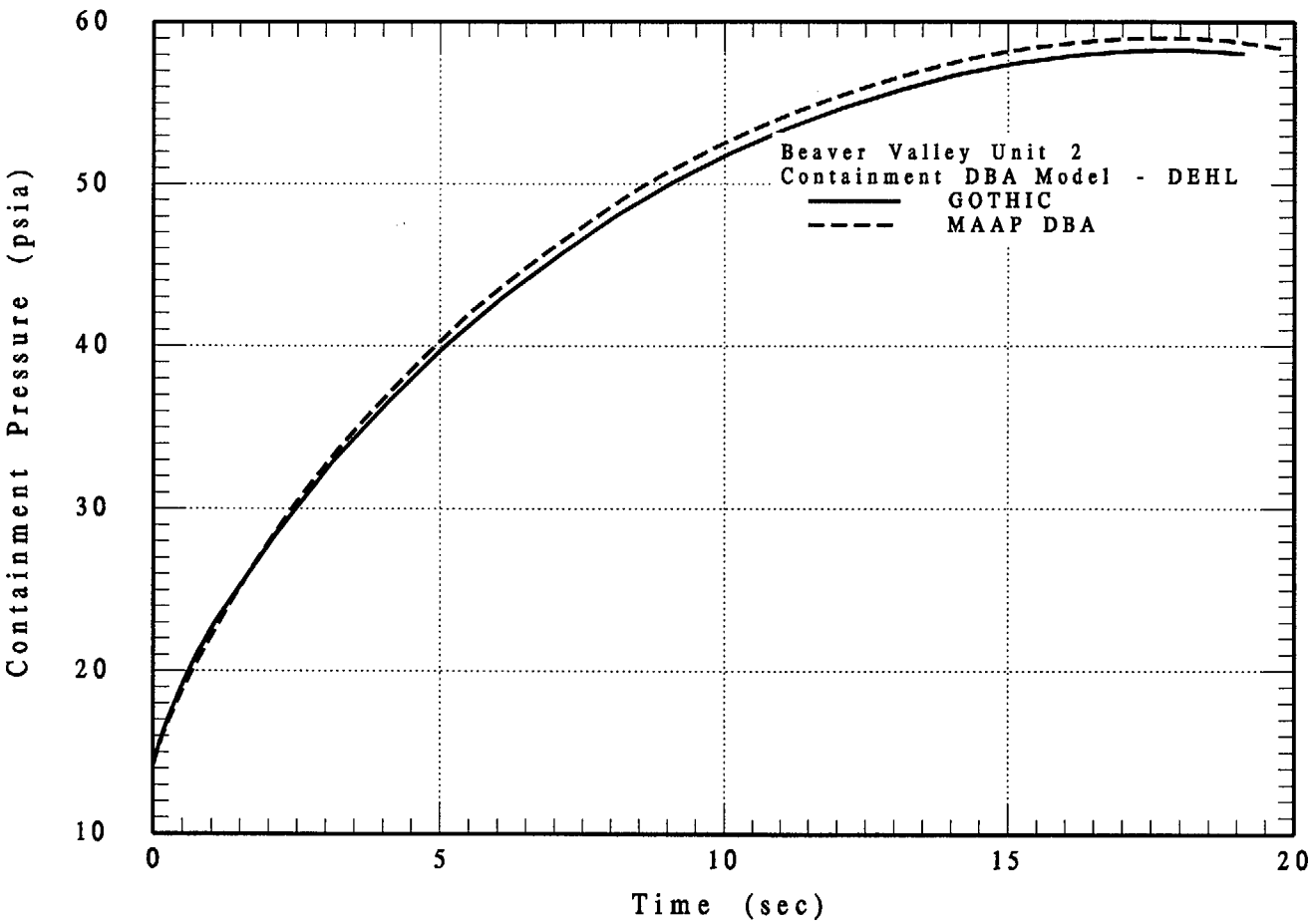


Figure 2-8 Comparison of Pressure Results from MAAP-DBA and GOTHIC for Large LOCA (BVPS Case3L)

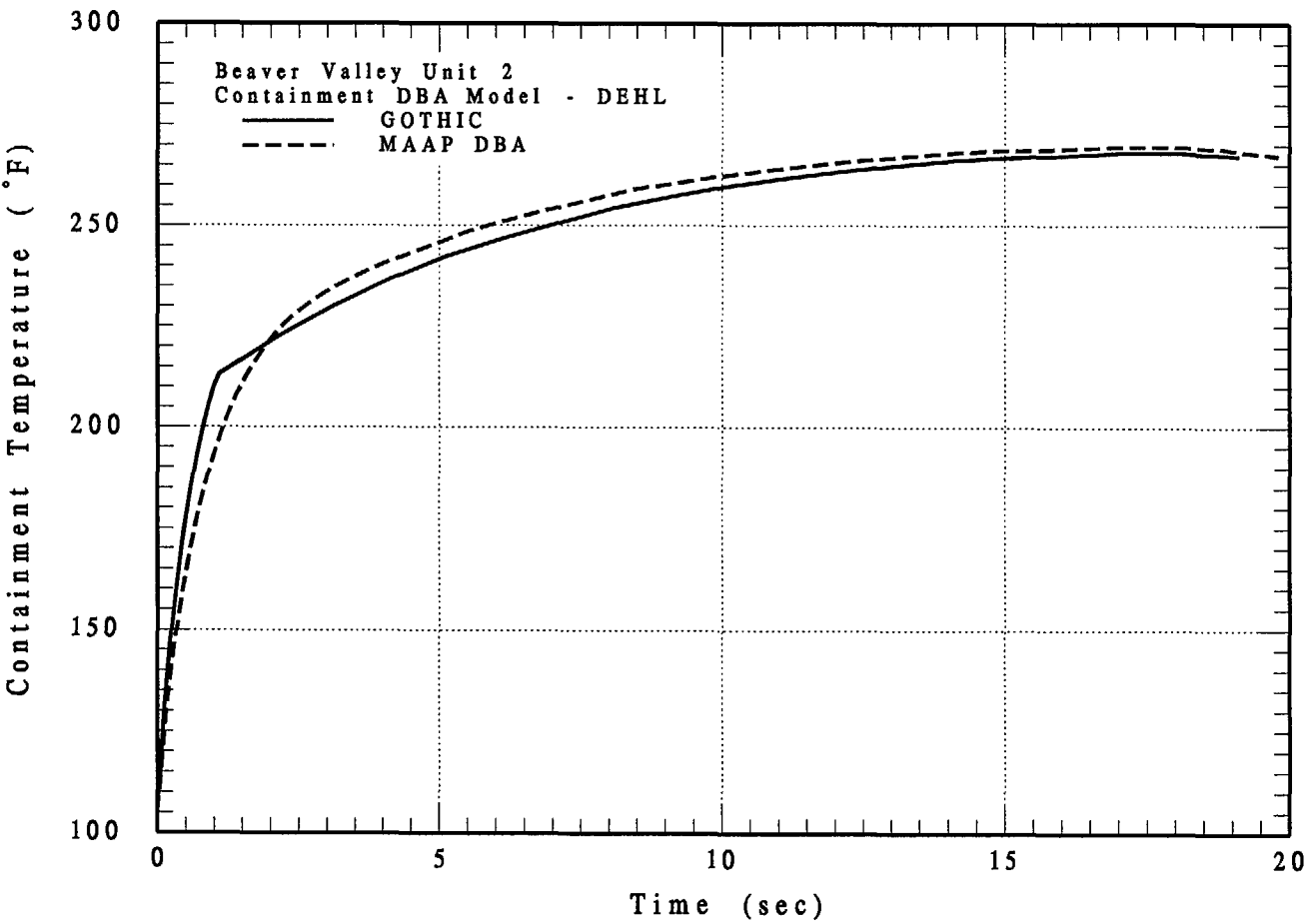


Figure 2-9 Comparison of Temperature Results from MAAP-DBA and GOTHIC for Large LOCA (BVPS Case3L)

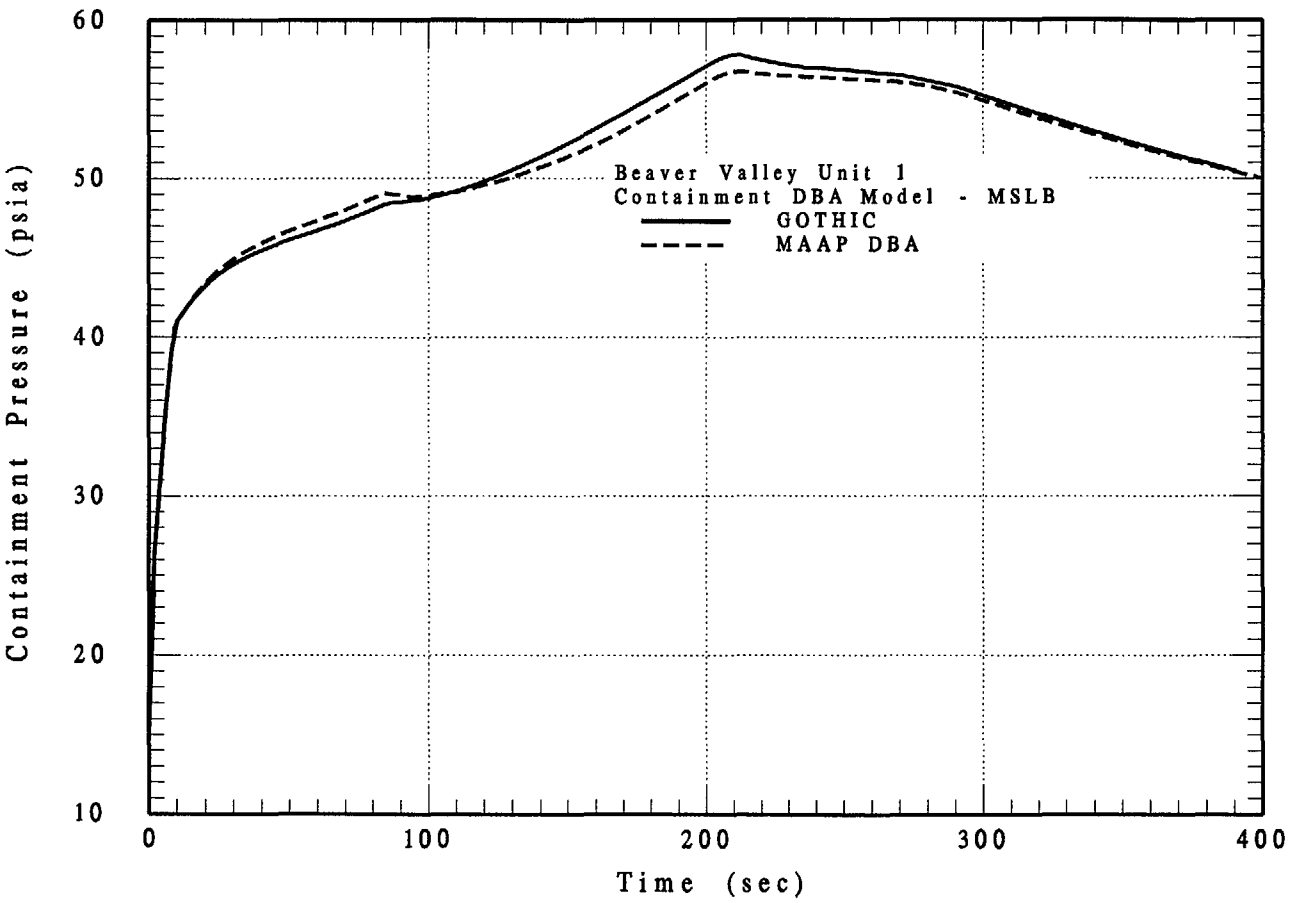


Figure 2-10 Comparison of Pressure Results from MAAP-DBA and GOTHIC for MSLB (BVPS Case15M)

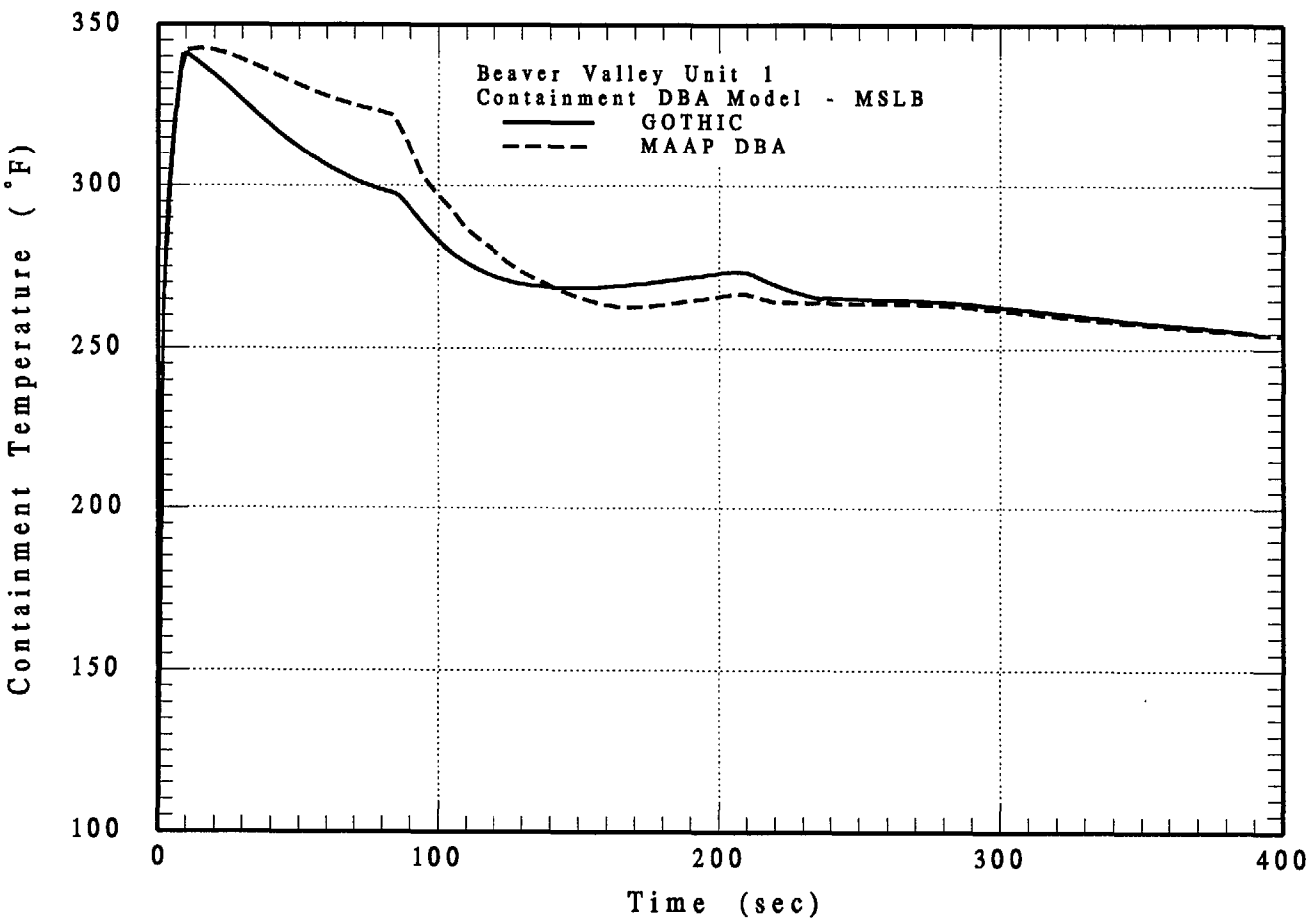


Figure 2-11 Comparison of Temperature Results from MAAP-DBA and GOHTIC for MSLB (BVPS Case15M)

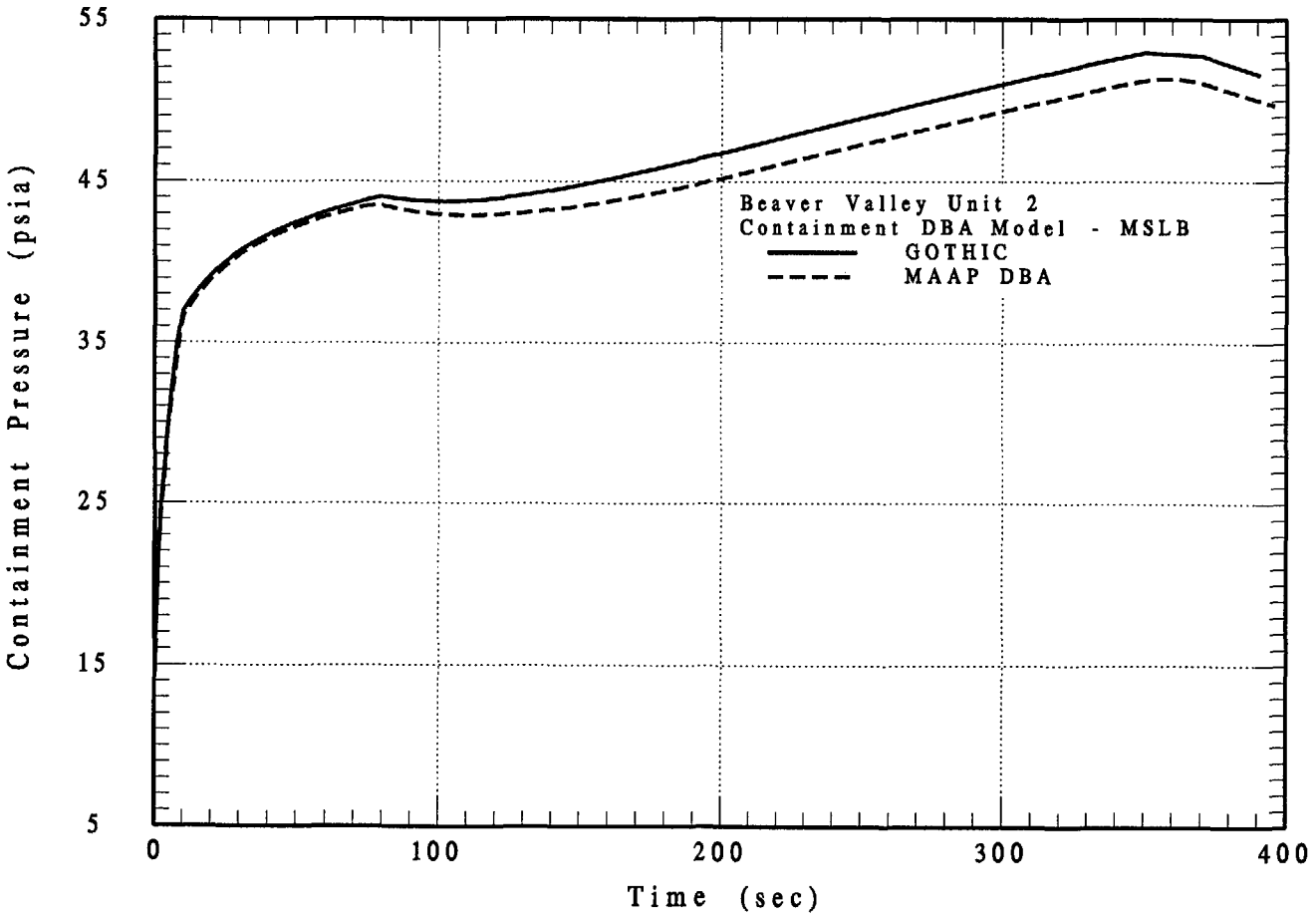


Figure 2-12 Comparison of Pressure Results from MAAP-DBA and GOTHIC for MSLB (BVPS Case 16M)

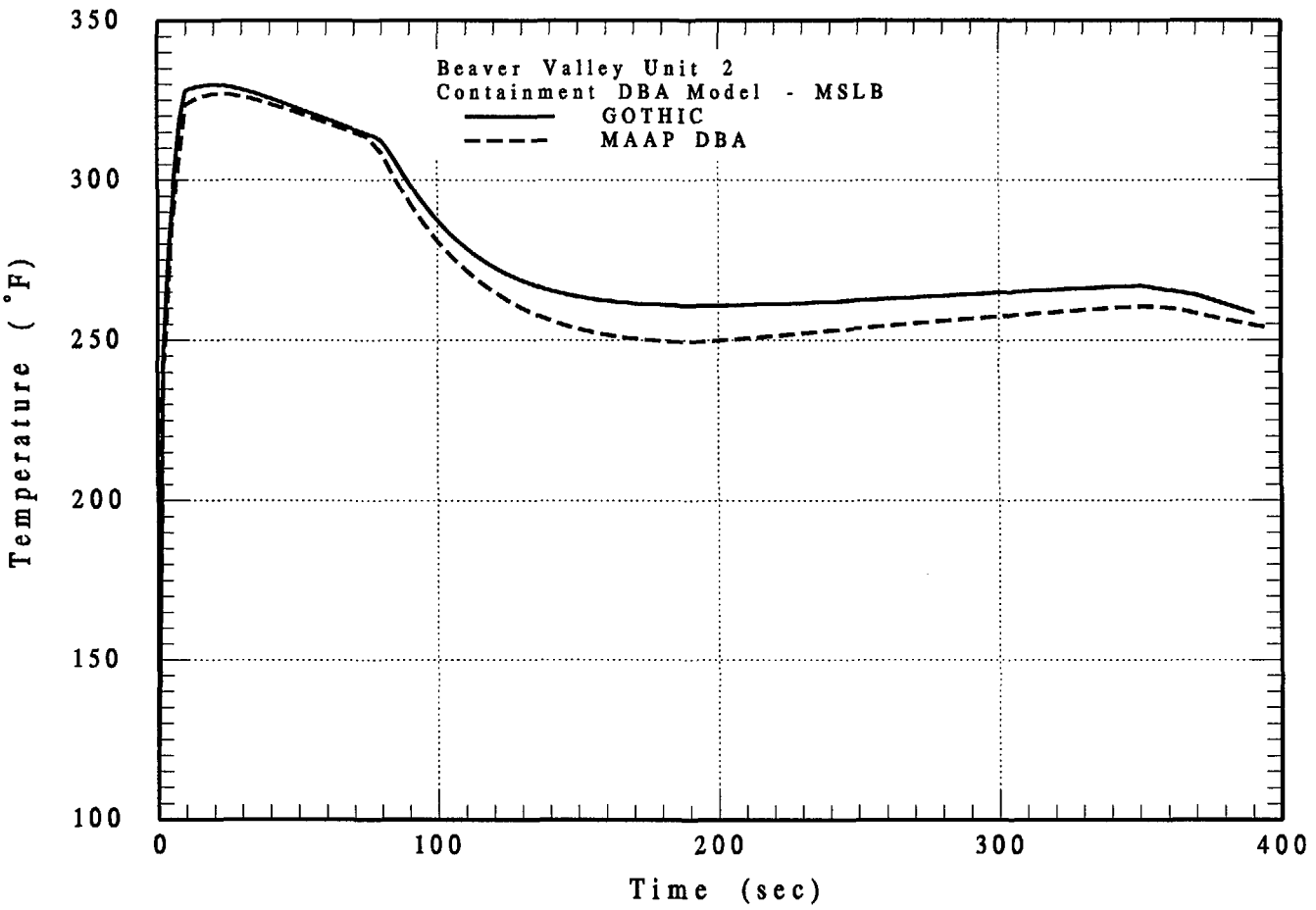


Figure 2-13 Comparison of Temperature Results from MAAP-DBA and GOTHIC for MSLB (BVPS Case 16M)

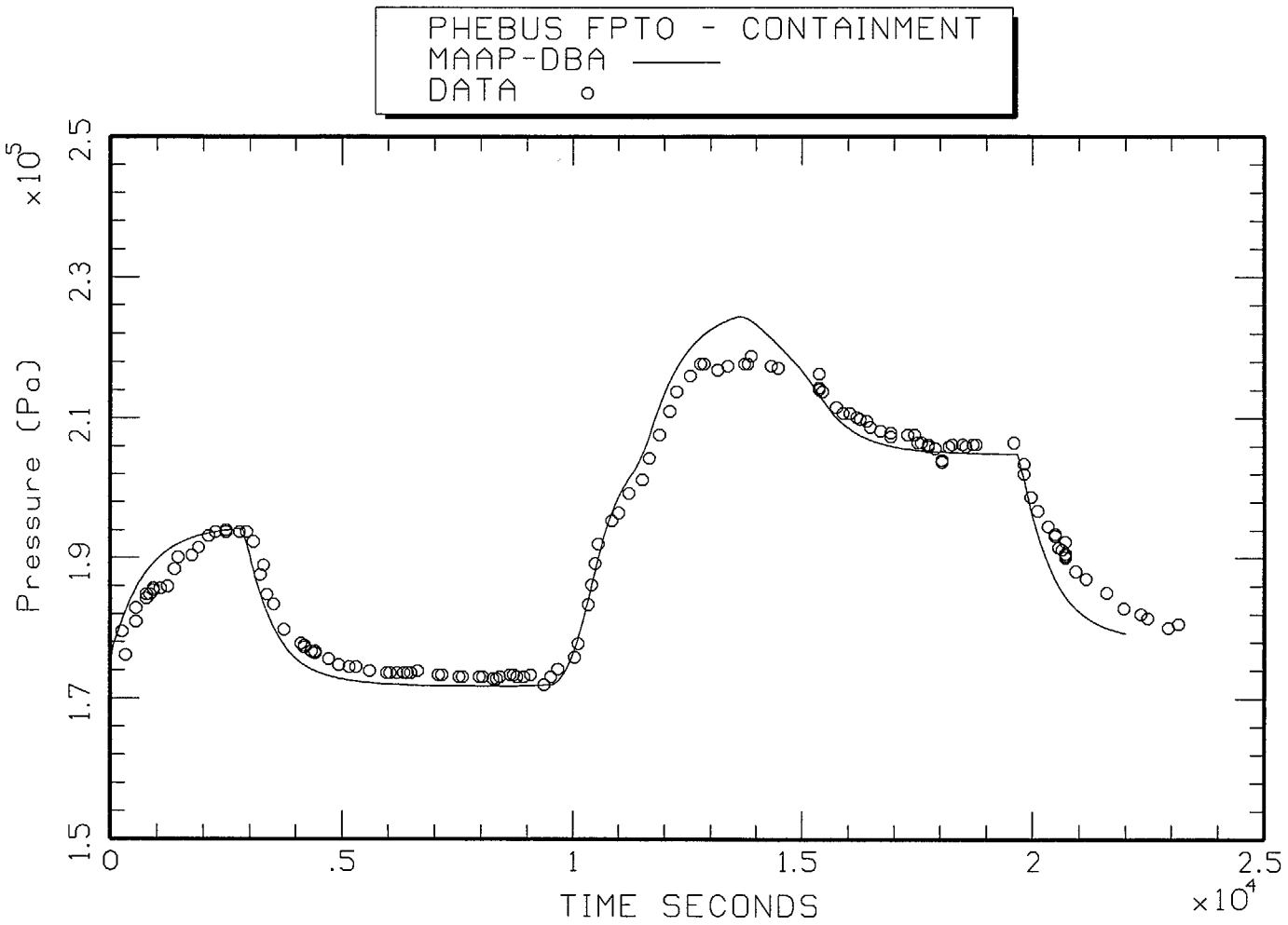


Figure 2-14 PHEBUS FTP0 Pressure Profile

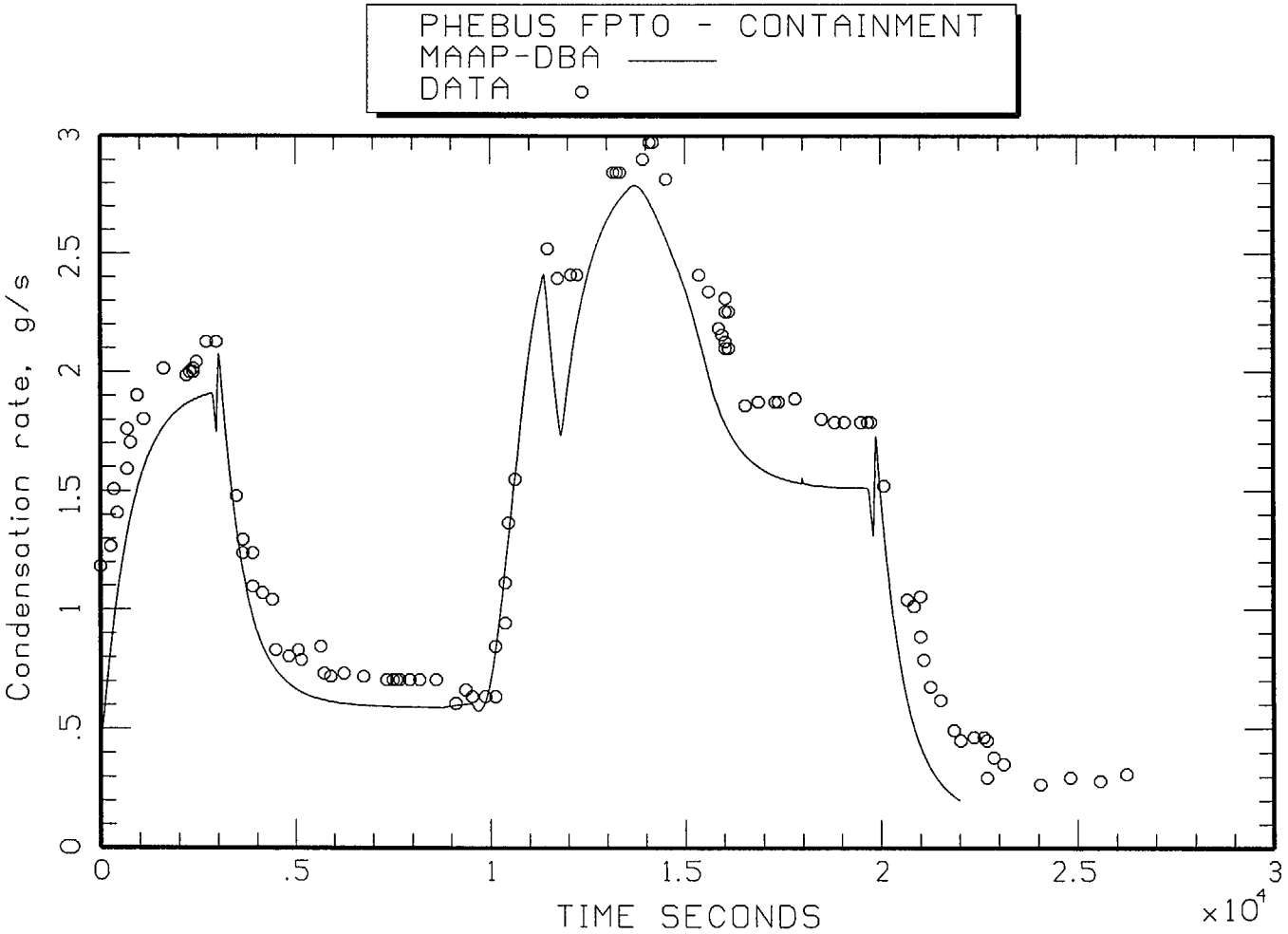


Figure 2-15 PHEBUS FPTO Condensation Rate Profile

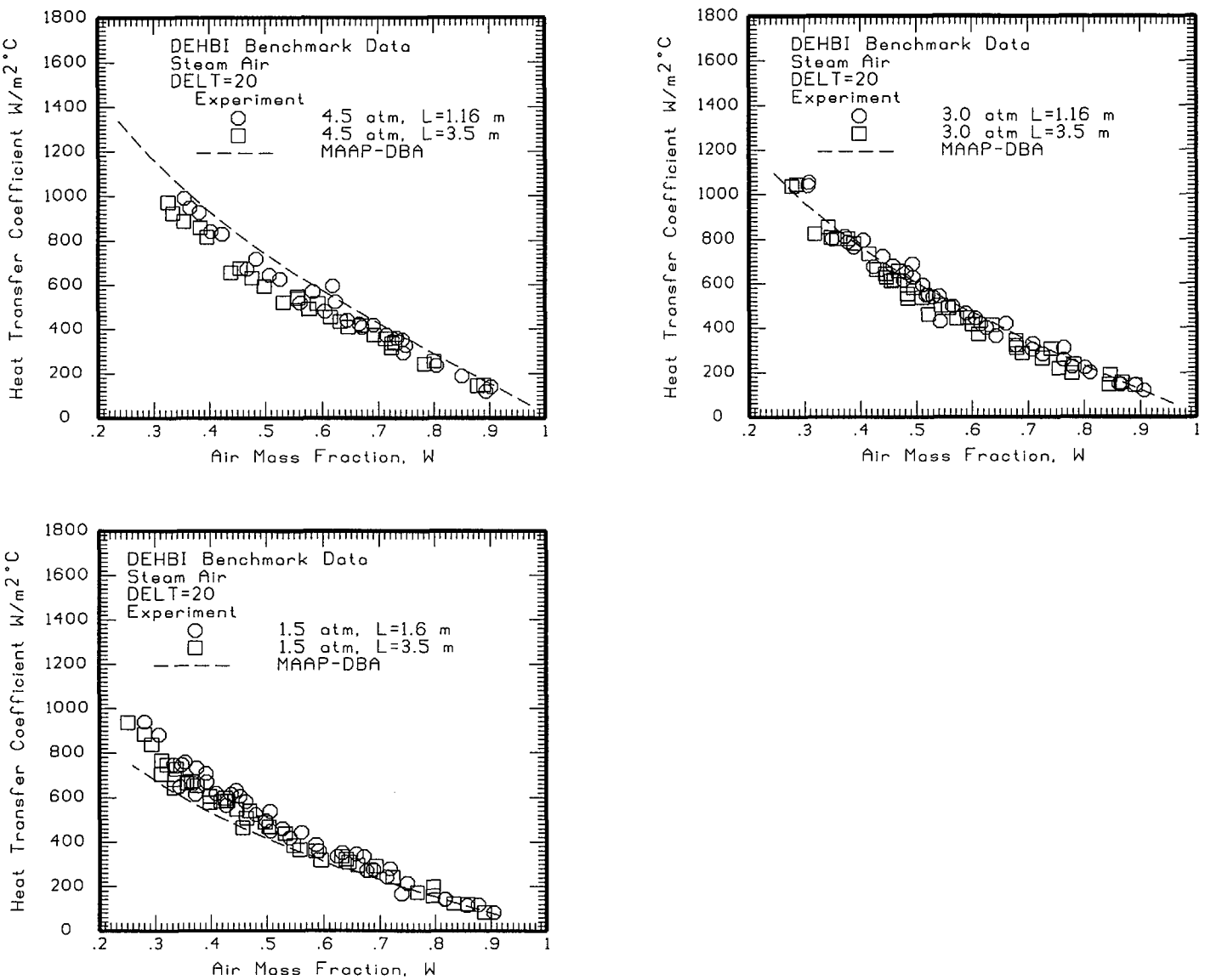


Figure 2-16 Comparison of the MAAP-DBA Condensation Heat Transfer Model with the Experimentally Determined Steam-Air Condensing Heat Transfer Coefficients

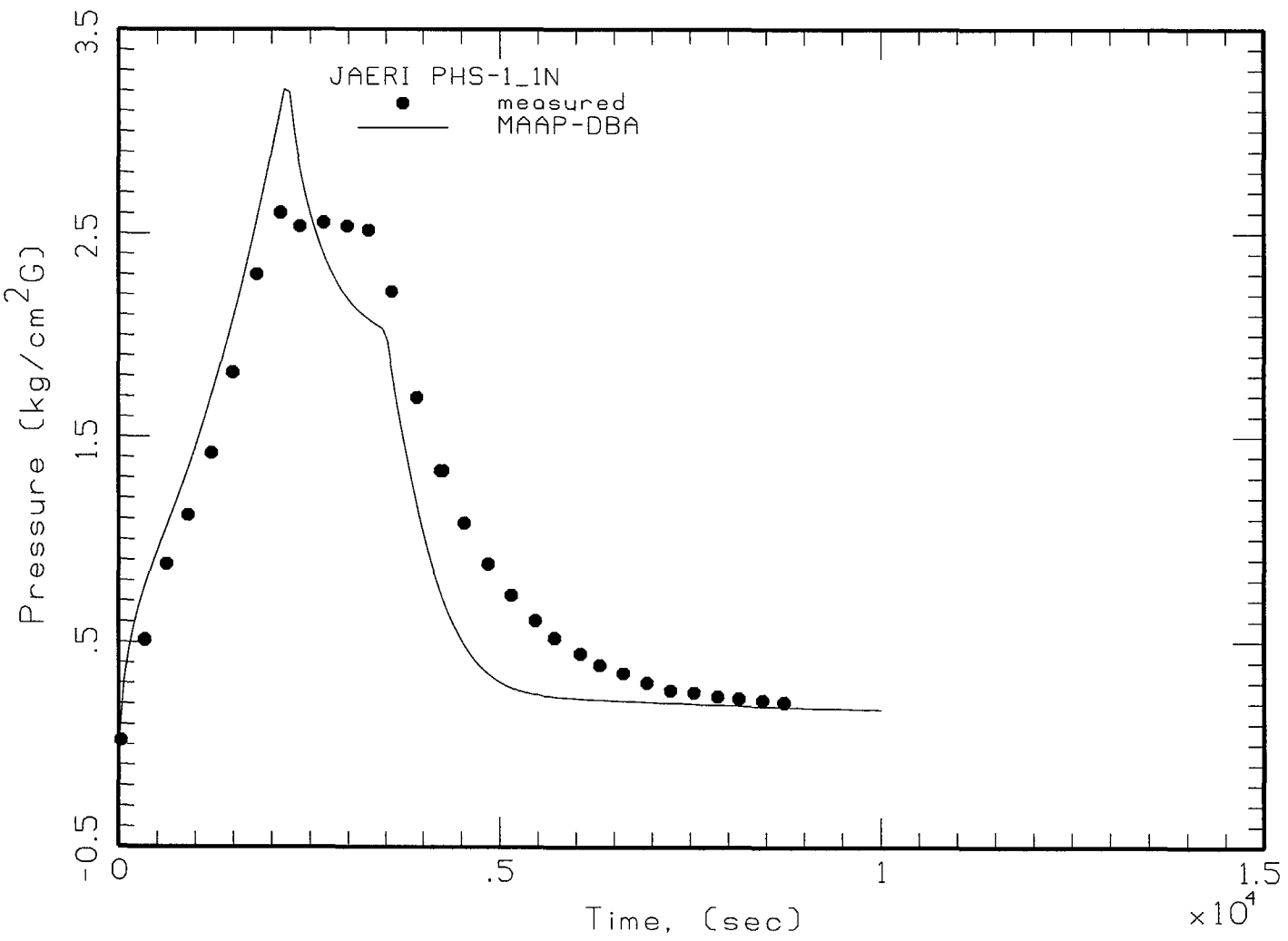


Figure 2-17 MAAP-DBA Single Node Model Pressure Profile for JAERI Test PHS-1

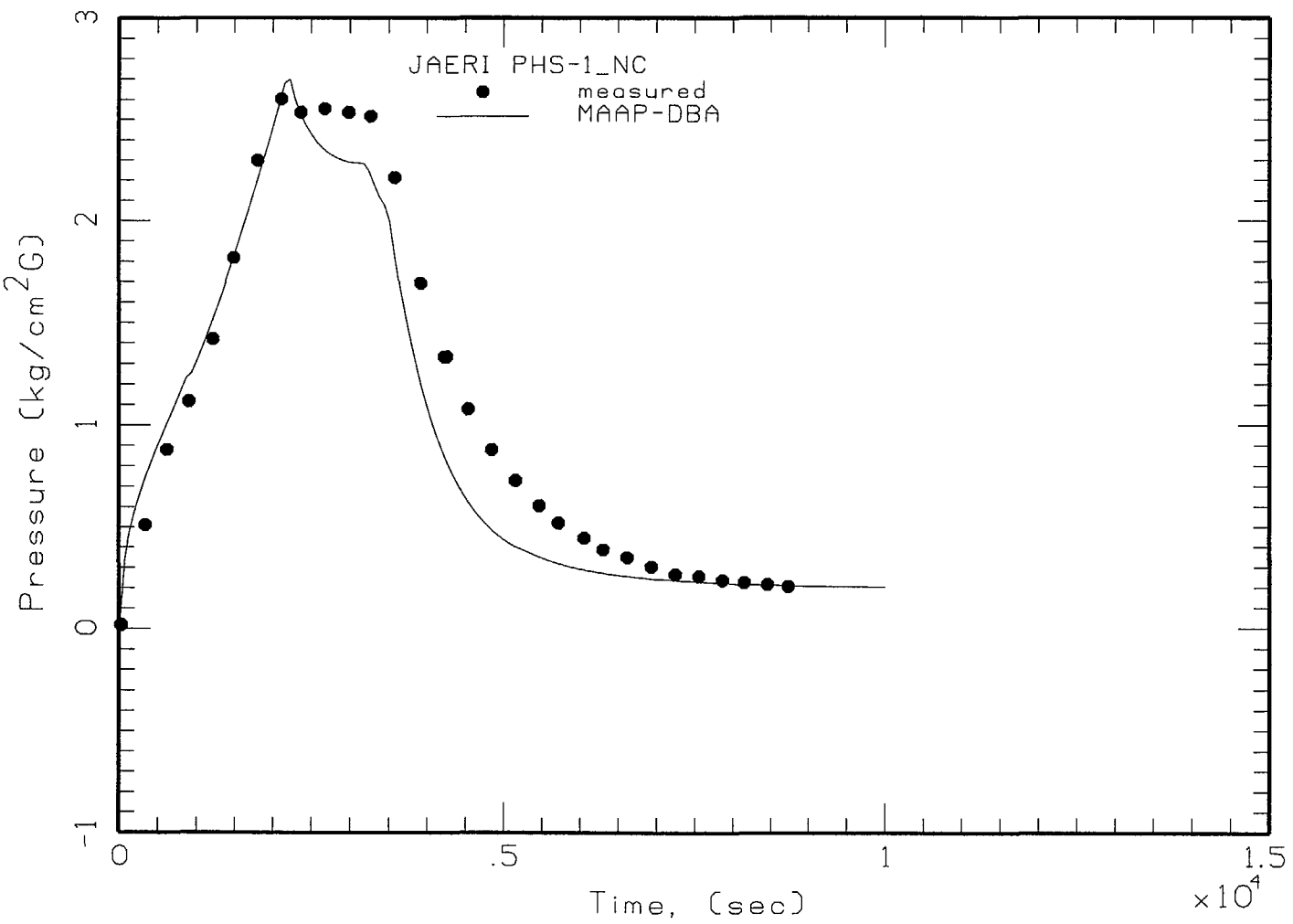


Figure 2-18 MAAP-DBA Multiple Node Model Pressure Profile for JAERI Test PHS-1

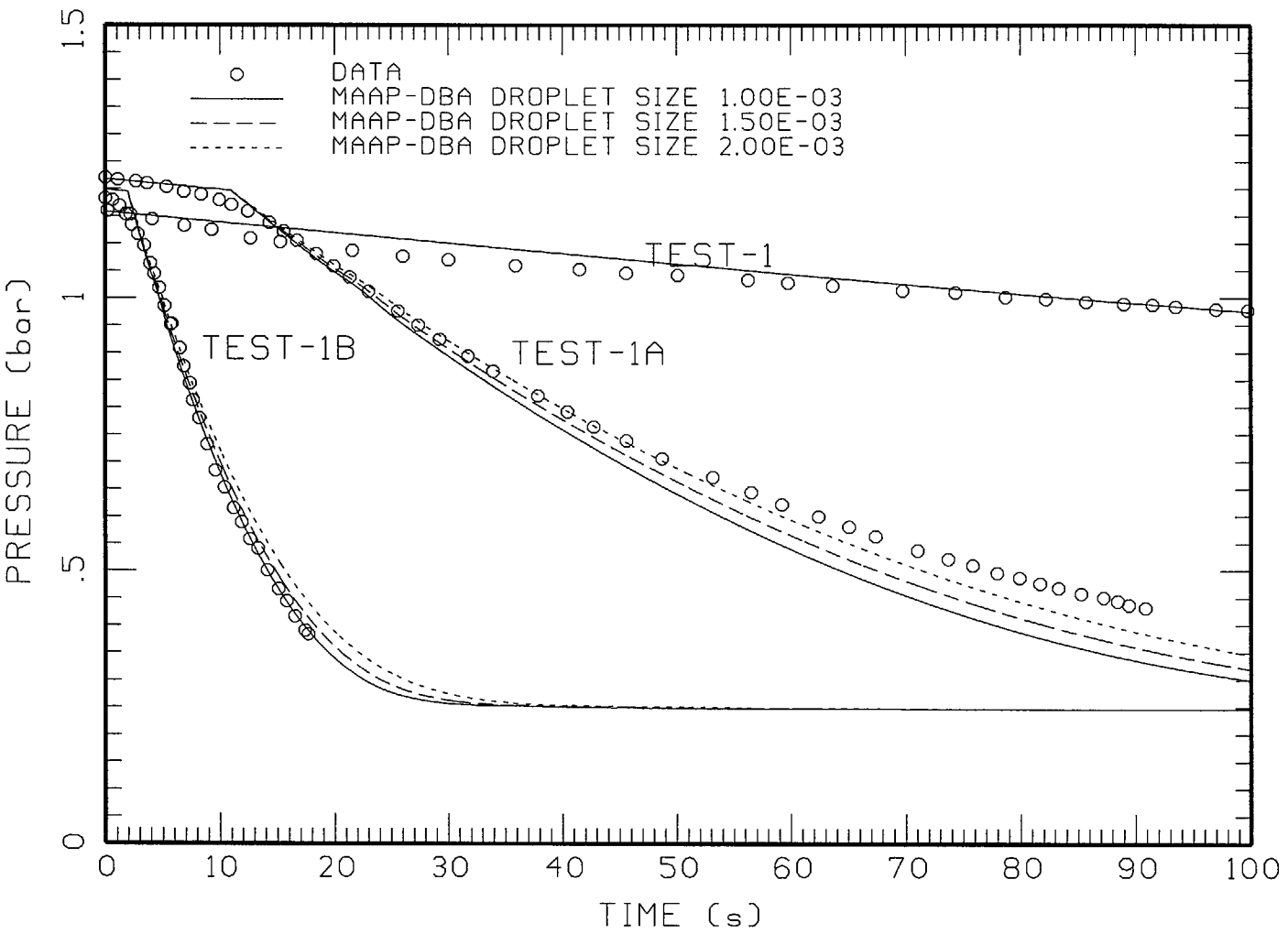


Figure 2-19 MAAP-DBA Pressure Profiles for Kulic Spray Tests

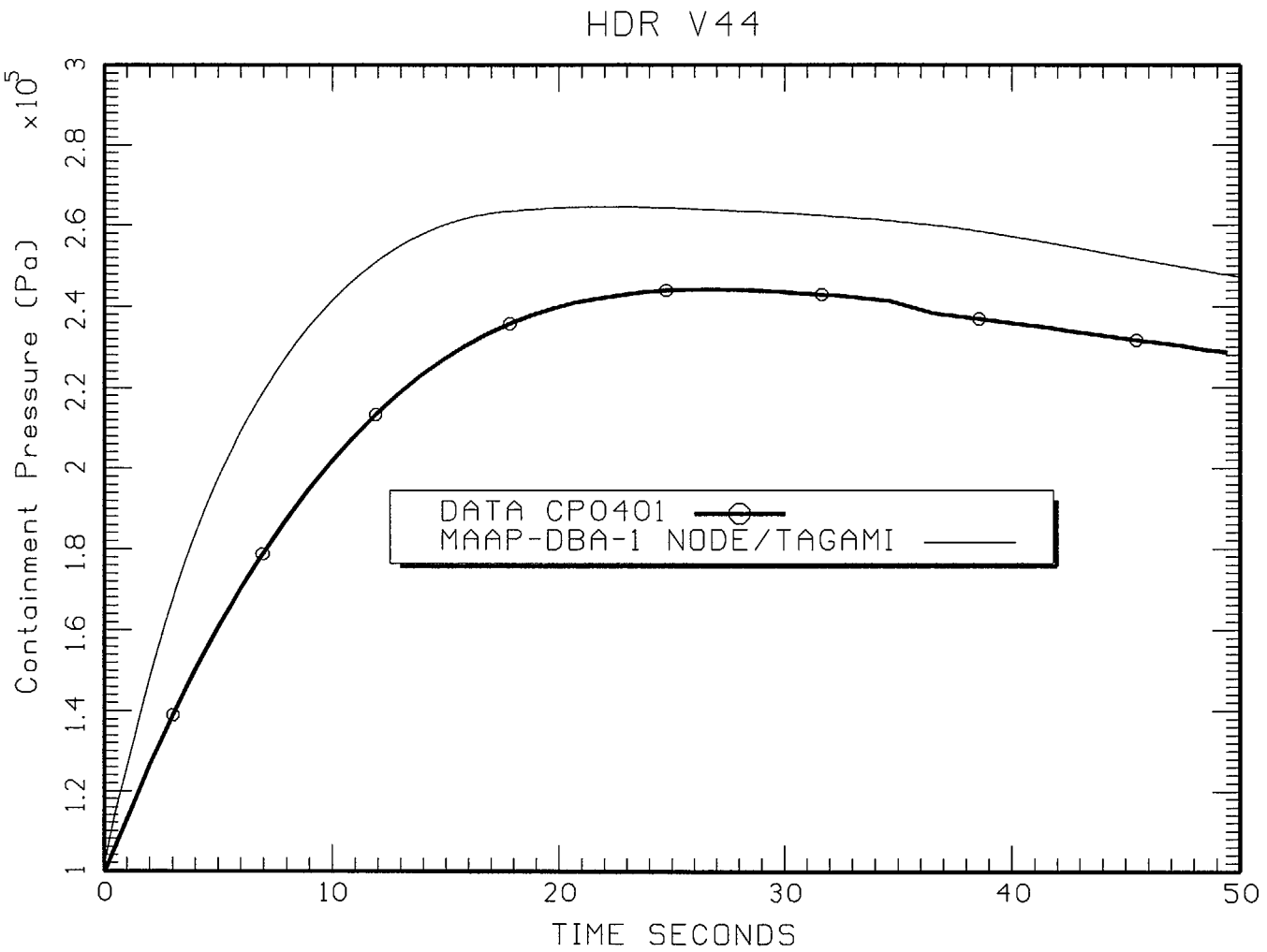


Figure 2-20 HDR-V44 Pressure Profile

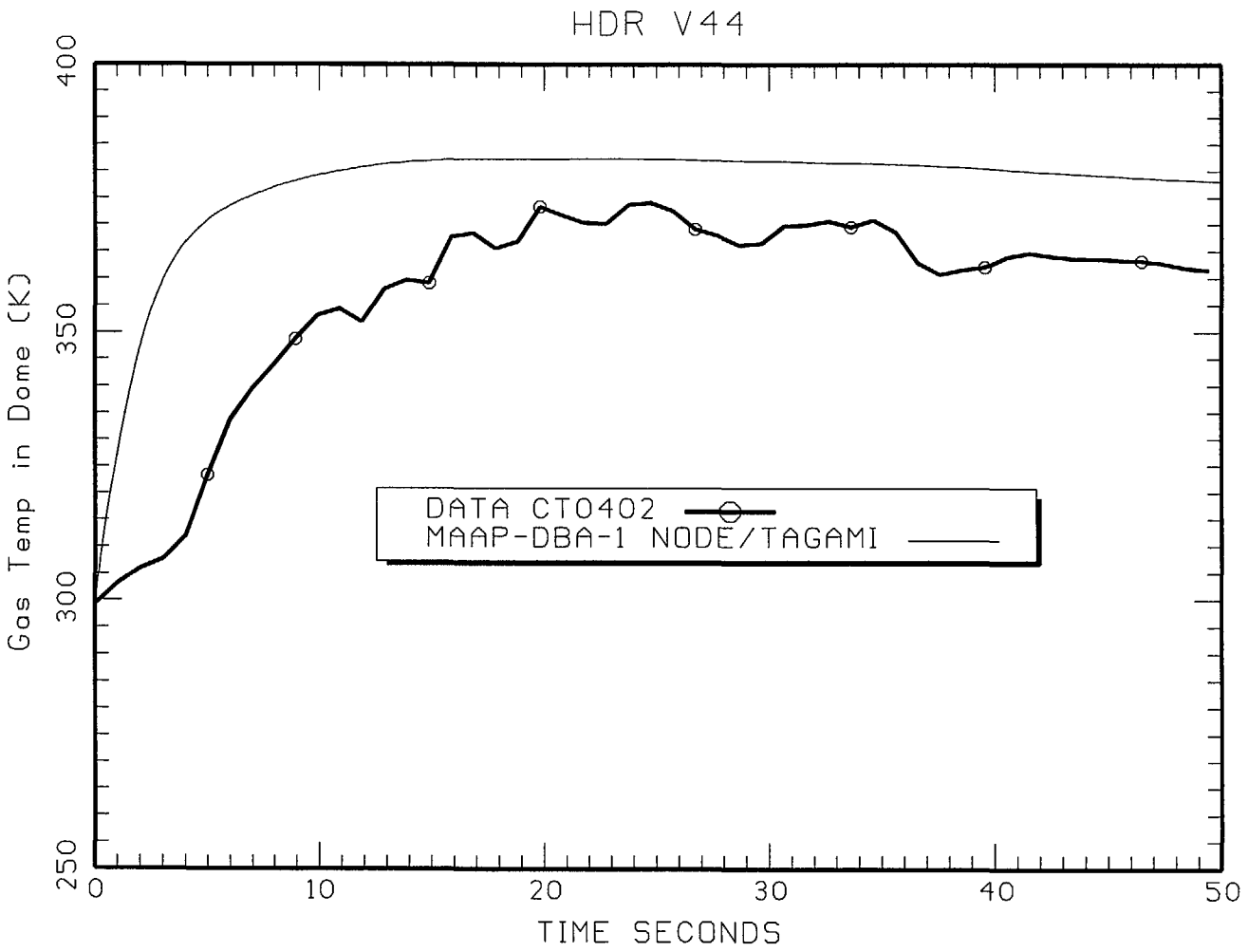


Figure 2-21 HDR-V44 Gas Temperature Profile

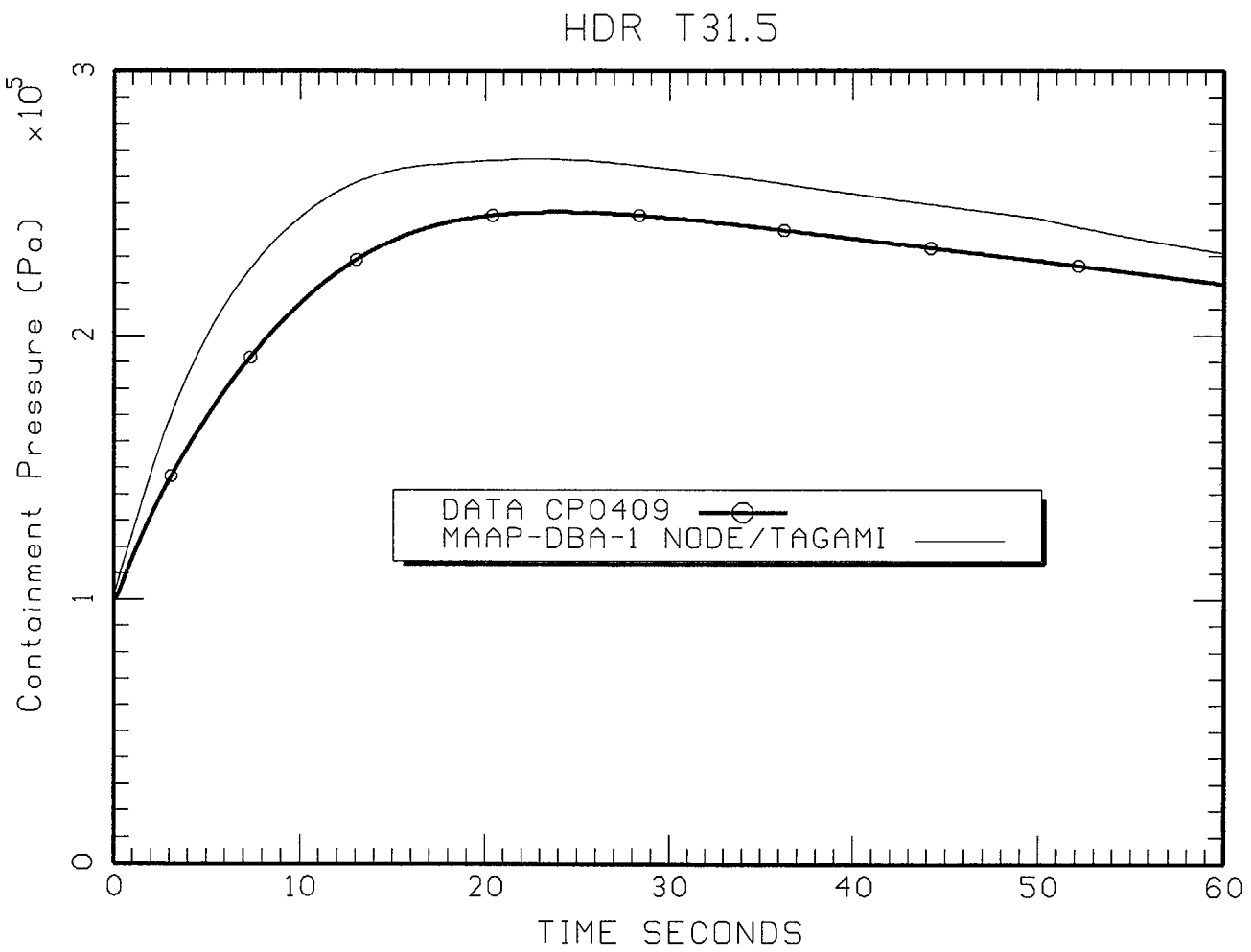


Figure 2-22 HDR-T31.5 Pressure Profile

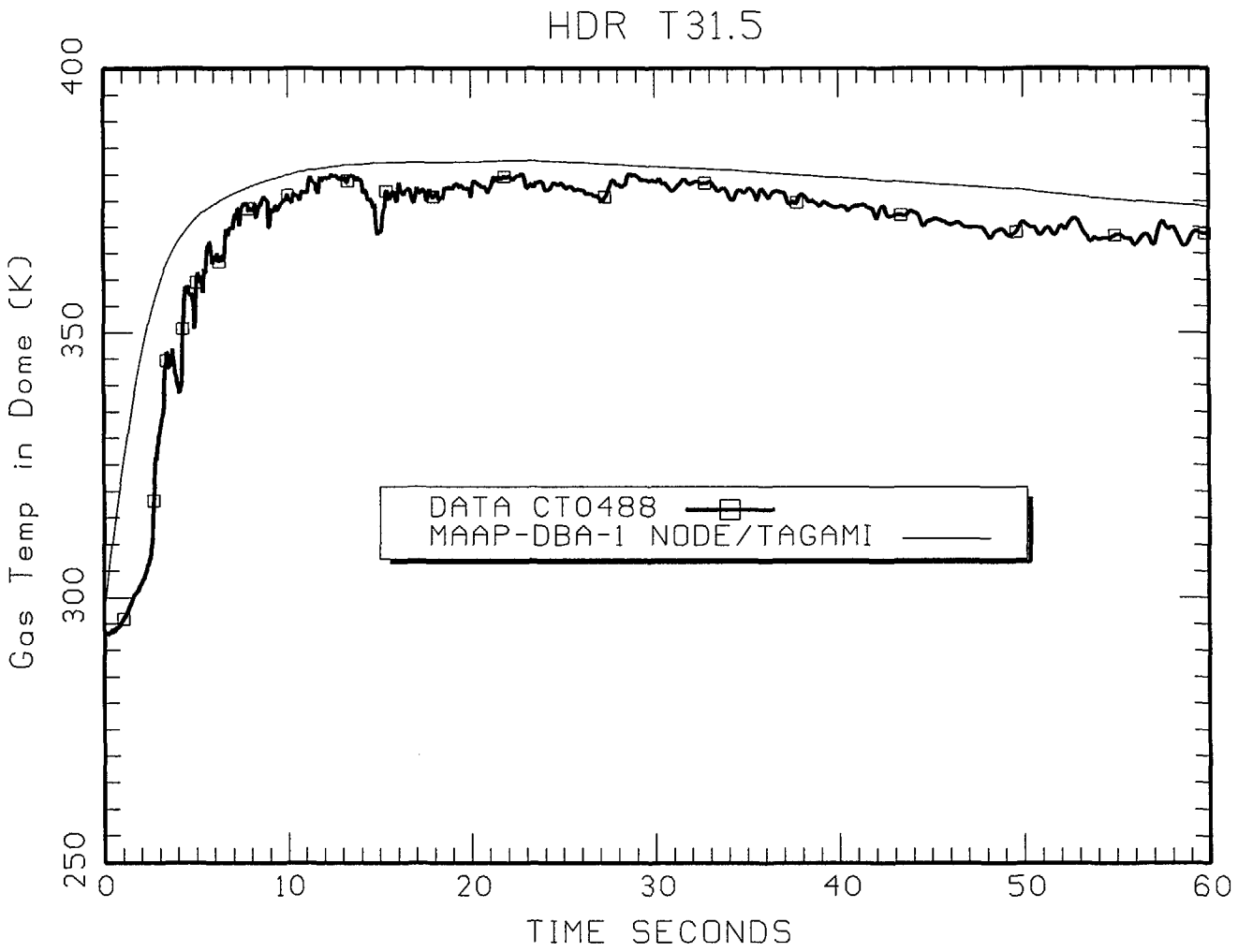


Figure 2-23 HDR-T31.5 Gas Temperature Profile

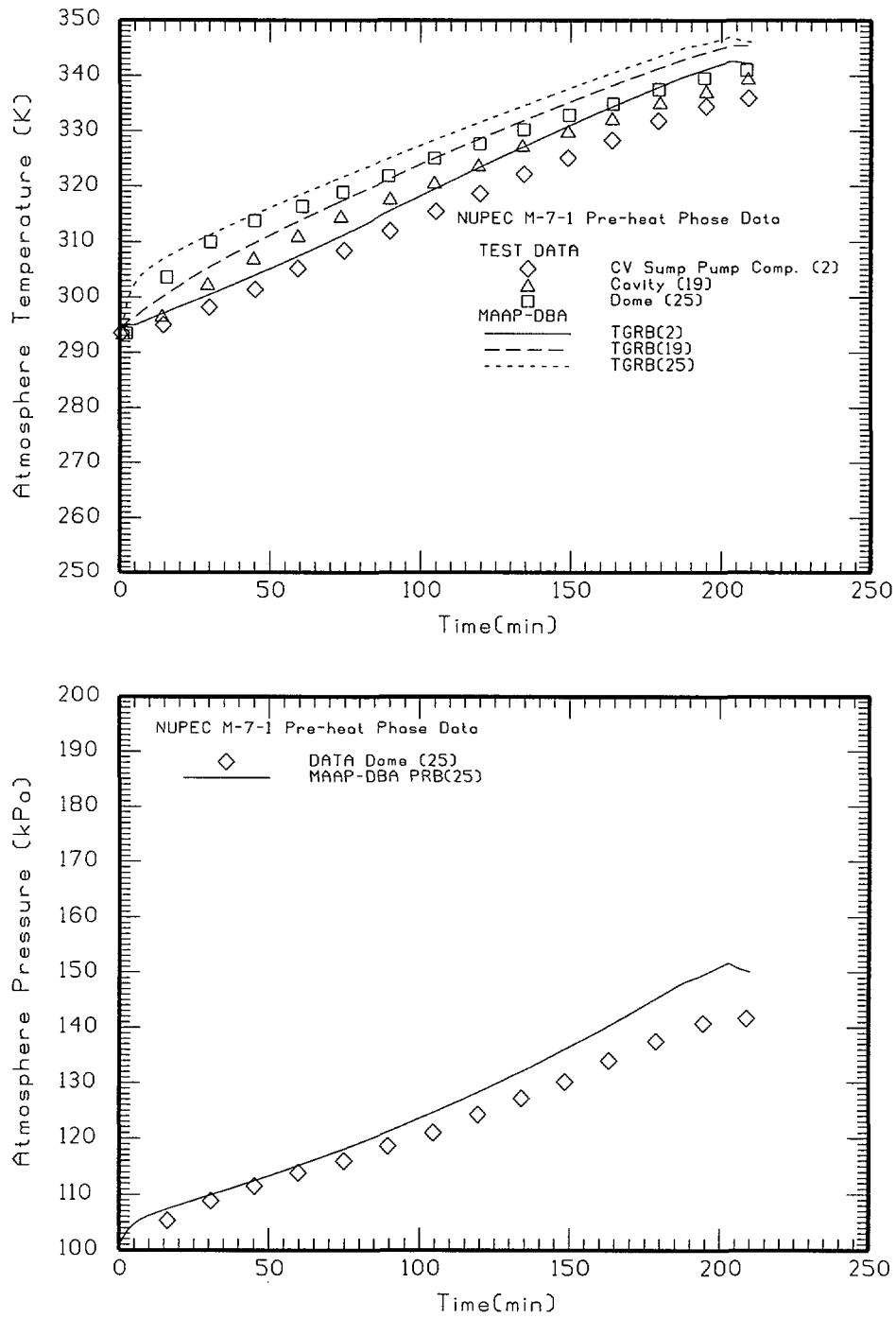


Figure 2-24 Comparison of NUPEC M-7-1 Preheat Phase Gas Temperatures and Containment Pressure

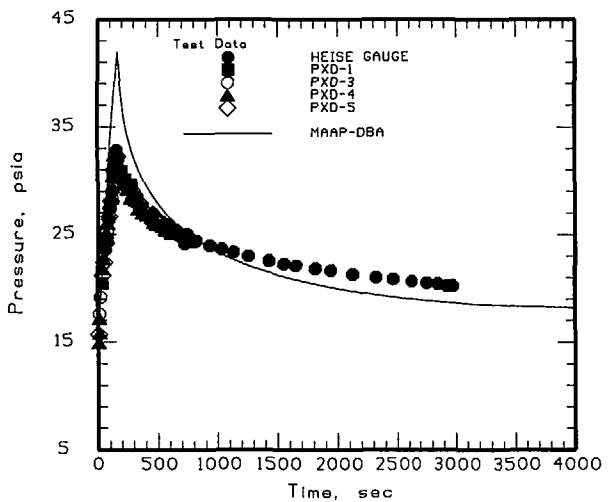
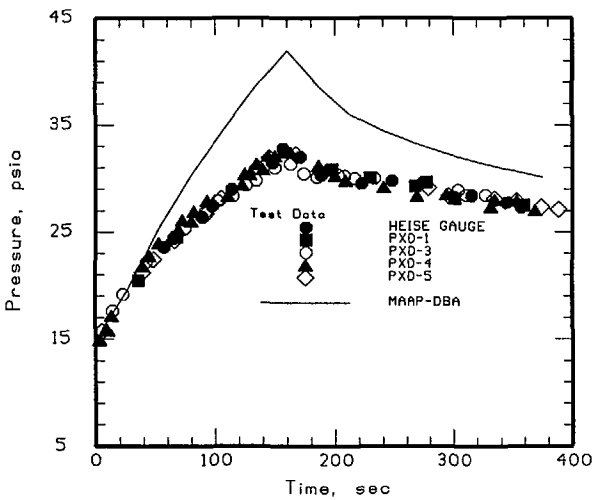
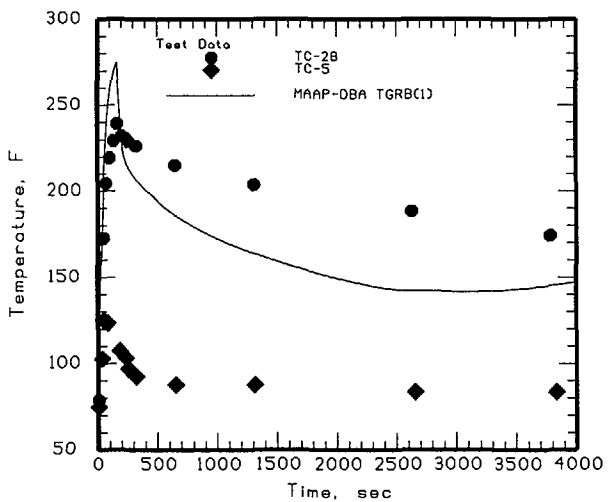
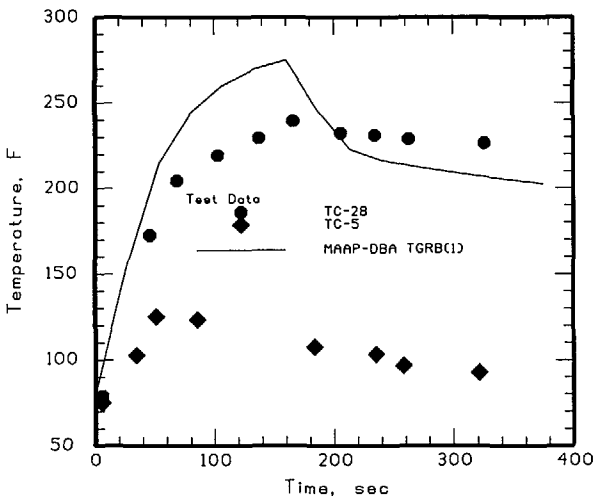


Figure 2-25 Comparison of CVTR Test 3 Containment Pressure

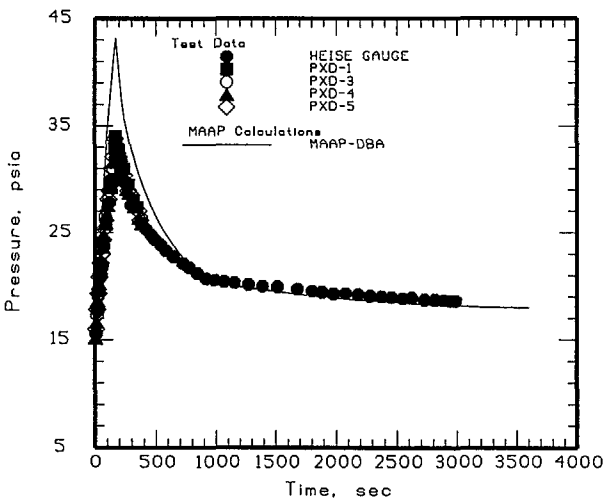
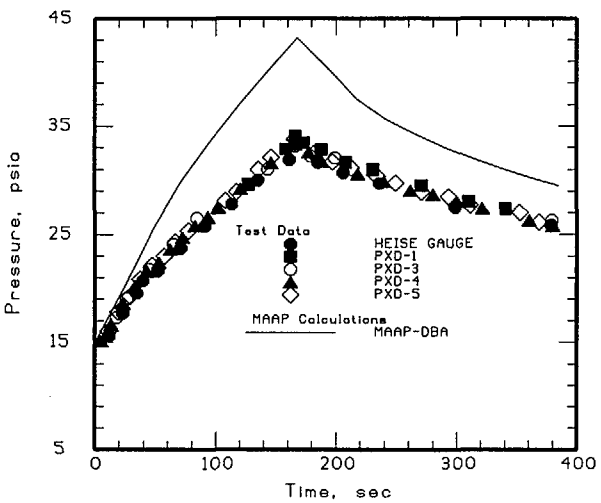
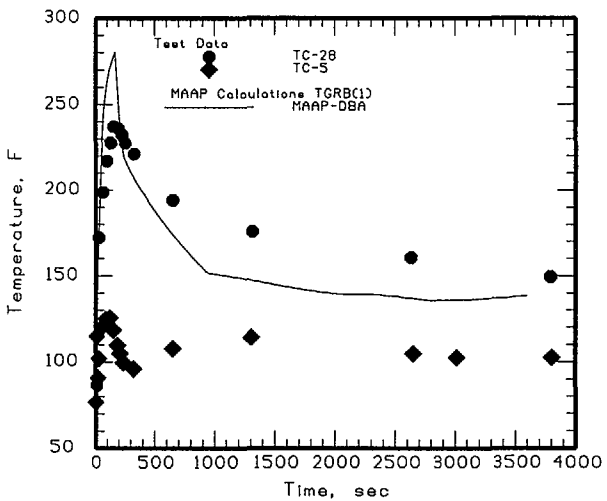
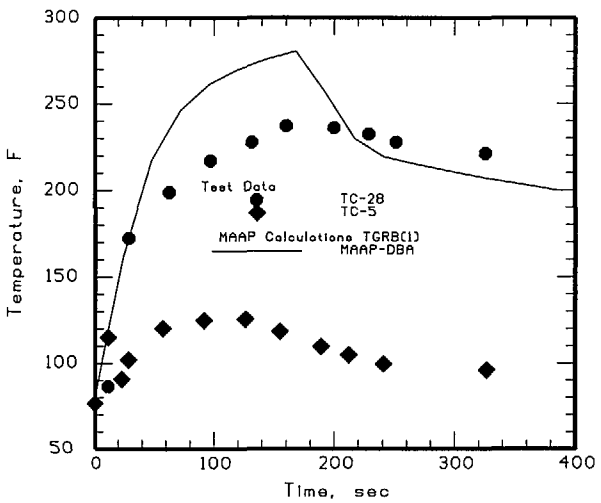


Figure 2-26 Comparison of CVTR Test 4 Containment Pressure

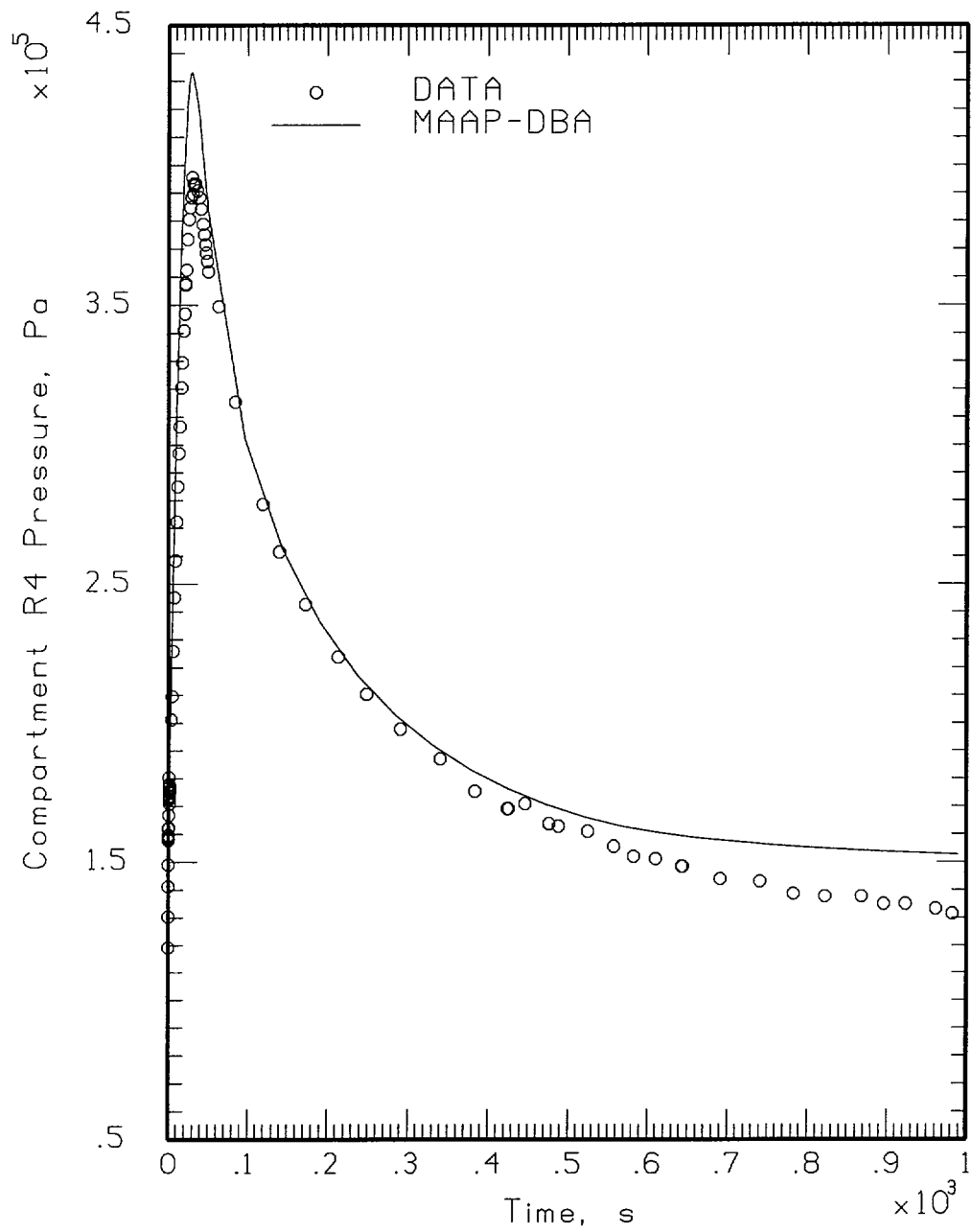


Figure 2-27 Comparison of BFMC D-16 Pressure History in the Break Compartment

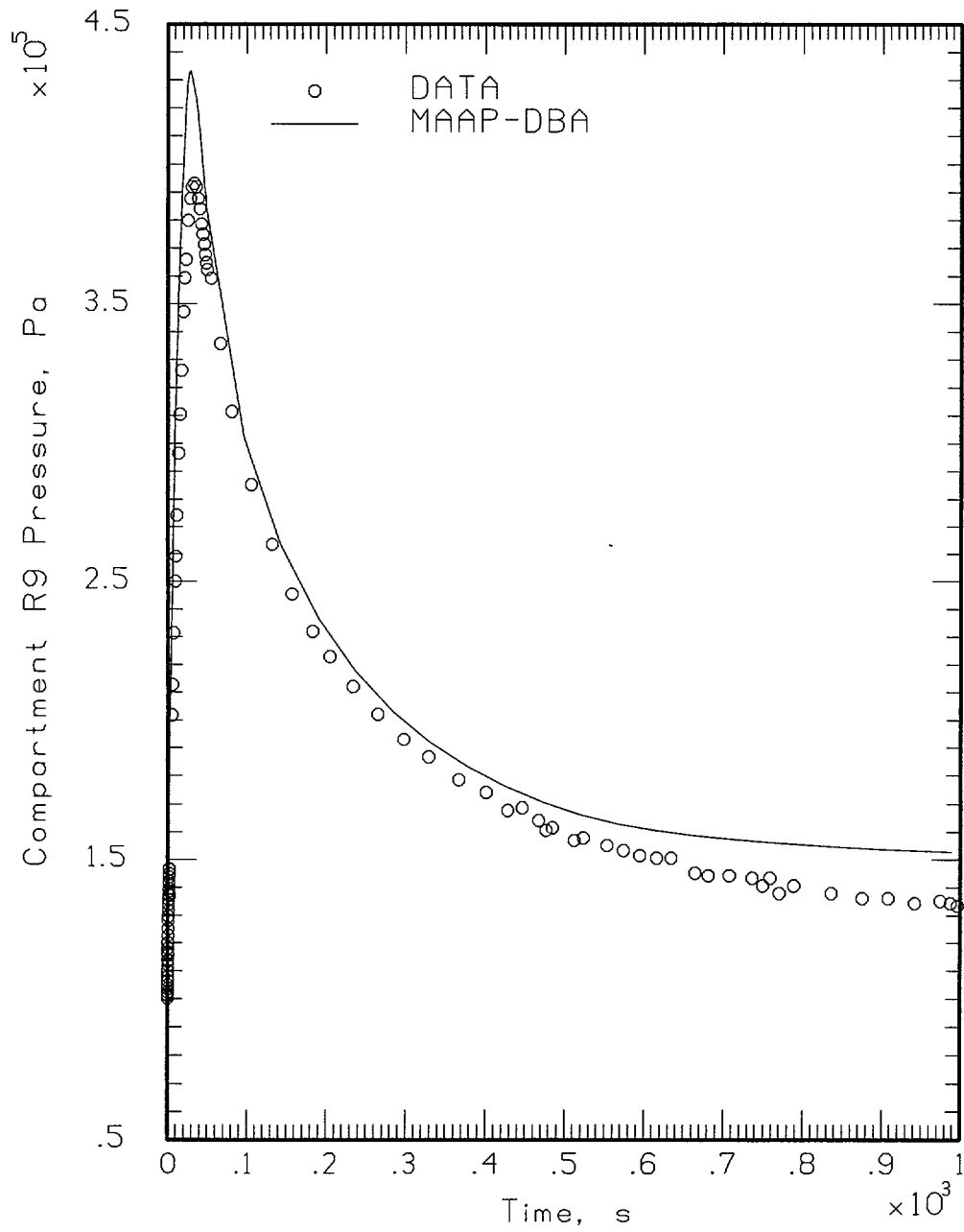


Figure 2-28 Comparison of BFMC D-16 Pressure History for Outer Room

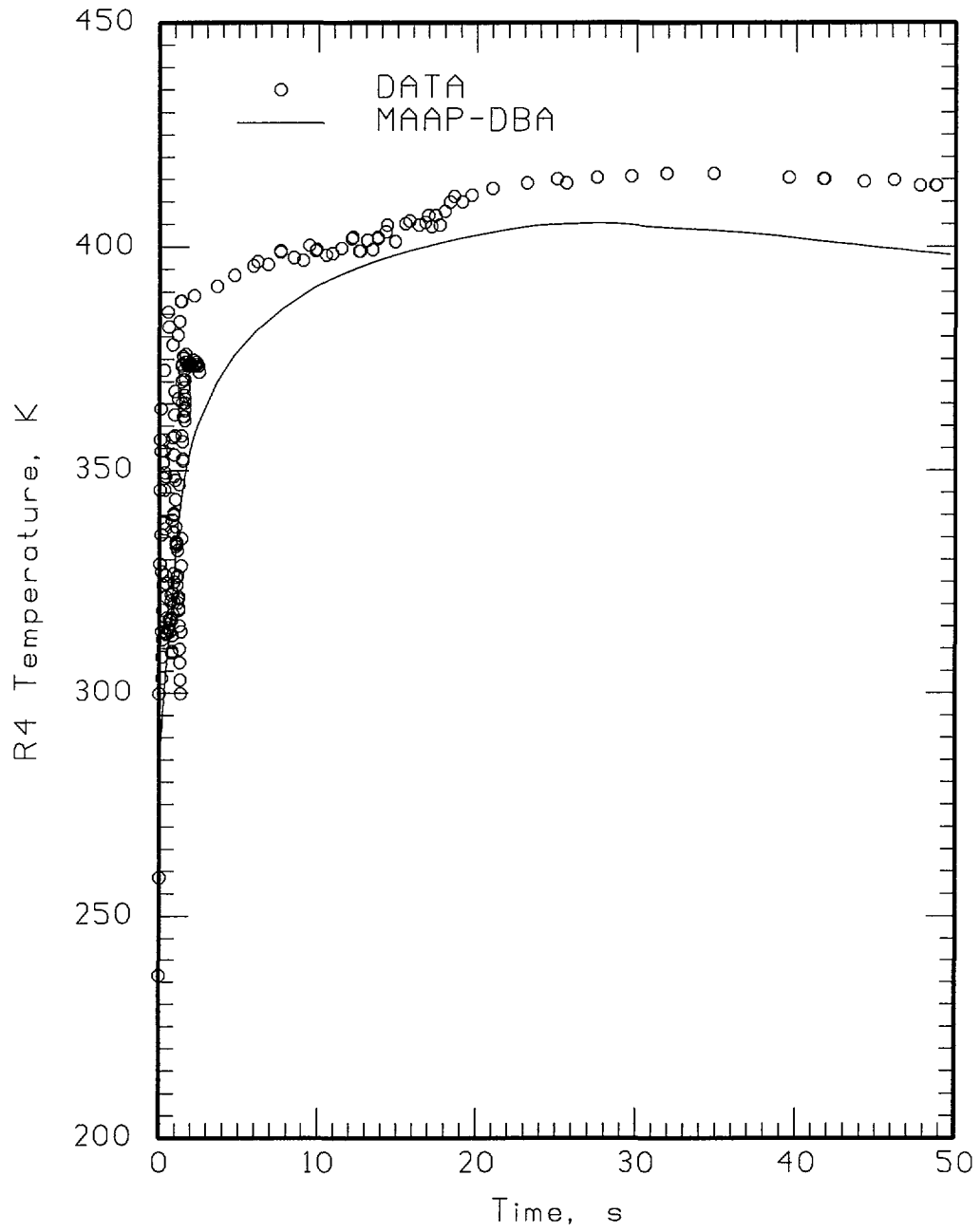


Figure 2-29 Comparison of BFMC D-16 Temperature History for Break Room

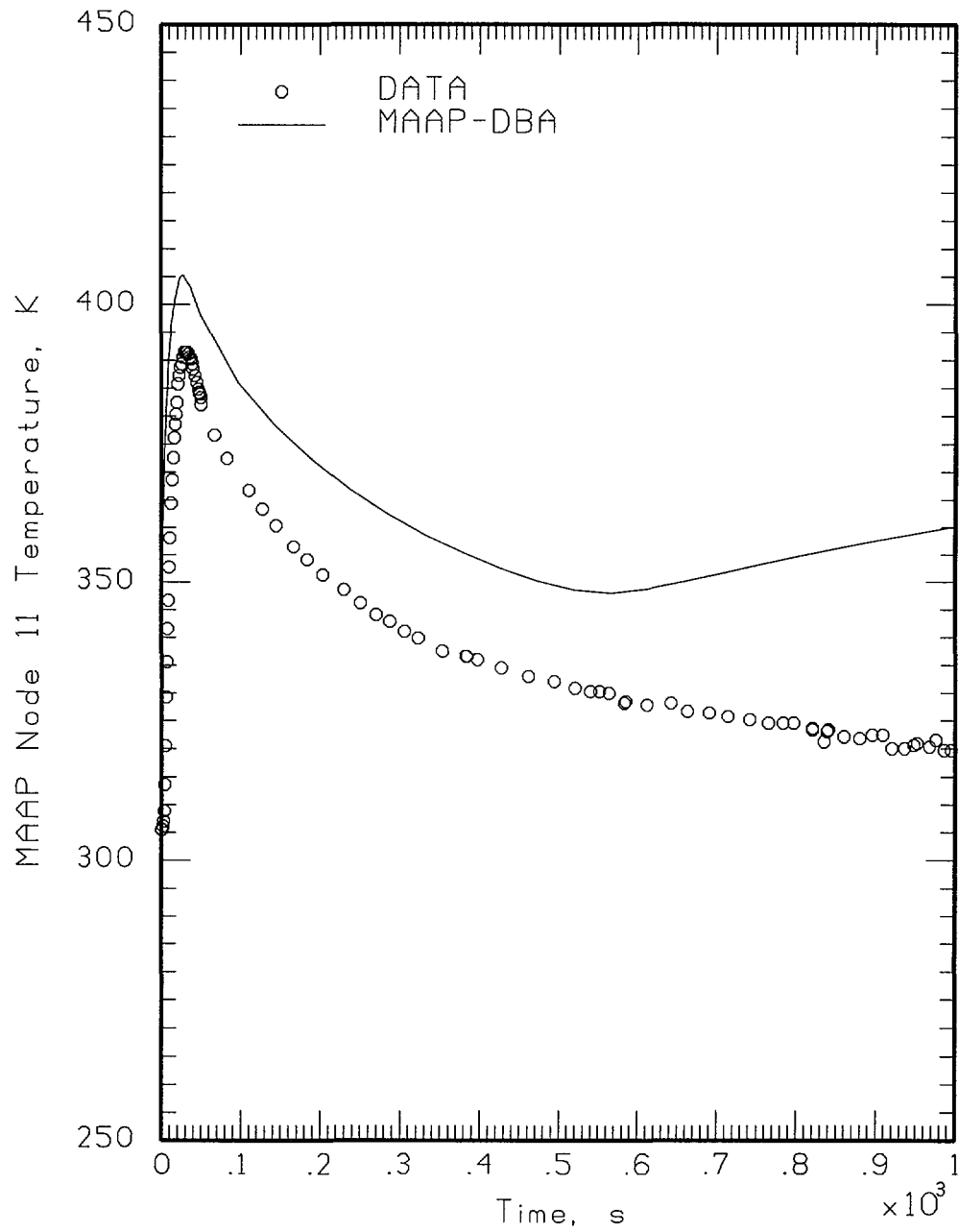


Figure 2-30 Comparison of BFMC D-16 Temperature History for Outer Room

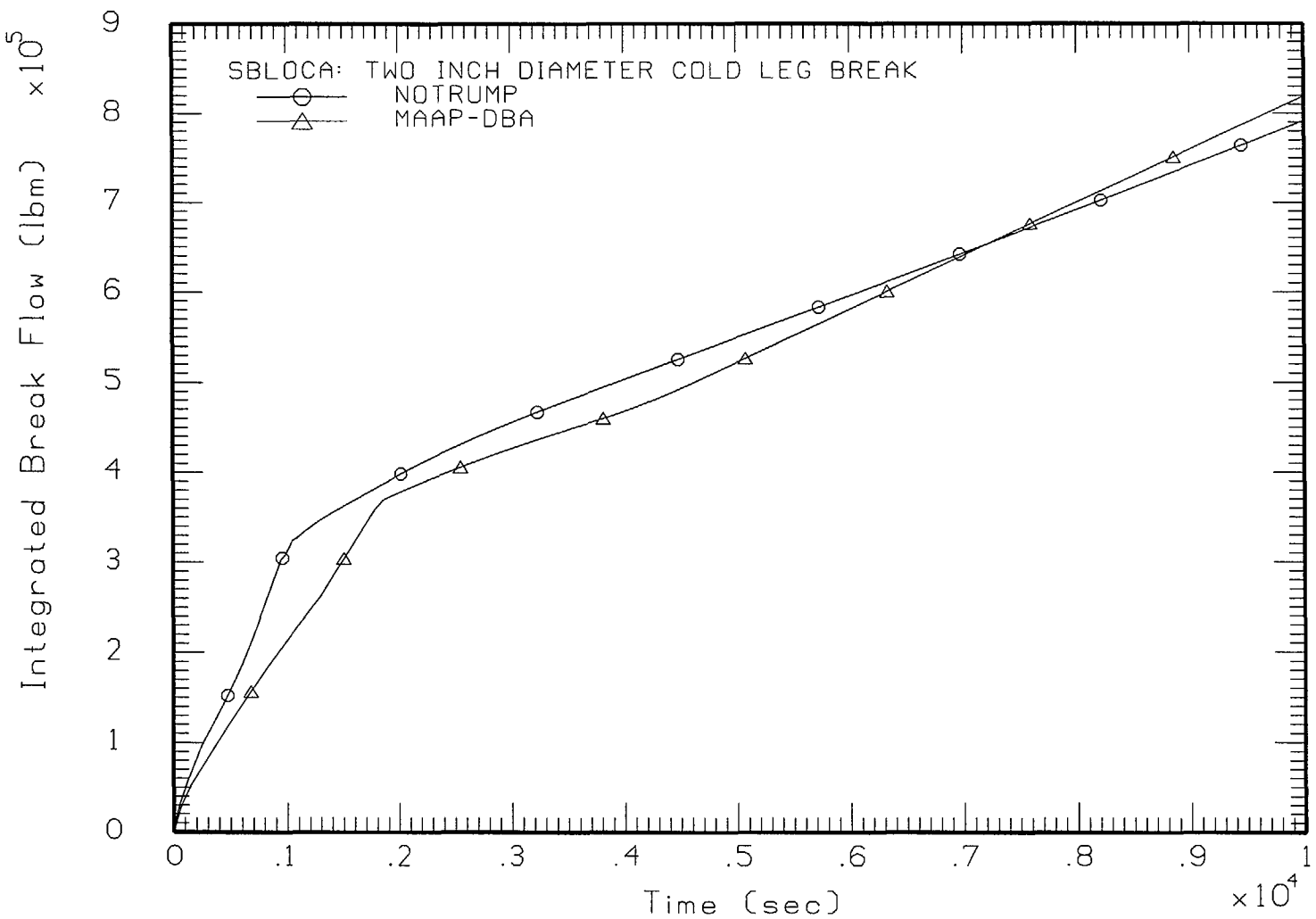


Figure 2-31a Comparison of 2 Inch Cold Leg Releases for SBLOCA Analysis

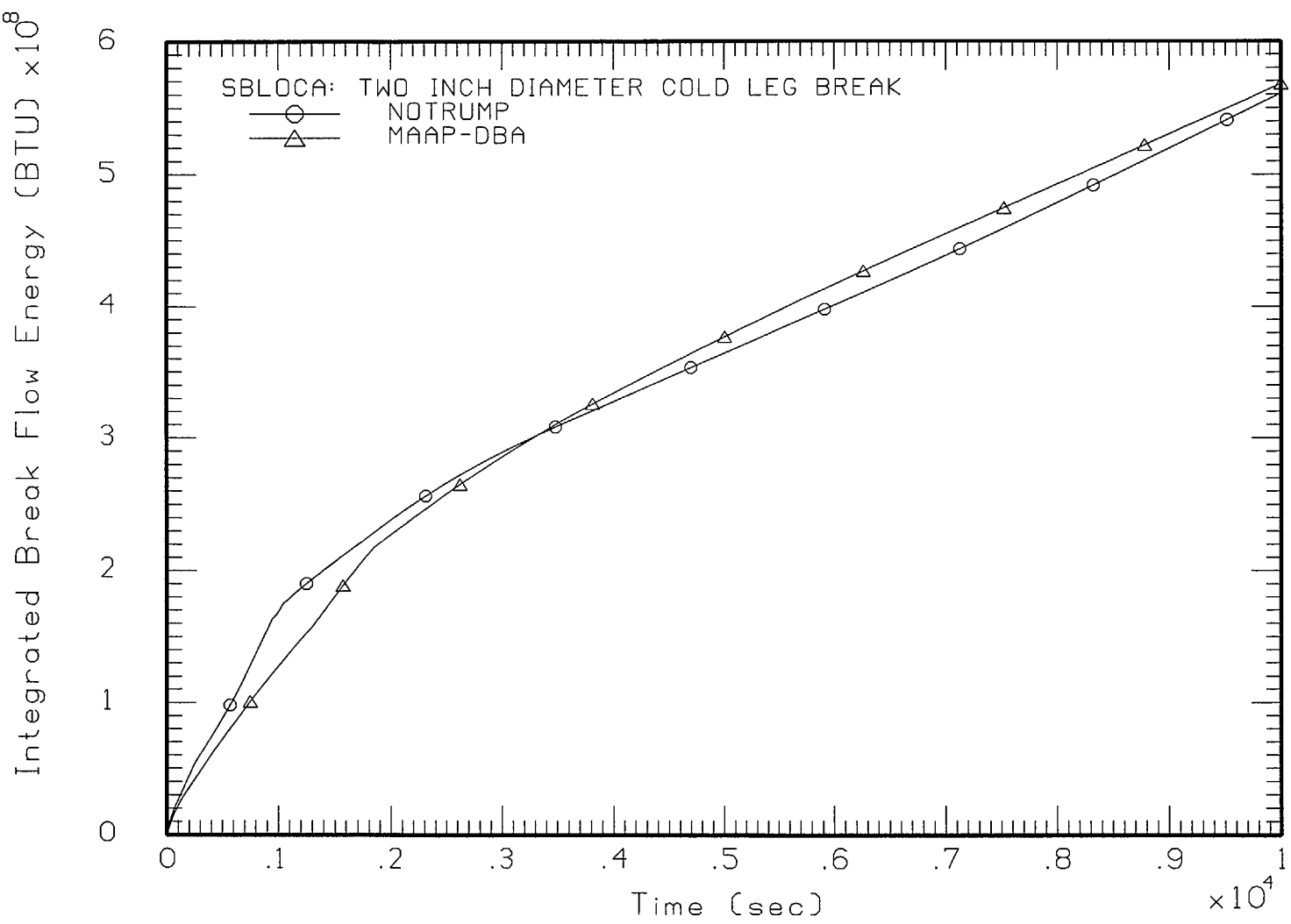


Figure 2-31b Comparison of 2 Inch Cold Leg Releases for SBLOCA Analysis

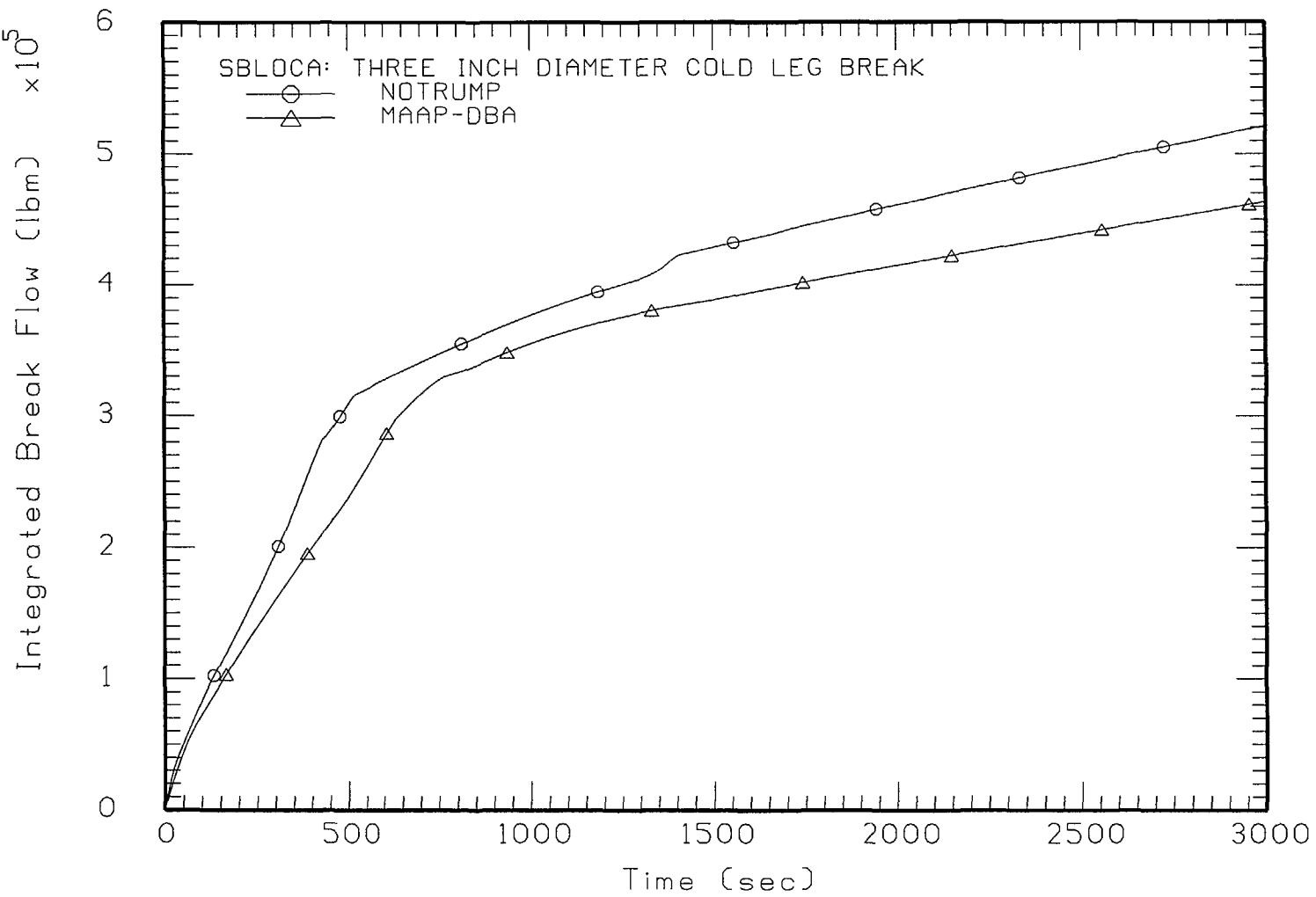


Figure 2-32a Comparison of 3 Inch Cold Leg Releases for SBLOCA Analysis

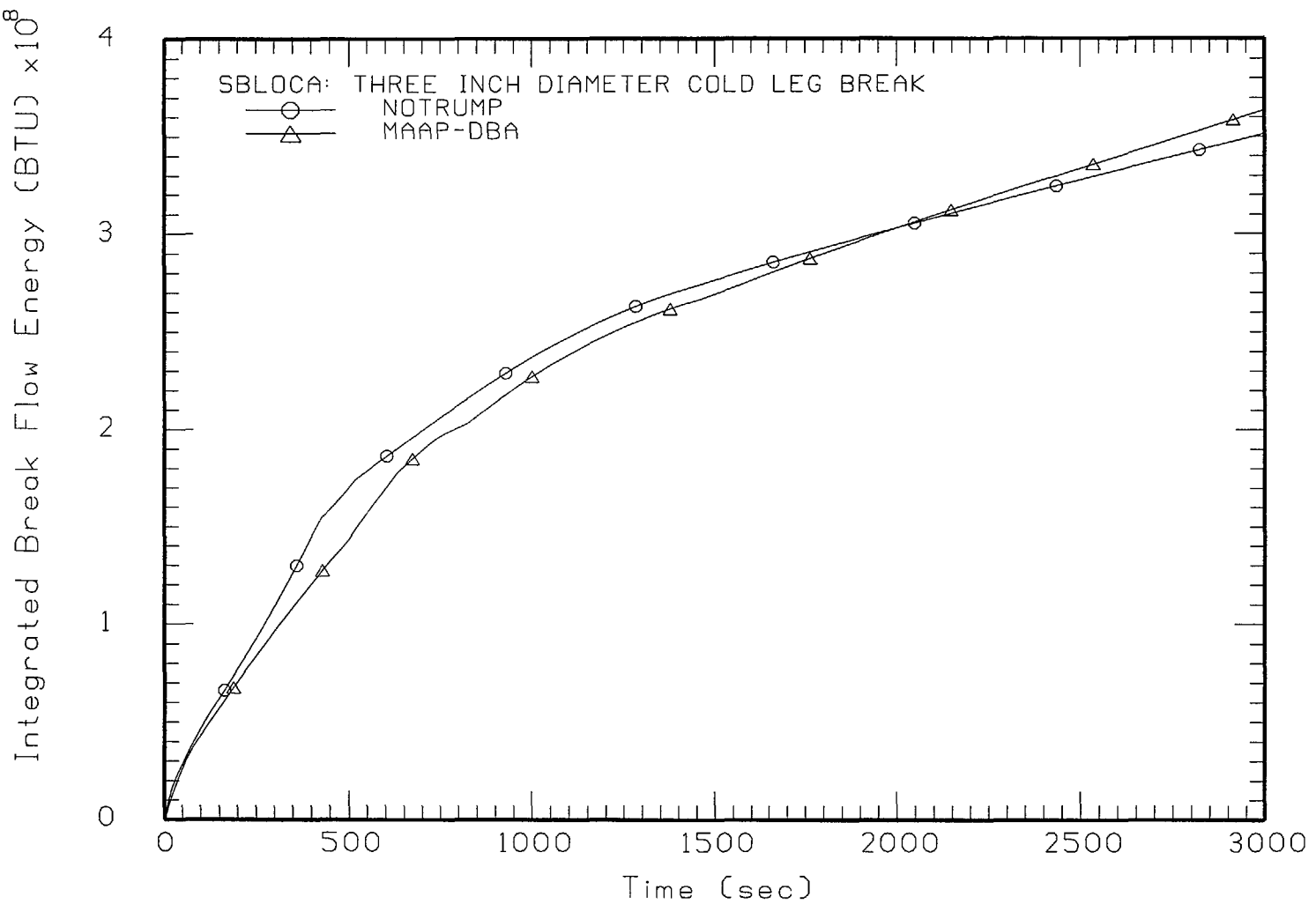


Figure 2-32b Comparison of 3 Inch Cold Leg Releases for SBLOCA Analysis

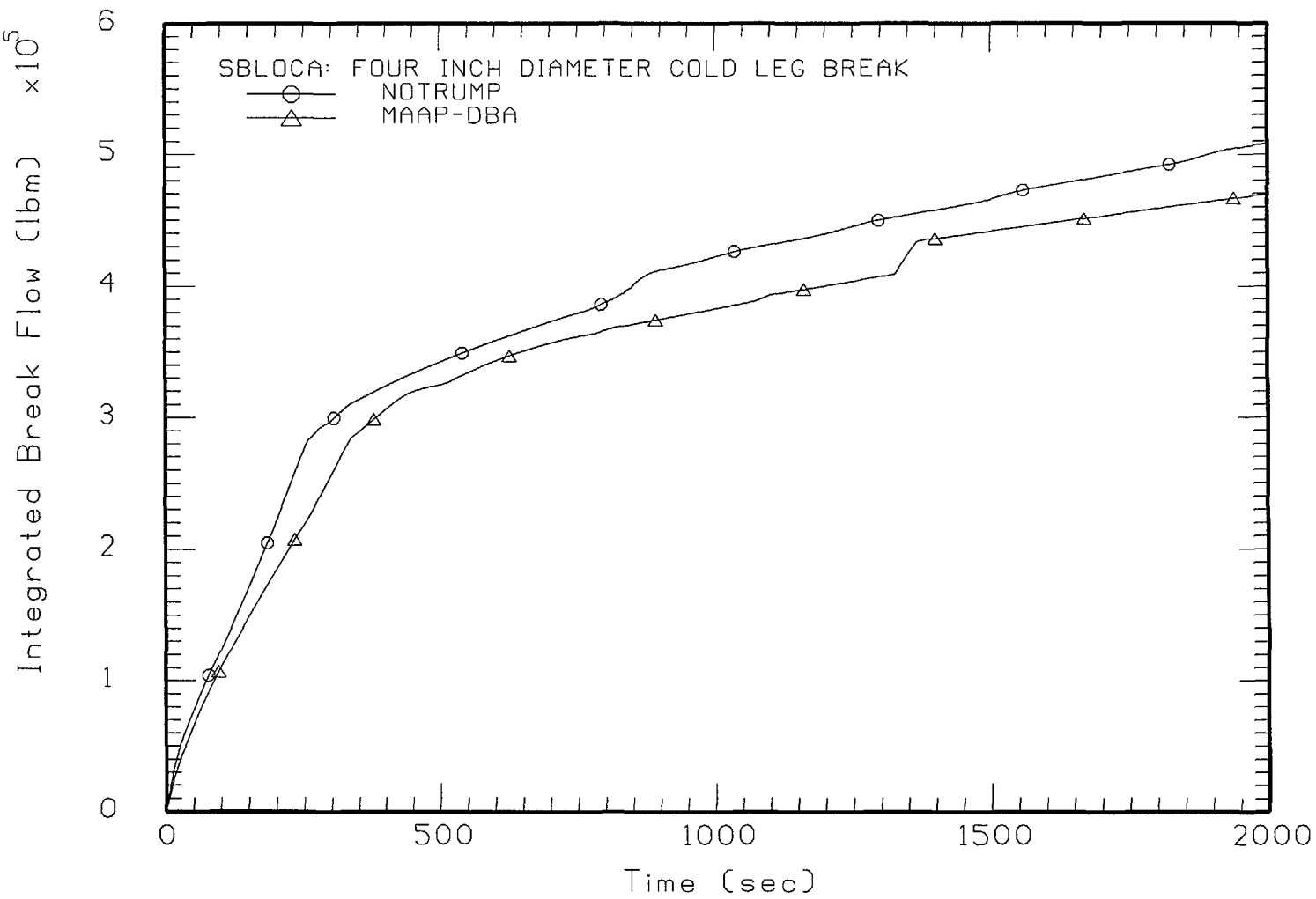


Figure 2-33a Comparison of 4 Inch Cold Leg Releases for SBLOCA Analysis

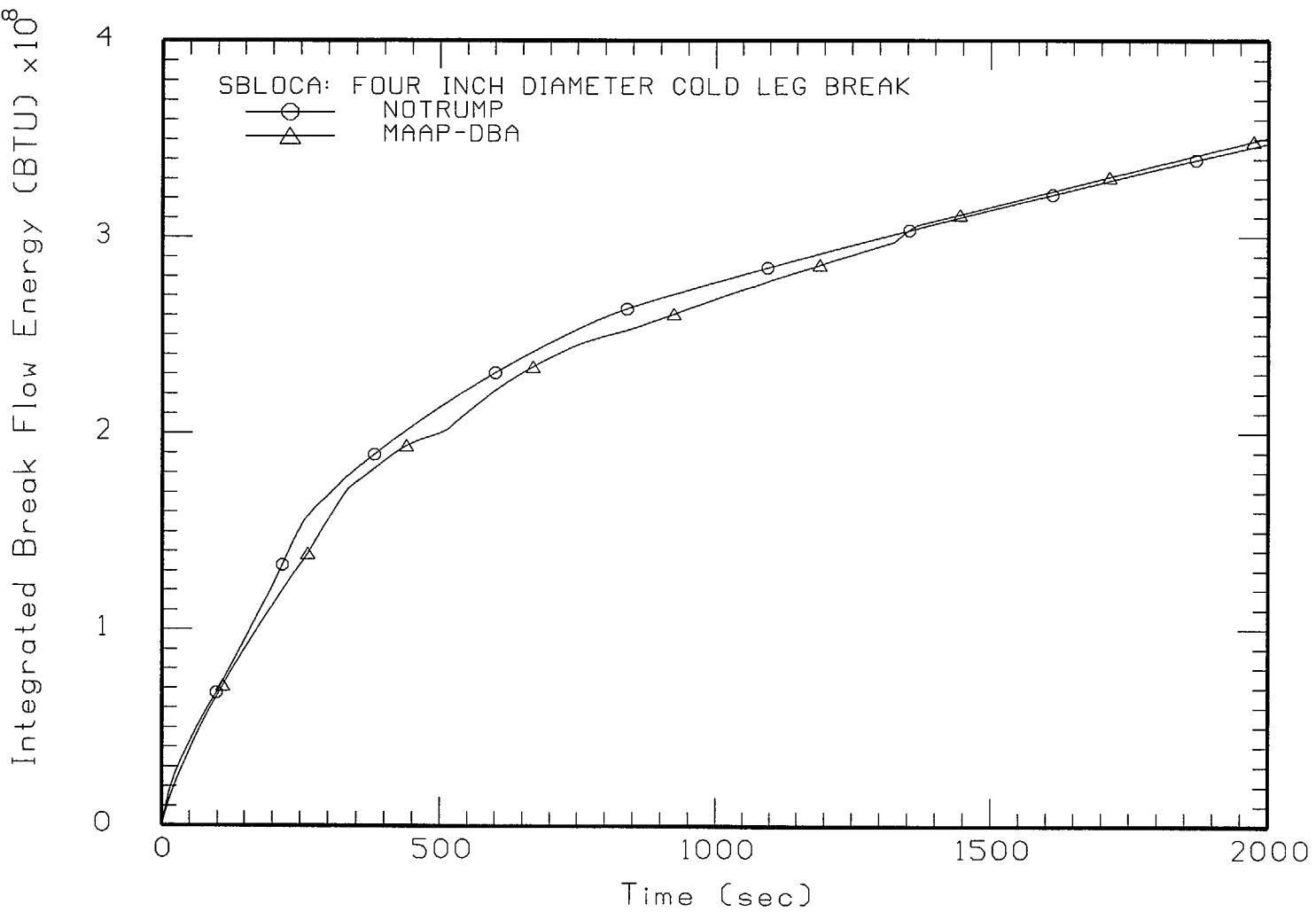


Figure 2-33b Comparison of 4 Inch Cold Leg Releases for SBLOCA Analysis

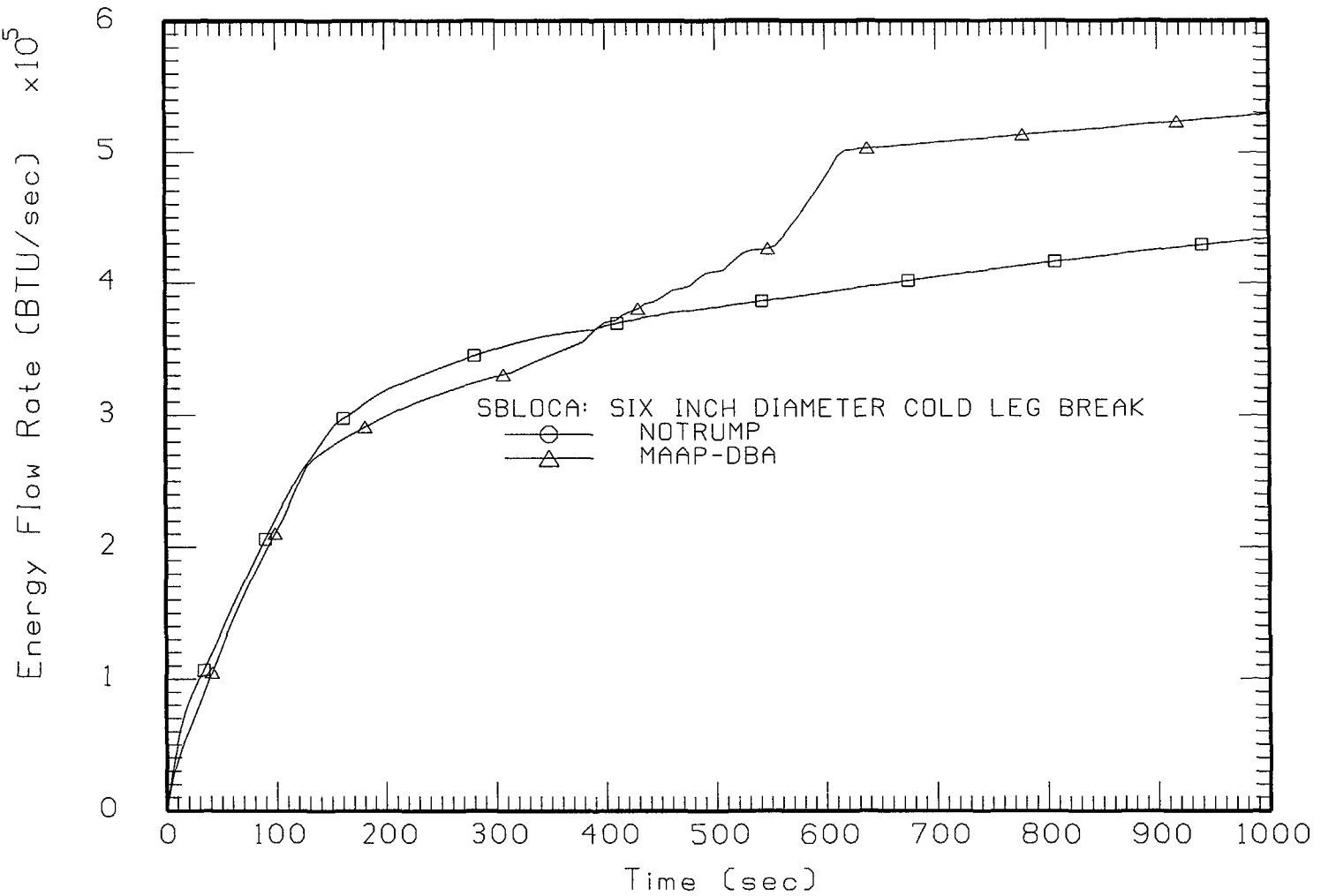


Figure 2-34a Comparison of 6 Inch Cold Leg Releases for SBLOCA Analysis

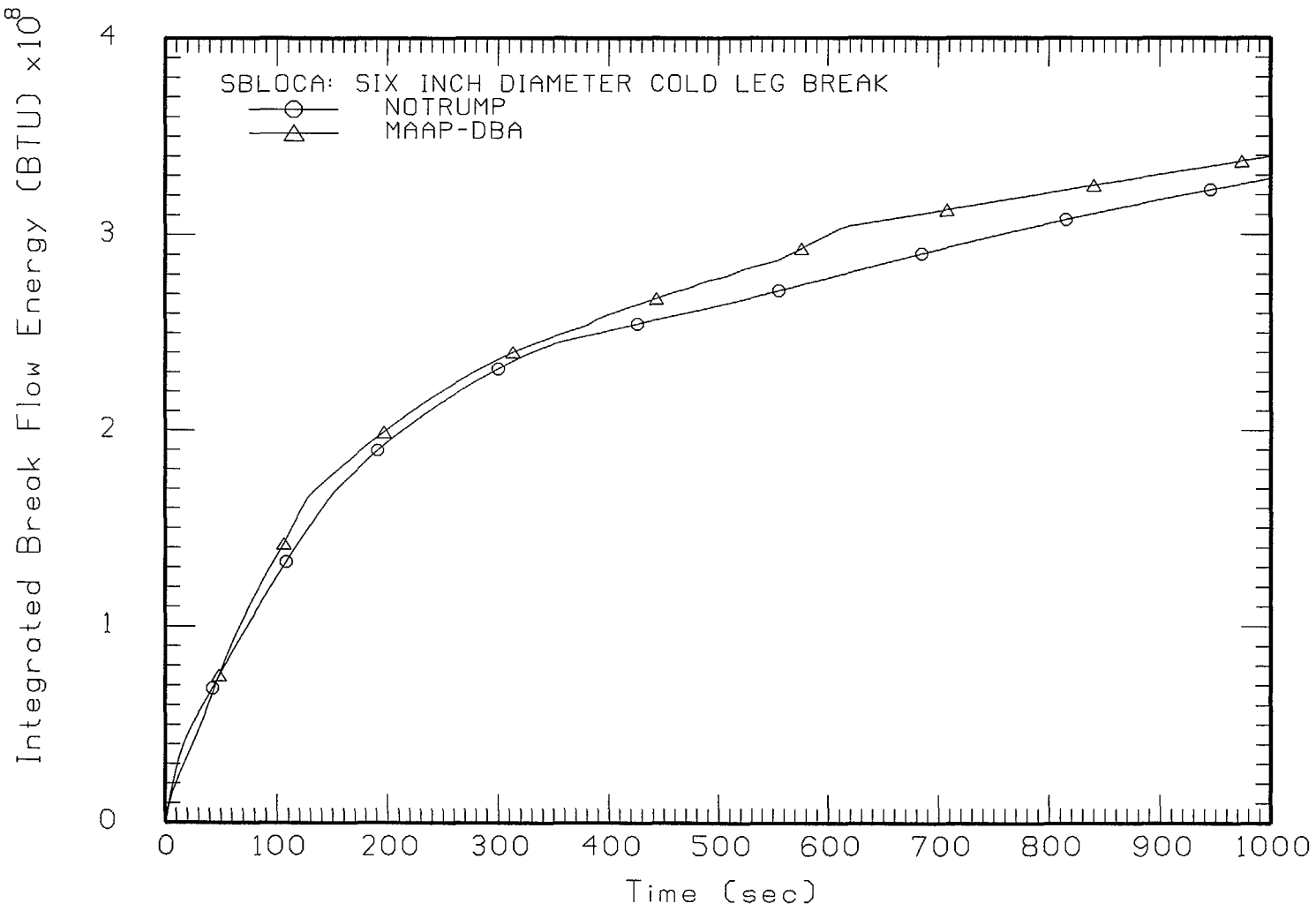


Figure 2-34b Comparison of 6 Inch Cold Leg Releases for SBLOCA Analysis

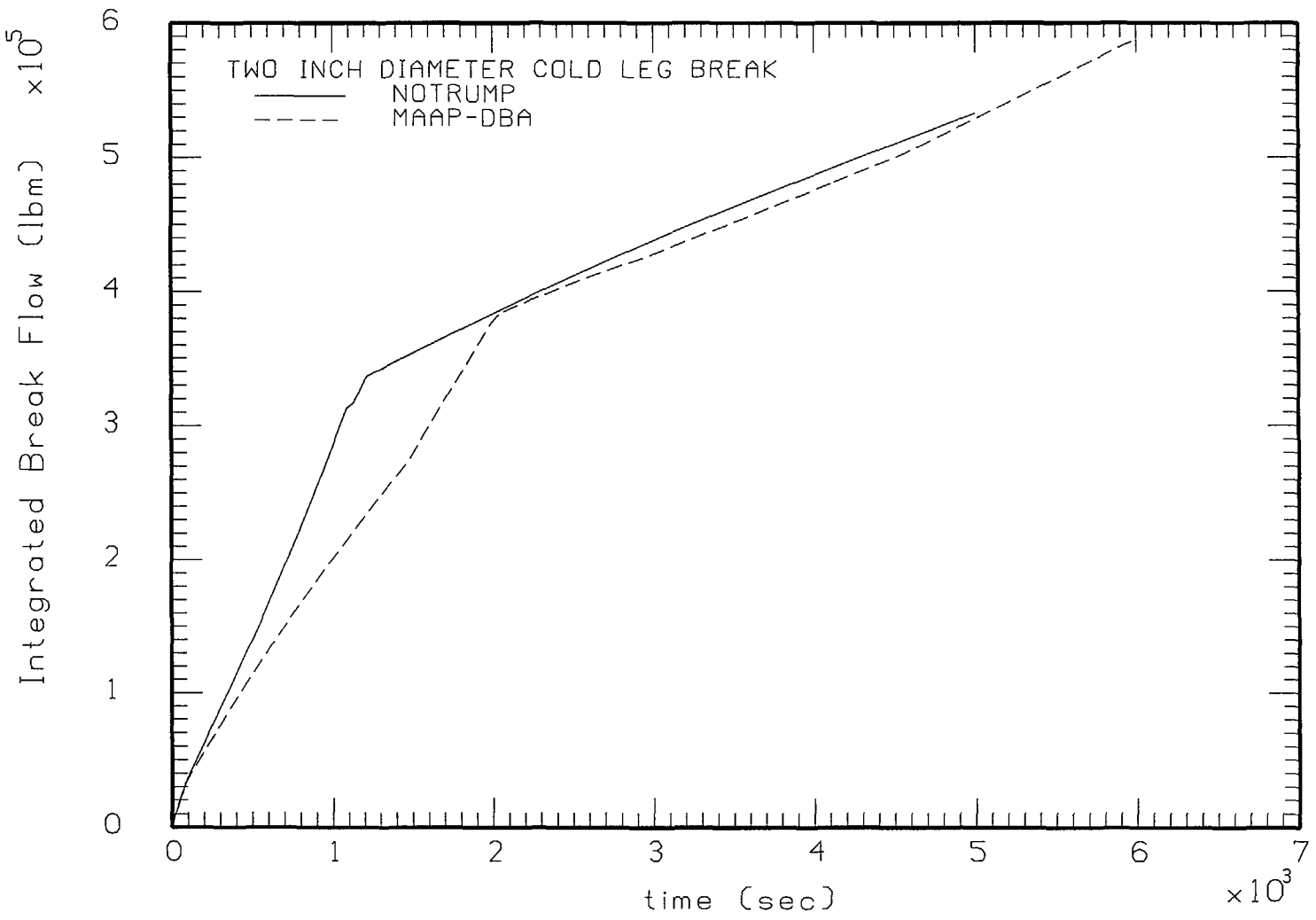


Figure 2-35a Comparison of 2 Inch Cold Leg Releases

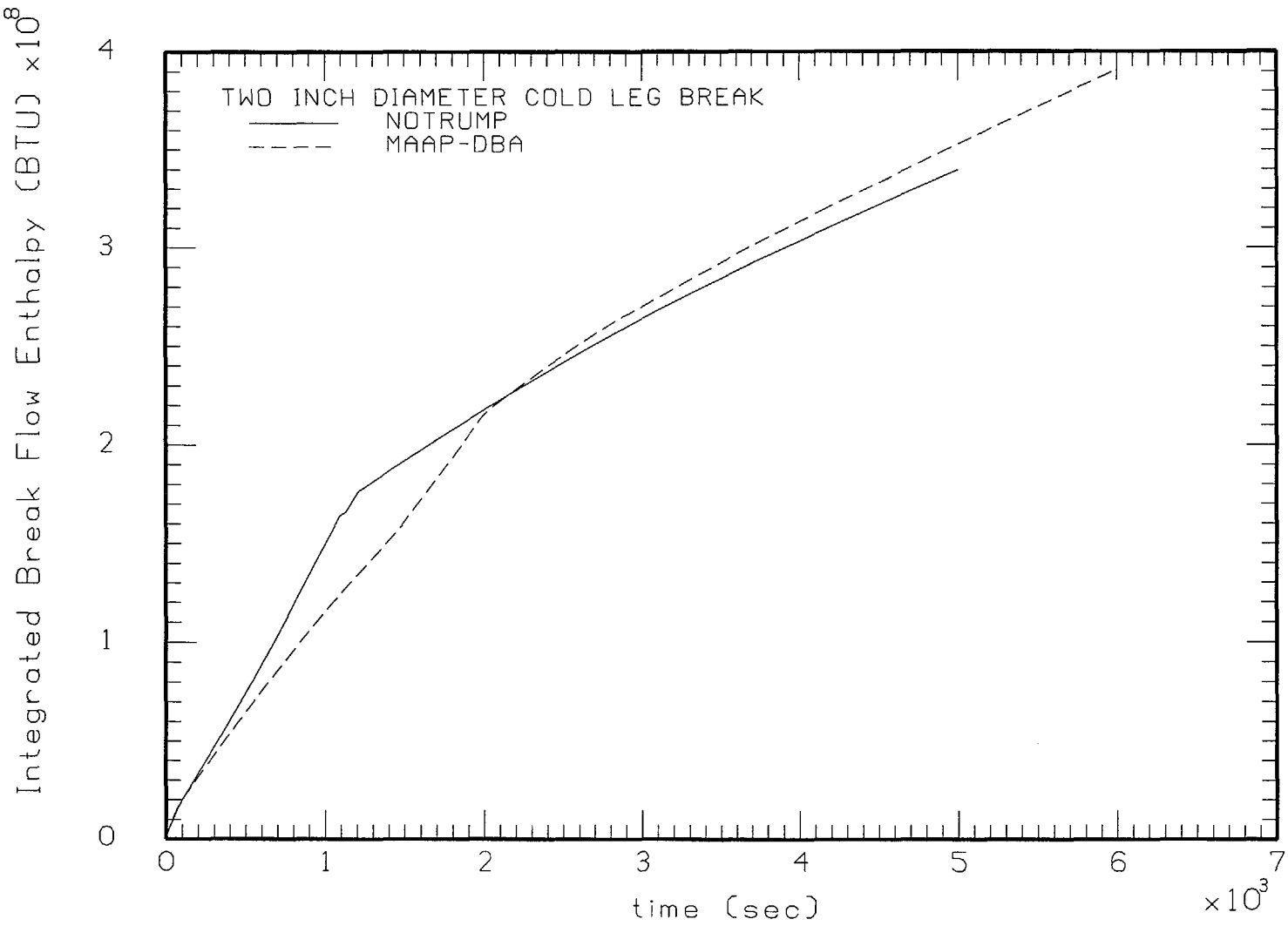


Figure 2-35b Comparison of 2 Inch Cold Leg Releases

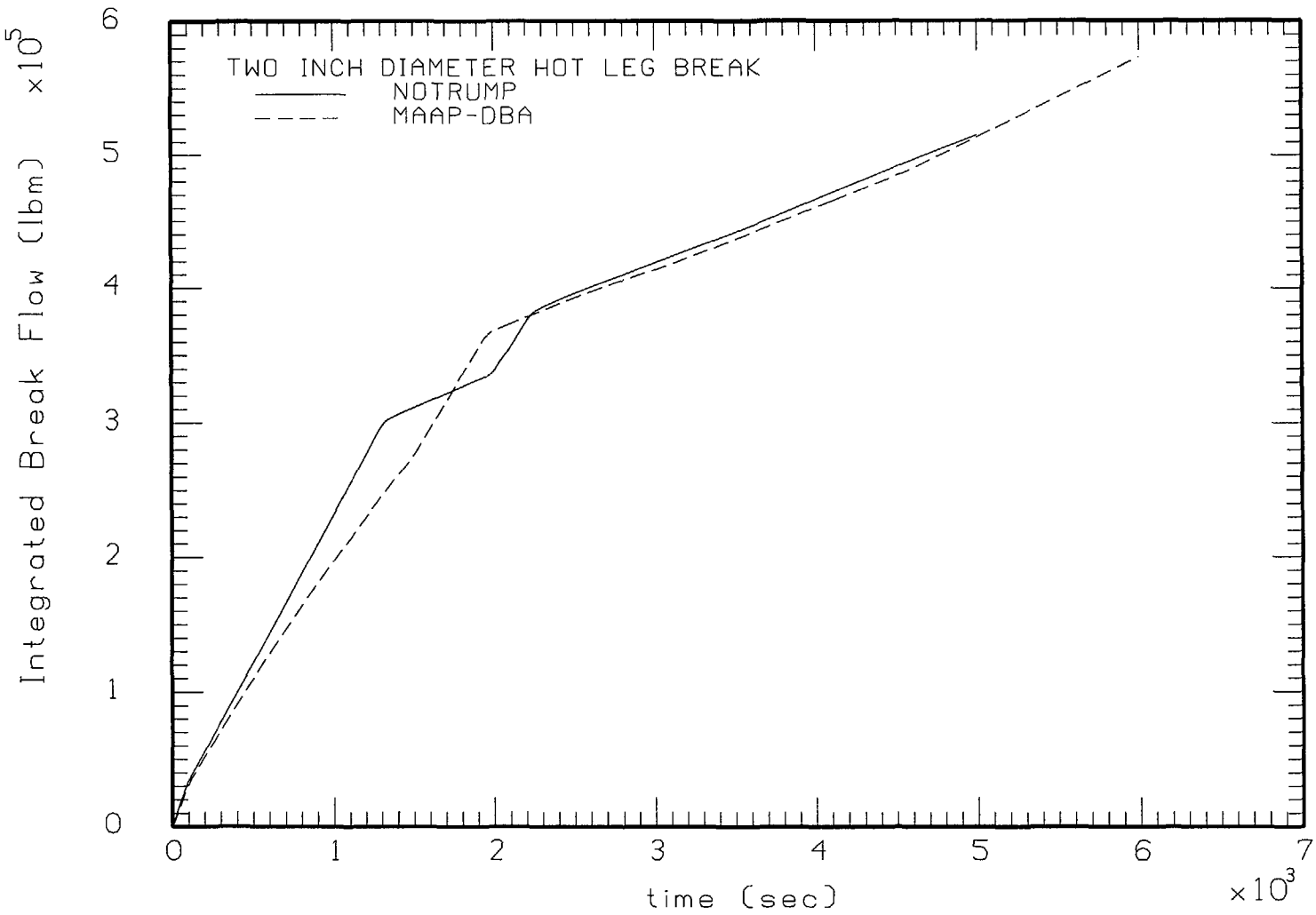


Figure 2-36a Comparison of 2 Inch Hot Leg Releases

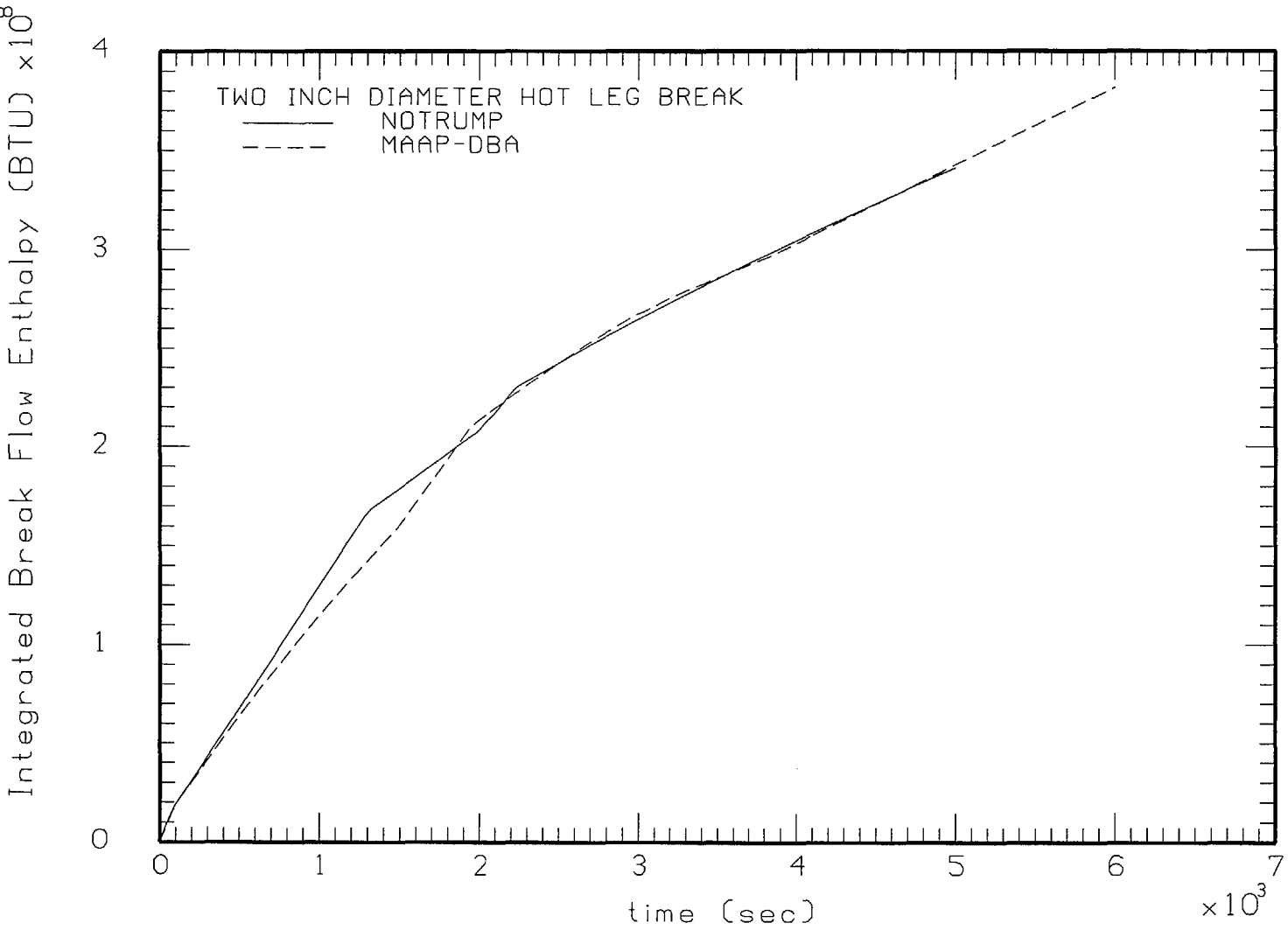


Figure 2-36b Comparison of 2 Inch Hot Leg Releases

3 RESULTS FOR BVPS-1 AND BVPS-2

The limiting large break LOCA and MSLB cases for both units have been quantified to determine the peak containment pressure and temperature responses. The single node MAAP-DBA model was used along with assumptions that comply with the guidance provided in the applicable Standard Review Plan. The single node MAAP-DBA models used the Tagami and Uchida heat transfer correlations to calculate the energy exchange with the passive containment heat sinks. The key model assumptions used for containment peak pressure calculations are summarized in Table 3-1.

The mass and energy release histories for both large break LOCA and MSLB were generated using NRC approved Westinghouse methodologies and computer codes. Those Westinghouse generated mass and energies were then inputted in the MAAP-DBA containment analyses code.

In producing the mass and energies, Westinghouse used realistic core reactivity coefficients and accounted for the fact that integral steam flow restrictors will be installed in the Unit 1 replacement steam generators. As a result, the MSLB was found to be no longer design pressure limiting compared to LOCA.

The large LOCA double ended hot leg (DEHL) was selected for the LOCA peak pressure and temperature assessment for both units, because it has been previously shown to be limiting for containment design.

The peak pressure results are summarized in Table 3-2 and Figures 3-1 and 3-2 for both units. The peak calculated pressures using MAAP-DBA and these modeling assumptions are less than the 45 psig containment design pressure.

The corresponding gas temperature responses for these cases are presented in Figures 3-3 and 3-4.

These results indicate that the current containment design basis for peak pressure will continue to be met following the conversion to an atmospheric containment mode of operation.

Nodes	Single
Entrainment (Pools and Films)	No
Forced Convection	No
LOCA Airborne Water Droplet Fraction	10%
Spray Droplet Diameter	1000 microns
LOCA Airborne Water Droplet Diameter	100 microns
Re-vaporization	8%
Initial Containment Pressure	14.2 psia
LOCA: Heat Transfers (Short Term)	Tagami
MSLB: Heat Transfers	Uchida with 8% revaporization

Unit	Case	Accident Type	Peak Pressure (psig)	Peak Gas Temperature (°F)
1	Case 8L	LOCA	43.1	267.3
1	Case 15M	MSLB	42.4	342.6
2	Case 3L	LOCA	44.6	269.7
2	Case 16M	MSLB	36.9	327.1

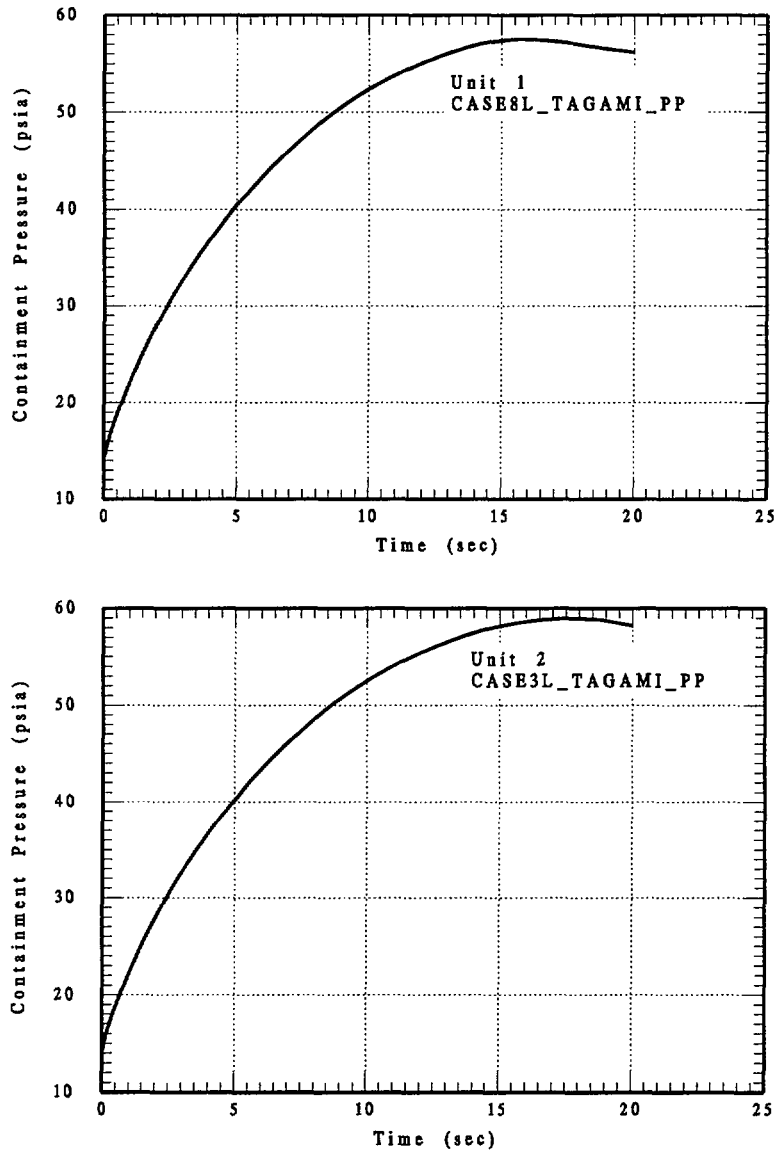


Figure 3-1 BVPS Large LOCA Pressure Profile (Tagami)

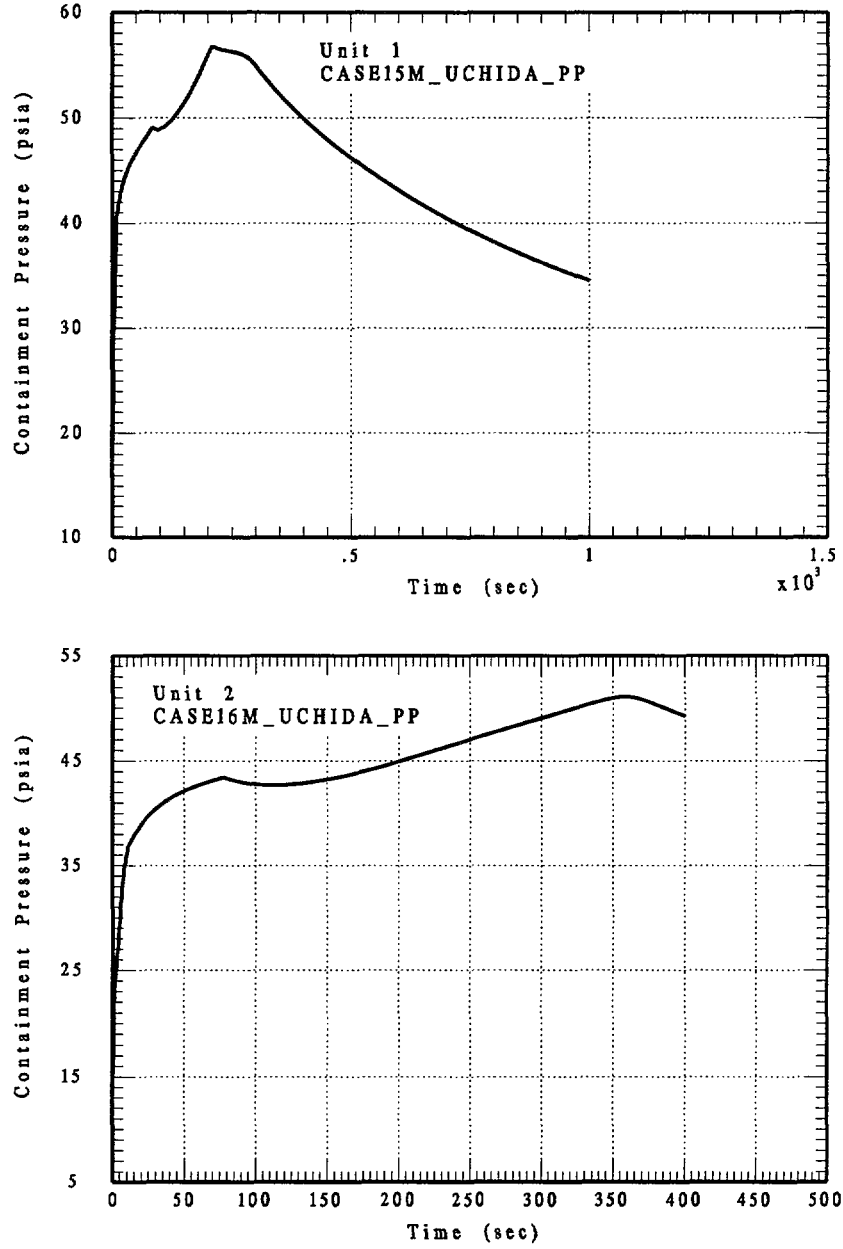


Figure 3-2 BVPS MSLB Pressure Profile (Uchida)

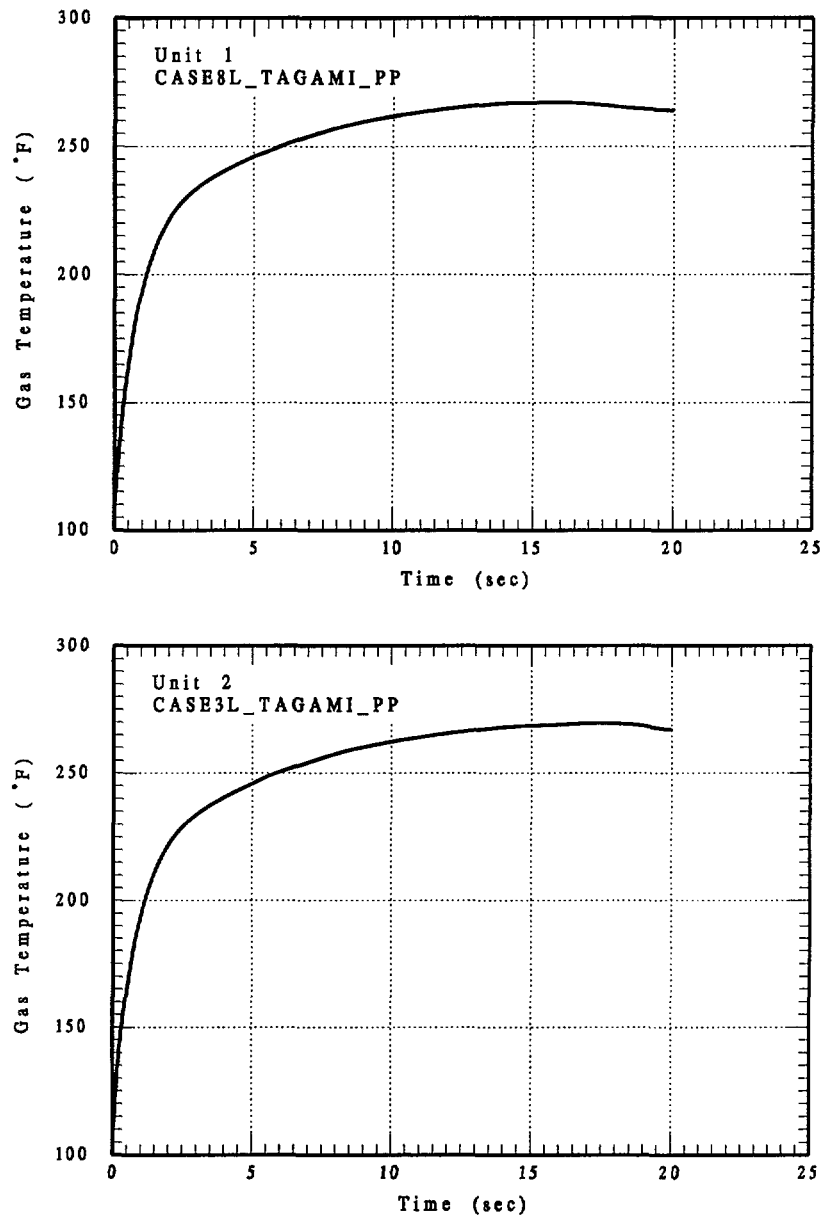


Figure 3-3 BVPS Large LOCA Gas Temperature Profile (Tagami)

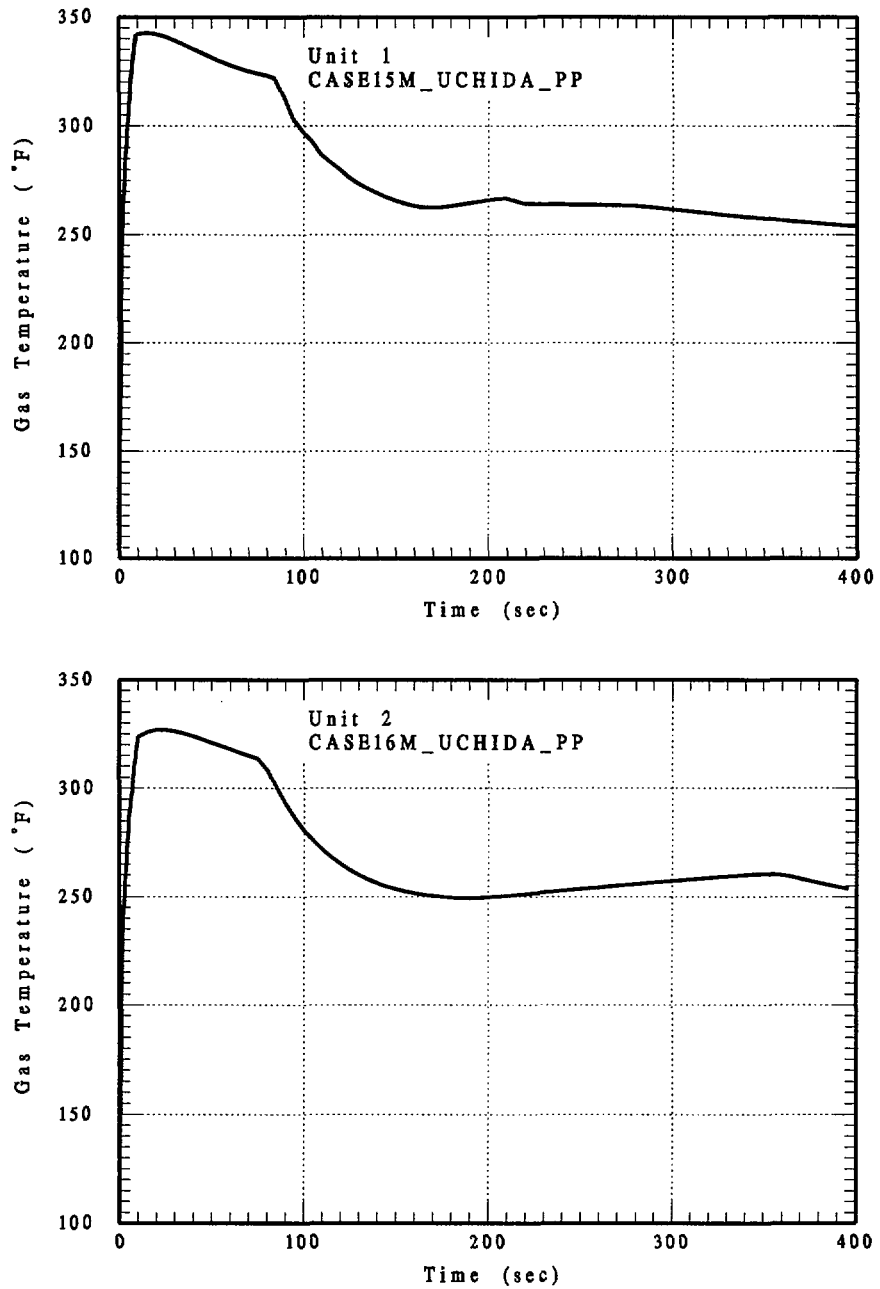


Figure 3-4 BVPS MSLB Gas Temperature Profile (Uchida)